

Interaction and Phase Relaxation in Disordered Nanowires and Quantum Hall Systems

T. Ludwig

Institut für Nanotechnologie

März 2006

Forschungszentrum Karlsruhe

in der Helmholtz-Gemeinschaft

Wissenschaftliche Berichte

FZKA 7204

**Interaction and phase relaxation
in disordered nanowires
and Quantum Hall Systems**

Thomas Ludwig

Institut für Nanotechnologie

von der Fakultät für Physik
der Universität Karlsruhe (TH) genehmigte Dissertation

Forschungszentrum Karlsruhe GmbH, Karlsruhe
2006

Für diesen Bericht behalten wir uns alle Rechte vor

Forschungszentrum Karlsruhe GmbH
Postfach 3640, 76021 Karlsruhe

Mitglied der Hermann von Helmholtz-Gemeinschaft
Deutscher Forschungszentren (HGF)

ISSN 0947-8620

urn:nbn:de:0005-072044

**Interaction and phase relaxation
in disordered nanowires
and Quantum Hall Systems**

**Wechselwirkung und Phasenrelaxation
in ungeordneten Nanodrähten
und Quanten-Hall-Systemen**

Zur Erlangung des akademischen Grades eines
DOKTORS DER NATURWISSENSCHAFTEN
von der Fakultät für Physik der
Universität Karlsruhe (TH)

genehmigte
DISSERTATION

von
Dipl.-Phys. Thomas Ludwig
aus Hamburg

Tag der mündlichen Prüfung: 27.01.2006
Referent: Prof. Dr. Alexander D. Mirlin
Korreferent: Prof. Dr. Peter Wölfle

Hofstadter's Law:

It always takes longer than you expect,
even when you take Hofstadter's Law into account.

Zusammenfassung:

Wechselwirkung und Phasenrelaxation in ungeordneten Nanodrähten und Quanten-Hall-Systemen

Die vorliegende Arbeit untersucht das Wechselspiel von Elektron-Elektron-Wechselwirkung und Unordnung in mesoskopischen Systemen.

Der Einfluß von inelastischen Prozessen auf Aharonov-Bohm-Oszillationen in metallischen Ringen wird mit der Pfadintegralmethode untersucht. Es ergibt sich eine Phasenrelaxationslänge, die sich parametrisch von der bekannten Relaxationslänge für schwache Lokalisierung unterscheidet. Der Unterschied entsteht dadurch, daß für Aharonov-Bohm-Oszillationen die Länge relevanter Trajektorien durch die Systemgröße gegeben ist (obwohl die Phasenrelaxationslänge viel kürzer ist), da nur Trajektorien die den Ring umlaufen zu Aharonov-Bohm-Oszillationen beitragen.

Ferner wird die Amplitude mesoskopischer Leitwertfluktuationen im Nichtgleichgewicht berechnet. Diese zeigt eine nichtmonotone Spannungsabhängigkeit, die durch mehrere Mechanismen entsteht. Eine Erhöhung der Fluktuationen ergibt sich durch den Einfluß von Variationen des elektrochemischen Potentials auf alle Leitungselektronen im verfügbaren Energiefenster. Bei sehr hohen Spannungen werden Leitwertfluktuationen durch inelastische Prozesse unterdrückt. Diese sind ortsabhängig, so daß die Leitwertfluktuationen durch die Teile der Probe in der Nähe der Reservoirs bestimmt sind.

Schließlich wird der Einfluß von Eichfeldfluktuationen auf Quanteninterferenzeffekte untersucht. Typische Eichfeldfluktuationen sind viel langsamer als die Zeitskalen des Elektronentransports. Daher entstehen Dephasingeffekte vor allem durch Ensemblemitteilung und Brechung der Zeitumkehrsymmetrie. Diese Effekte werden in zwei- und quasi-eindimensionalen Systemen untersucht. Die resultierenden Phasenrelaxationsraten sind wesentlich größer als die Rate, die den Verlust des Phasengedächtnisses des einzelnen Teilchens beschreibt.

Abstract:

Interaction and phase relaxation in disordered nanowires and Quantum Hall Systems

This thesis investigates the interplay of electron-electron interaction and disorder in mesoscopic systems.

The suppression of Aharonov-Bohm oscillations in metallic rings is calculated using the path-integral method. The resulting dephasing length is parametrically different from the usual dephasing length applicable to weak localisation. The difference is due to the length of relevant trajectories being given by the system size, even if the dephasing length is much shorter, since Aharonov-Bohm oscillations arise only from trajectories encircling the ring.

Further, the voltage dependence of mesoscopic conductance fluctuations in the nonequilibrium situation is calculated. The amplitude of conductance fluctuations is a nonmonotonic function of the voltage due to several different effects. An enhancement results from variations of the electrochemical potential affecting all electrons in the energy window available for transport. At very high voltages, inelastic processes lead to a suppression of the conductance fluctuations. The dephasing effect is position dependent, with the residual conductance fluctuations originating from the regions of the sample close to the reservoirs.

Finally, the effect of transverse gauge field fluctuations on quantum interference effects is investigated. Typical gauge field fluctuations are much slower than the timescales set by the electron motion. Therefore dephasing effects are mainly due to ensemble-averaging and time-reversal breaking. These effects are investigated for two- and quasi-one-dimensional systems. The resulting dephasing rates are very high compared to the rate describing the loss of phase memory of the single particle.

Deutsche Zusammenfassung

Die vorliegende Arbeit beschäftigt sich mit dem Wechselspiel von Elektron-Elektron-Wechselwirkung und Unordnung in mesoskopischen Systemen. Gerade in niedrigen Dimensionen, also in zweidimensionalen Filmen und quasi-eindimensionalen¹ Drähten, sind Wechselwirkungseffekte besonders ausgeprägt, weil sich diffusiv bewegende Leitungselektronen länger miteinander wechselwirken als ballistische und in niedrigen Dimensionen die Rückkehrwahrscheinlichkeit zu einem gegebenen Punkt höher ist. Ferner sind aufgrund von Phasenraumargumenten in niedrigen Dimensionen kleine Impulse (von der Größenordnung der inversen Systemgröße) besonders relevant für das Verhalten der Systeme, so daß nichttriviale Geometrien interessante Effekte haben.

In Kapitel 2 wird daher die Aharonov-Bohm Ringgeometrie untersucht. Interferenz von Pfaden, die den Ring umlaufen, führt zu Oszillationen des Leitwerts als Funktion des magnetischen Flusses durch den Ring mit einer fundamentalen Periode von h/e bzw. $h/2e$. Diese Effekte entsprechen den bekannten mesoskopischen Leitwertfluktuationen bzw. der schwachen Lokalisierung. Durch Anpassung des Pfadintegralformalismus [18, 29, 85] auf die Ringgeometrie, insbesondere eine Formulierung der abgeschirmten Coulombwechselwirkung im Ortsraum, wird eine mikroskopische Theorie des Einflusses inelastischer Prozesse auf Aharonov-Bohm-Oszillationen entwickelt. Es zeigt sich, daß die durch Gln. (2.30), (2.33) gegebene Unterdrückung von Aharonov-Bohm-Oszillationen sich parametrisch von der Unterdrückung schwacher Lokalisierung oder mesoskopischer Leitwertfluktuationen unterscheidet. Dies ergibt sich daraus, daß in niedrigdimensionalen Systemen inelastische Prozesse mit kleinen Impulsüberträgen (von der Größenordnung der inversen Systemgröße) dominieren. Während der Infrarotcutoff für schwache Lokalisierung und mesoskopische Leitwertfluktuationen selbstkonsistent gesetzt wird (die Probe kann gedanklich in kohärente Segmente von der Größe der Phasenrelaxationslänge L_φ geteilt werden), entstehen Aharonov-Bohm-Oszillationen nur durch Trajektorien, die den Ring umlaufen und daher nicht kürzer als der Ringumfang sein können. Diese Bedingung, die selbst bei starkem Dephasing ($L_\varphi \ll R$, wobei R der Ringradius ist) erfüllt sein muß, führt zu dem Verhalten (2.33), das sich durch die Dekohärenzlänge (2.34) beschreiben lässt. Die Formulierung mit Hilfe einer Dekohärenzlänge, die von der Sy-

¹Hiermit sind Drähte gemeint, deren Breite viel größer ist als die elastische freie Weglänge, aber viel kleiner als ihre Länge. Die Diffusionsbewegung der Leitungselektronen kann daher eindimensional beschrieben werden. Es handelt sich nicht um streng eindimensionale Systeme, die als Luttingerflüssigkeit zu beschreiben wären.

stemgröße abhängt, ist physikalisch motiviert durch den systemgrößenabhängigen Gehalt an relevanten Fluktuationen.

Ferner wurde in Kapitel 2.3 die in [85] aufgestellte Beziehung (2.41) zwischen schwacher Lokalisierung und mesoskopischen Leitwertfluktuationen durch eine Formulierung mit Hilfe von Pfadintegralen auf eine allgemeinere Basis gestellt und u.a. auf die Ringgeometrie verallgemeinert (siehe Gleichung (2.48)). Die für h/e -Oszillationen entwickelte Theorie läßt sich also direkt auf $h/2e$ -Oszillationen übertragen. Eine experimentelle Bestätigung der Ergebnisse von Kapitel 2 ist vor kurzem erfolgt [104].

Eine andere interessante Situation ist eine mesoskopische Probe im Nichtgleichgewicht. Durch die kompliziertere Form der Verteilungsfunktion der Elektronen haben auch Wechselwirkungseffekte einen qualitativ anderen Charakter. Insbesondere hat eine endliche Spannung einen qualitativ anderen Effekt als eine endliche Temperatur. In Kapitel 3 wird das Verhalten von mesoskopischen Fluktuationen des differentiellen Leitwerts als Funktion der angelegten Spannung untersucht. Die Ergebnisse bestätigen Experimente neueren Datums, die ein interessantes nichtmonotones Verhalten mit steigender Spannung beobachtet haben. Für hohe, aber nicht zu hohe Spannungen V , $V_c \ll V \ll gV_c$ (wobei g der dimensionslose Leitwert und eV_c die Thoulessenergie ist) spielen inelastische Effekte keine wesentliche Rolle. Die Elektron-Elektron-Wechselwirkung ist allerdings auch in dieser Situation wichtig, denn erst die Abschirmung der Wechselwirkung zwischen den Leitungselektronen durch eben diese Leitungselektronen ermöglicht die Definition des elektrochemischen Potentials. Variationen des elektrochemischen Potentials beeinflussen alle Elektronen im zur Verfügung stehenden Energiefenster der Breite eV , das für $eV \gg eV_c$ in unkorrelierte Intervalle der Breite eV_c zerfällt, und führen dadurch zu einem Anstieg der Leitwertfluktuationen mit der Spannung, der asymptotisch linear mit der Spannung verläuft [34]. Die mit Hilfe der Keldysh-Diagrammtechnik gewonnenen Ergebnisse zeigen, daß dieser Anstieg nach einem steilen Verlauf im Crossover-Bereich sehr flach verläuft und von Termen dominiert wird, die formal von höherer Ordnung sind.

Die Notwendigkeit, inelastische Elektron-Elektron-Streuung zu berücksichtigen, zeigt sich schon darin, daß für Spannungen $V \gg g^2V_c$ die Leitwertfluktuationen die Größenordnung des Leitwerts erreichen würden, so daß Spannungsbereiche mit negativem differentielltem Widerstand auftreten müssten. Dies ist an metallischen Proben nie beobachtet worden, stattdessen zeigen alle Experimente bei genügend hoher Spannung einen Abfall der Leitwertfluktuationen. Eine genaue Betrachtung von Dephasingeffekten im Nichtgleichgewicht findet in Kapitel 3.3 statt. Es zeigt sich, daß Dephasingeffekte für Spannungen $V \gtrsim gV_c$ relevant werden, und damit der Bereich $V \gtrsim g^2V_c$ nicht im nichtwechselwirkenden Bild beschrieben werden kann. Für starkes Dephasing ($V \gg gV_c$) ergibt sich der durch Gleichung (3.99) beschriebene Abfall der Leitwertfluktuationen. In diesem Regime kann die Probe nicht durch eine konstante Relaxationslänge L_φ beschrieben werden, sondern die Stärke inelastischer Prozesse ist ortsabhängig. Die Leitwertfluktuationen (3.99) entstehen im wesentlichen in den Teilen der Probe in der Nähe der Reservoirs. In diesen Bereichen ist der Effekt inelastischer Prozesse auch bei

hohen Spannungen klein. Die in Kapitel 3 präsentierten Ergebnisse stimmen gut mit experimentellen Daten [86, 87] überein.

Prinzipiell existieren in ungeordneten Metallen nicht nur skalare Fluktuationen, sondern auch transversale magnetische Fluktuationen. In gewöhnlichen Metallen sind diese relativistisch klein gegenüber den skalaren Fluktuationen und von eher konzeptionellem Interesse. Eichfeldfluktuationen mit den gleichen qualitativen Eigenschaften treten aber auch in Modellen stark korrelierter Systeme auf, wie zum Beispiel der Composite-Fermion-Beschreibung [45, 47, 52, 71] des halb gefüllten Landau-Niveaus im Quanten-Hall-Effekt. Die Quasiteilchen dieses Systems, sogenannte Composite Fermions, entstehen durch eine statistische Transformation aus den Leitungselektronen und bewegen sich in einem reduzierten magnetischen Feld (das bei halber Füllung gerade verschwindet), wechselwirken aber andererseits mit einem Chern-Simons-Eichfeld, wobei die Kopplungskonstante von der Größenordnung 1 ist. Composite Fermions lassen sich als Elektronen mit zwei an sie gebundenen magnetischen Flußquanten auffassen. Aus der ungeordneten Bewegung der Elektronen resultiert daher automatisch auch ein fluktuierendes ungeordnetes Magnetfeld, bzw. Fluktuationen des Chern-Simons-Eichfelds. Die Composite Fermions wechselwirken miteinander über den Austausch von Eichfeldfluktuationen wesentlich stärker als über die Coulombwechselwirkung. In Kapitel 4 werden dadurch verursachte Dephasingeffekte untersucht. Charakteristisch für die betrachteten Systeme sind die unterschiedlichen Zeitskalen: Die Dynamik des Eichfeldes ist viel langsamer als die der Composite Fermions. Daher kann die Eichfeldkonfiguration für ein einzelnes Fermion als statisch betrachtet werden; allerdings verändert sie sich zwischen verschiedenen Messungen. Die Dephasingeffekte beruhen also vorwiegend auf dem Auseinanderlaufen der Phasen im Ensemble der quasistatischen Eichfeldkonfigurationen, und lassen sich auf topologische Effekte zurückführen. Die entsprechende Phasenrelaxationsrate ist wesentlich höher als die inverse Temperatur, allerdings stellt sich heraus daß das Bild der Fermiflüssigkeit [3] gültig bleibt, da die Zeitskala auf der das einzelne Fermion seine Phasenkohärenz verliert viel länger ist. Während in zwei Dimensionen, bedingt durch mehrfache Rückkehrprozesse eine logarithmische Korrektur zur Dekohärenzrate entsteht (siehe Gl. (4.40)), ergibt sich in der quasi-eindimensionalen Geometrie die durch Gl. (4.47) gegebene Dekohärenzrate proportional zur Temperatur. Diese entsteht auf nichttriviale Weise aus dem Wechselspiel zwischen Rückkehrprozessen und der geometrischen Beschränkung der quasi-eindimensionalen Trajektorien. Aufgrund der Abwesenheit von Infrarotdivergenzen unterscheidet sich auch die Relaxationsrate für Aharonov-Bohm-Oszillationen (4.58) nicht qualitativ von derjenigen im einfachen Draht, im Gegensatz zur in Kapitel 2 betrachteten Coulombwechselwirkung.

Obwohl bei oberflächlicher Betrachtung schwache Lokalisierung und Leitwertfluktuationen auf verschiedene Weise durch langsame Eichfeldfluktuationen unterdrückt werden (schwache Lokalisierung durch Brechung der Zeitumkehrinvarianz und Leitwertfluktuationen durch Ensemblemittelung über die quasistatischen Konfigurationen), gilt eine der in Kapitel 2.3 bewiesenen vergleichbare Beziehung zwischen schwacher Lokalisierung und Leitwertfluktuationen auch für den Fall von Eichfeldfluktuationen: Die Effekte von Bre-

chung der Zeitumkehrinvarianz und Ensemblemittelung werden gerade aufeinander abgebildet. Da in beiden Fällen kein “echtes” Dephasing (Verlust des Phasengedächtnisses des einzelnen Fermions) vorliegt, stellt sich die Frage ob die Effekte von “langsamen” und “schnellen” Eichfeldfluktuationen ($\omega_{\text{gf}} \gtrsim 1/\tau_\varphi$) voneinander getrennt werden können, also die Phasenrelaxation des einzelnen Fermions beobachtet werden kann. Theoretisch gibt es zur schwachen Lokalisierung in *zweiter* Ordnung in $1/k_F l$ Beiträge, die nur auf schnelle Eichfeldfluktuationen sensibel sind. Leider scheinen diese nicht sinnvoll für Experimente zugänglich zu sein. Eine selbstkonsistente Berechnung der nur durch schnelle Fluktuationen verursachten Relaxationsrate für schwache Lokalisierung in erster Ordnung in $1/k_F l$ bestätigt das Bild der Fermiflüssigkeit für typische Quanten-Hall-Systeme bei $\nu = 1/2$ im experimentell relevanten Parameterbereich.

Wechselwirkungs- und Unordnungseffekte in niedrigen Dimensionen bleiben ein spannendes Thema. Zwar ist das Verhalten von wechselwirkenden Elektronen in ungeordneten Metallen gut verstanden, aber zum Verhalten von Composite-Fermion-Systemen bleiben noch offene Fragen. Insbesondere das Verhalten des Composite-Fermion-Systems unterhalb der durch Gleichung (4.68) gegebenen Temperatur konnte im Rahmen dieser Arbeit nicht untersucht werden. Das verfügbare Spektrum von thermischen “schnellen” Eichfeldfluktuationen (mit Frequenzen größer als die inverse Phasenrelaxationsrate) verschwindet unterhalb dieser Temperatur. Die Eigenschaften des Systems bei noch tieferen Temperaturen sind bisher nur unzureichend verstanden.

Contents

1	Introduction	1
1.1	Quantum interference and phase relaxation effects in disordered metals	1
1.1.1	Weak localization	3
1.1.2	Mesoscopic conductance fluctuations	6
1.1.3	Aharonov-Bohm oscillations of conductance	10
2	Effect of Coulomb interaction on Aharonov-Bohm oscillations	17
2.1	Dephasing on a phenomenological level	17
2.2	Dephasing of h/e Aharonov-Bohm oscillations by Coulomb interaction	18
2.2.1	Screened Coulomb interaction in real space	18
2.2.2	Effect of Coulomb interaction on Aharonov-Bohm interference	20
2.2.3	Analytic solution of the strong-dephasing case	23
2.2.4	Aharonov-Bohm dephasing time and dephasing length	28
2.2.5	Relation to experiments	30
2.3	Relation of h/e oscillations and $h/2e$ oscillations	31
2.4	Summary	37
3	Nonequilibrium mesoscopic conductance fluctuations	39
3.1	Overview of previous results and available experimental data	39
3.2	Voltage dependence of conductance fluctuations in a noninteracting system	41
3.2.1	Keldysh diagrammatic method for disordered systems	41
3.2.2	Voltage-induced enhancement of conductance fluctuations in a quasi-onedimensional wire	44
3.2.3	Effect of finite temperature	54
3.3	Effect of Coulomb interaction at high voltage	57
3.3.1	Nonequilibrium noise: Boltzmann-Langevin approach	57
3.3.2	Strong-dephasing limit	59
3.3.3	Comparison with experimental data	65
3.4	Summary	67

4	Effect of gauge-field interactions on quantum interference	69
4.1	Coupling to transverse gauge fields	69
4.2	Previous results on dephasing in fermion-gauge field systems	71
4.3	Relation of weak localization and conductance fluctuations	73
4.4	Weak localization with slow transverse gauge field fluctuations	77
4.4.1	Two-dimensional case	77
4.4.2	Quasi-onedimensional case	83
4.5	Aharonov-Bohm oscillations with slow transverse gauge field fluctuations	86
4.6	Fast versus slow gauge field fluctuations	89
4.7	Summary	94
5	Conclusions	97
A	Preexponential factor of Aharonov-Bohm oscillations	99
B	Keldysh diagram for the current	101
C	Keldysh diagrams for current fluctuations	105
D	Crossover between the linear response and the high-voltage enhancement	109
E	Subleading terms in the high-voltage strong-dephasing regime	111
F	Thermal averaging factor for $T \ll E_c$	115
G	Consistency checks for the fermion-gauge field system	117
H	Saddle-point evaluation of the $h/2e$ amplitude with gauge field fluctuations	121
	Bibliography	123
	Acknowledgments	131

1 Introduction

1.1 Quantum interference and phase relaxation effects in disordered metals

Quantum interference effects in the transport theory of disordered metals arise from the fact that the probability of a classical trajectory needs to be replaced by a quantum-mechanical complex probability amplitude. Considering two trajectories connecting the same initial and final points, the probability for a conduction electron to travel from the initial to the final point is given by the absolute square of the sum of the amplitudes,

$$|A_1 + A_2|^2 = |A_1|^2 + |A_2|^2 + 2 \operatorname{Re} A_1 A_2^* , \quad (1.1)$$

with the quantum interference term (the last term) usually oscillating quickly on the scale of the Fermi wavelength λ_F , which is much shorter than the elastic mean free path l . The interference term therefore usually averages out, one exception being the weak localization correction (see Section 1.1.1), where the phase relation between the paths under consideration is fixed. Another phenomenon is the case of mesoscopic conductance fluctuations (see Section 1.1.2), which are due to the fact that, unlike in the classical case, for a quantum-coherent sample the conductance is not a self-averaging quantity. Instead, as is typical for a mesoscopic system (i.e. a system with a size of the order of the phase-coherence length), details of the microscopic configuration carry over to the macroscopically observable conductance.

For all quantum interference phenomena, it is important to describe how the phase memory (with respect to the initial point) along a trajectory gets lost. This generally happens through processes which scatter the particle into a new quantum state. As a result, characteristic phase coherence times τ_φ and lengths L_φ arise, beyond which quantum interference effects are suppressed.

At low temperatures ($\lesssim 1$ K), spin-flip scattering from magnetic impurities and electron-electron interaction are the most important dephasing processes. While spin-flip scattering can be regarded as an extrinsic dephasing source and can be highly suppressed in a suitable setup [88], electron-electron interaction is an intrinsic property of the conduction electrons, raising the need for a well-understood theoretical treatment.

In low dimensions, the interplay of disorder and interaction is particularly interesting because the disorder enhances the interaction between diffusively moving electrons [29]: A ballistic electron moves through a region of size $1/q$, where q is the momentum

transfer of the collision, in the time $1/qv_F$, where v_F is the Fermi velocity. When this region is crossed by diffusion, the time instead is $1/Dq^2$ (D is the diffusion constant), so that the interaction time is given by the diffusion time or by the inverse energy transfer [29]. As a result, of particular interest in low dimensions are processes with small energy transfers. These do not alter the trajectory in a substantial way, they do however change the phase of the wave function in an appreciable way. Also, in low dimensions interference phenomena depend more sensitively on the large-scale cutoffs τ_φ , L_φ , due to the momenta governing the behaviour of the system being of the order of the inverse system size. A well-established theory of inelastic electron-electron collisions in disordered systems is available [18, 29, 72, 85].

This thesis considers effects of electron-electron interaction in several situations which are characterized by a rich interplay of different effects.

In Chapter 2, the Aharonov-Bohm configuration [5, 17, 25, 48, 88] is considered. Due to the importance of low momentum transfers combined with the complicated geometry, a real-space formalism is needed which properly accounts for the geometry, including the boundary conditions. Surprisingly, up to now the treatment of dephasing in this situation has happened mainly on a phenomenological level [17, 37, 38]. Chapter 2 presents a microscopic theory which refines the previously available results and indeed shows some remarkable differences compared to them.

Another situation in which electron-electron interaction gains extra features is the nonequilibrium situation. When a mesoscopic sample is subject to a finite voltage, the electron distribution function becomes position-dependent, making the electrochemical potential (which is ultimately due to interactions and can only be defined on length-scales larger than the screening length) position-dependent. Already on this level, the nonequilibrium situation is remarkably different from the equilibrium one [34]. Moreover, also the phase space available for inelastic processes is more complicated than in the situation of a thermally broadened distribution function. In Chapter 3, a theory of mesoscopic conductance fluctuations in nonequilibrium is presented, which takes these features into account. A rich behaviour with several different regimes is found.

In some situations, electron-electron interaction results in the forming of new, strongly correlated states. One example is the half-filled lowest Landau level [20, 45, 47, 52, 57, 67, 71], which can be described in terms of new quasiparticles (“Composite Fermions”) which can be thought of as electrons with two magnetic flux quanta attached. As a result, they move in a magnetic field which is diminished by the absorbed flux quanta (and thus vanishes at half filling), but interact via a Chern-Simons gauge field in addition to the Coulomb interaction. The quasi-particle picture of Composite Fermions forming a Fermi sea [3] at half filling is supported by the Composite Fermions showing many of the transport phenomena known from electrons (see e.g. Refs. [54, 70, 84], for a review see Ref. [66]). In Chapter 4, the effect of the Chern-Simons interaction on transport properties of Composite Fermions is analyzed. From the properties of the Chern-Simons field, several issues arise which do not exist in the case of the Coulomb interaction, for example breaking of time-reversal symmetry and the appearance of new timescales

different from the scales set by the electron dynamics. As a result, the dephasing of Composite Fermions is dominated by geometric effects rather than those arising from energy exchange along the trajectories.

1.1.1 Weak localization

The weak localization of electrons in a disordered conductor is an effect of quantum interference of the conduction electrons. While the phase associated with an electron trajectory usually oscillates quickly as a function of small variations of the trajectory for most trajectories (and therefore just averages away), a path and its time-reversed version visit the same impurities and therefore feature a fixed phase relation (see Fig. 1.1). The interference is constructive because in the presence of time-reversal symmetry the phases accumulated along the direct and the time-reversed trajectory are identical. As a result, the probability to diffuse away from the origin of the trajectory is diminished (this is sometimes referred to as coherent backscattering), and the conductivity is decreased compared to the result obtained by the classical Drude-Boltzmann theory.

An estimate of the magnitude of the weak-localization effect can be obtained in the following way (see e.g. Refs. [29, 72]): The classical probability for a diffusive particle to return into a volume element dV is given by

$$dP = \frac{dV}{(Dt)^{d/2}} , \quad (1.2)$$

where D is the diffusion constant and d the number of dimensions. The relevant volume element is given by $dV = v_F dt \lambda_F^{d-1}$, i.e. by a cylinder of diameter λ_F and length $v_F dt$ where the returning trajectory may interfere with its initial part. On average, the returning trajectory will be directed opposite to the initial direction, so the correction to the conductivity is negative.¹ The weak localization correction $\delta\sigma_{\text{WL}}$ is therefore estimated as

$$\frac{\delta\sigma_{\text{WL}}}{\sigma} = -v_F \lambda_F^{d-1} \int \frac{dt}{(Dt)^{d/2}} , \quad (1.3)$$

where, if necessary in the dimensionality under consideration, the integral is cut off at the lower limit by the elastic scattering time τ (since a returning trajectory needs to visit at least one scattering site) and at the upper limit by the dephasing time τ_φ . In particular, the weak localization correction diverges at the upper limit in one and two dimensions if no cutoff τ_φ is taken into account. This ultimately means that for arbitrarily weak disorder all one-particle states are localized in one and two dimensions and therefore no states are available for conduction [4, 13, 14].

¹For strong spin-orbit coupling, the opposite situation is the case (weak antilocalization). Since the direction of the spin is locked to the direction of the trajectory, and thus rotated on average by π for a closed trajectory, the returning trajectory acquires an extra phase factor of -1 .

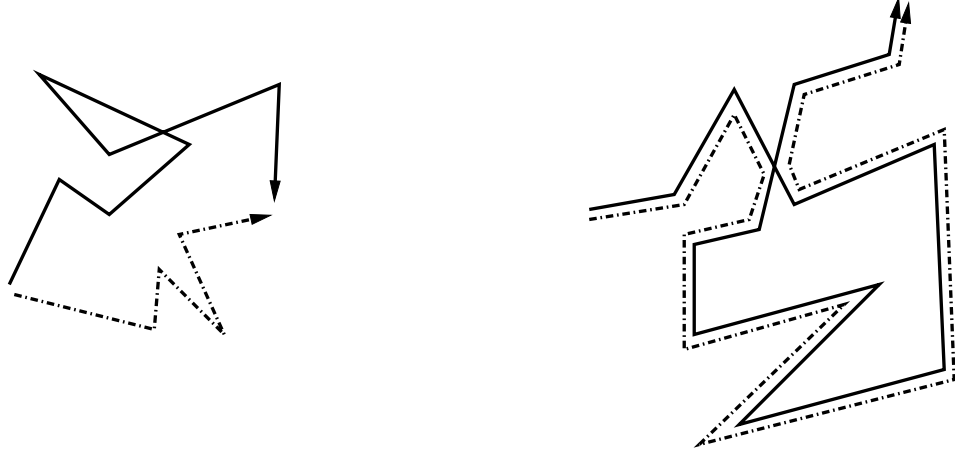


Figure 1.1: Left: Two paths visiting different impurity sites interfere with a random phase. Summing over all paths, most of the interference is averaged away. Right: Two paths visiting the same impurities but some in reversed order. These paths interfere constructively, thus reducing the probability for the particle to diffuse away. This is the origin of the weak localization correction.

Since weak localization requires interference with the time-reversed trajectory, it depends on the presence of the time-reversal symmetry. Time-reversal symmetry is broken by magnetic fields, and the weak localization effect then is destroyed because the direct and the time-reversed trajectory acquire opposite phases from the magnetic flux they enclose. This gives rise to the well-known negative magnetoresistance [16], since in strong magnetic fields only short trajectories enclosing less than one magnetic flux quantum give an appreciable contribution to the interference.

The weak localization correction has been calculated more rigorously [15, 16, 32] to be

$$\frac{\delta\sigma_{\text{WL}}}{\sigma} = - \int_{\tau}^{\tau_{\varphi}} dt \mathcal{C}(\mathbf{r}, \mathbf{r}, t) , \quad (1.4)$$

where the Cooperon \mathcal{C} satisfies (see Fig. 1.2)

$$\left\{ \frac{\partial}{\partial t} + D (-i\nabla - e \mathbf{a}(\mathbf{r}, t/2) - e \mathbf{a}(\mathbf{r}, -t/2))^2 \right\} \mathcal{C}(\mathbf{r}, \mathbf{r}', t) = \delta(\mathbf{r} - \mathbf{r}') \delta(t) . \quad (1.5)$$

The Cooperon can also be represented as a path integral [18],

$$\mathcal{C}(\mathbf{r}, \mathbf{r}', t) = \int_{\mathbf{r}(-t)=\mathbf{r}'}^{\mathbf{r}(t)=\mathbf{r}} \mathcal{D}[\mathbf{r}(t)] \exp \left\{ - \int_{-t}^t dt' \left[\frac{\dot{\mathbf{r}}^2(t')}{4D} + ie \dot{\mathbf{r}}(t') \cdot [\mathbf{a}(\mathbf{r}, t'/2) + \mathbf{a}(\mathbf{r}, -t'/2)] \right] \right\} . \quad (1.6)$$

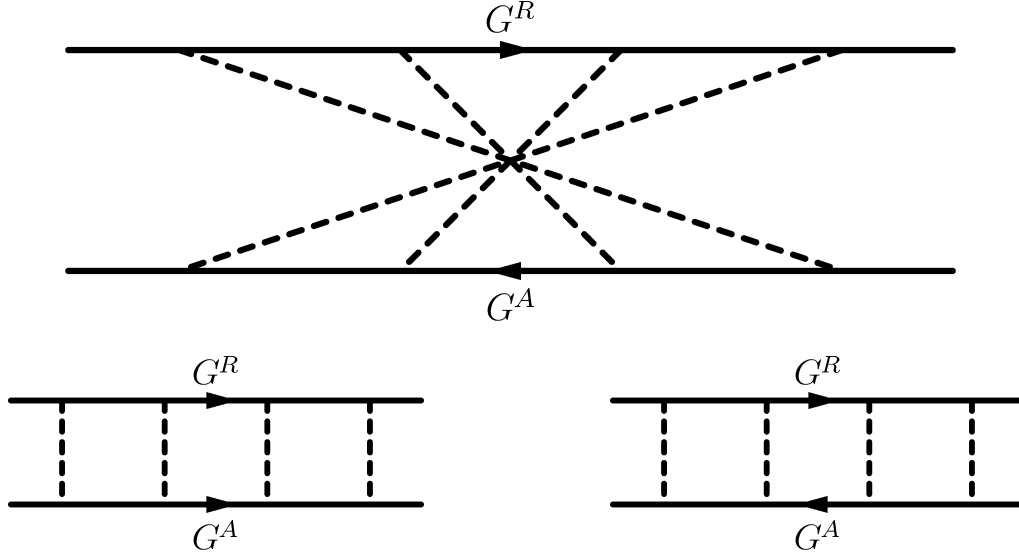


Figure 1.2: Top: diagrammatic representation of the Cooperon. The maximally crossed impurity lines result from the impurities visited in reverse order by the electron and hole trajectories. Here G^R denotes the retarded (electron) Green's function and G^A denotes the advanced (hole) Green's function. Lower left: equivalent diagram for the Cooperon. In the presence of time-reversal symmetry, this is equal to the diffuson (lower right).

Without a magnetic field, $\mathbf{a} = 0$, the Cooperon has the same form as the diffuson due to time-reversal symmetry, while the Cooperon is suppressed in the presence of a vector potential \mathbf{a} . Evaluating Eq. (1.4), the result is

$$\delta\sigma_{\text{WL}} = -\frac{e^2\sqrt{D\tau_\varphi}}{\pi} \frac{1}{[-\ln \text{Ai}(\tau_\varphi/\tau_H)]'} , \quad d = 1 , \quad (1.7)$$

$$\delta\sigma_{\text{WL}} = -\frac{e^2}{2\pi^2} \ln \frac{\tau_H\tau_\varphi}{\tau(\tau_H + \tau_\varphi)} , \quad d = 2 , \quad (1.8)$$

where τ_H is the timescale on which the magnetic field breaks time-reversal symmetry [16, 29, 72].

The weak localization effect is robust against thermal averaging, since the time-reversed version of a trajectory has the same energy even if the electron distribution function is thermally broadened. A temperature dependence of the weak localization arises from inelastic electron-electron collisions, which occur with increasing rate as the temperature is increased.

The dephasing rates due to inelastic processes have been calculated [18, 29, 72] for

different dimensions d to be

$$\frac{1}{\tau_\varphi} \sim \frac{T^{2/3}}{\nu^{2/3} D^{1/3}}, \quad d = 1, \quad (1.9)$$

$$\frac{1}{\tau_\varphi} \sim \frac{T}{\nu D} \ln k_F l, \quad d = 2, \quad (1.10)$$

where T is the temperature, D is the diffusion constant, l is the elastic mean free path, and ν is the density of states at the Fermi energy $E_F = k_F^2/2m$. The corresponding dephasing lengths are given by $L_\varphi = (D\tau_\varphi)^{1/2}$. In particular, for a quasi-onedimensional wire

$$L_\varphi \sim \frac{\nu^{1/3} D^{2/3}}{T^{1/3}}, \quad d = 1. \quad (1.11)$$

Recently it has been shown [85] that the same dephasing length also applies to the suppression of mesoscopic conductance fluctuations by inelastic electron-electron scattering (see Section 1.1.2, the connection between the two effects is investigated further in Section 2.3).

1.1.2 Mesoscopic conductance fluctuations

Universal conductance fluctuations [23, 24, 26, 33, 36] are one of the most prominent manifestations of quantum coherent transport in disordered conductors. When quantum coherence is retained over the entire sample, i.e. the dephasing length L_φ is larger than the system size, the variance $\langle \delta g^2 \rangle$ of the dimensionless conductance g (the conductance G measured in units of the conductance quantum $e^2/h = e^2/2\pi$) over the ensemble of disorder realizations assumes a value of order unity, which depends only on the spatial dimensionality and on global symmetries (time-reversal and spin-rotation) of the Hamiltonian. In particular, the variance of the conductance does not depend on the system size (the conductance is not self-averaging as long as quantum coherence is preserved over the entire sample) and does not depend on the average value of the conductance. This effect is due to different microscopic impurity configurations of macroscopically identical samples. The interference pattern of electron trajectories, and therefore the conductance, depends on these microscopic details (see Fig. 1.3).

The variance of the conductance at zero temperature can be calculated using the standard impurity diagram technique [7, 36, 39, 41, 42]. To obtain the variance of the conductivity, two conductivity bubble diagrams should be connected in all possible ways with diffuson or Cooperon impurity ladders. In principle, diagrams with up to four ladders exist, however it has been shown [33, 39] that diagrams with three and four ladders cancel in the leading order in $1/k_F l$, so that only the three two-diffuson diagrams shown in Fig. 1.4 and the corresponding Cooperon diagrams need to be taken into account.

To calculate the conductance from the conductivity (which is in general a long-ranged tensor), the conductivity should be convolved with the so-called “flow function” [39]

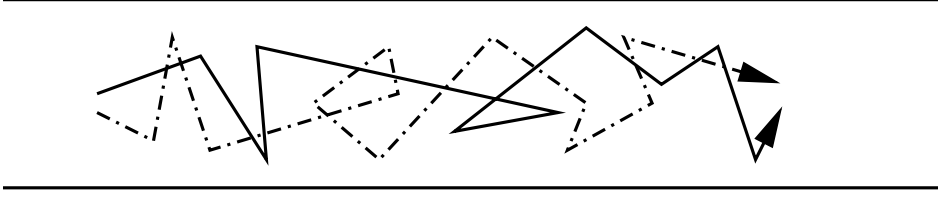


Figure 1.3: Trajectories visiting different impurities interfere with a random sample-specific amplitude. This results in a variance of the conductance over the disorder ensemble which is of order e^2/h .

and integrated over the sample. The flow function depends on the sample geometry and in general has a nontrivial structure.² For a quasi-onedimensional wire it is just a constant equal to the inverse of the system size. The conductance fluctuations of a quasi-onedimensional wire can thus be evaluated as

$$\begin{aligned} \langle \delta g^2 \rangle = 8 \int_{\text{sample}} \mathbf{dr} \mathbf{dr}' & \left[2 |\mathcal{D}(\mathbf{r}, \mathbf{r}')|^2 + \text{Re } \mathcal{D}^2(\mathbf{r}, \mathbf{r}') \right. \\ & \left. + 2 |\mathcal{C}(\mathbf{r}, \mathbf{r}')|^2 + \text{Re } \mathcal{C}^2(\mathbf{r}, \mathbf{r}') \right] , \end{aligned} \quad (1.12)$$

where the (rescaled) diffuson $\mathcal{D}(\mathbf{r}, \mathbf{r}')$ satisfies

$$\left\{ -\nabla^2 - \frac{i\omega}{D} + \frac{1}{D\tau_\varphi} \right\} \mathcal{D}(\mathbf{r}, \mathbf{r}') = \delta(\mathbf{r}, \mathbf{r}') , \quad (1.13)$$

and the rescaled Cooperon $\mathcal{C}(\mathbf{r}, \mathbf{r}')$ is equal to the diffuson in the absence of a time-reversal breaking magnetic field. For zero temperature ($1/\tau_\varphi = 0$) and in the linear response ($\omega = 0$), Eq. (1.12) simplifies to

$$\langle \delta g^2 \rangle = 48 \int_{\text{sample}} \mathbf{dr} \mathbf{dr}' |\mathcal{D}(\mathbf{r}, \mathbf{r}')|^2 . \quad (1.14)$$

In particular, for a quasi-onedimensional wire the variance of the conductance can be calculated as

$$\begin{aligned} \langle \delta g^2 \rangle &= 48 \text{Tr } |\mathcal{D}|^2 \\ &= 48 \sum_{n>0} \frac{1}{(q_n^2 L^2)^2} , \quad q_n = n\pi/L \\ &= \frac{8}{15} . \end{aligned} \quad (1.15)$$

²A comparison with the Keldysh formalism (see Section 3.2.1) shows that the flow function $\phi(\mathbf{r}_0, \mathbf{r})$ of Ref. [39], where \mathbf{r}_0 is located at a reservoir, is related to the impurity-averaged diagonal Keldysh function $\langle G_\epsilon^K(\mathbf{r}) \rangle$ by $\phi(\mathbf{r}_0, \mathbf{r}) = -\frac{1}{4\pi i\nu} \int \frac{d\epsilon}{eV} \nabla \langle G_\epsilon^K(\mathbf{r}) \rangle$; this follows from Eqs. (3.35), (3.36), and the equation for the flow function given in Ref. [39].

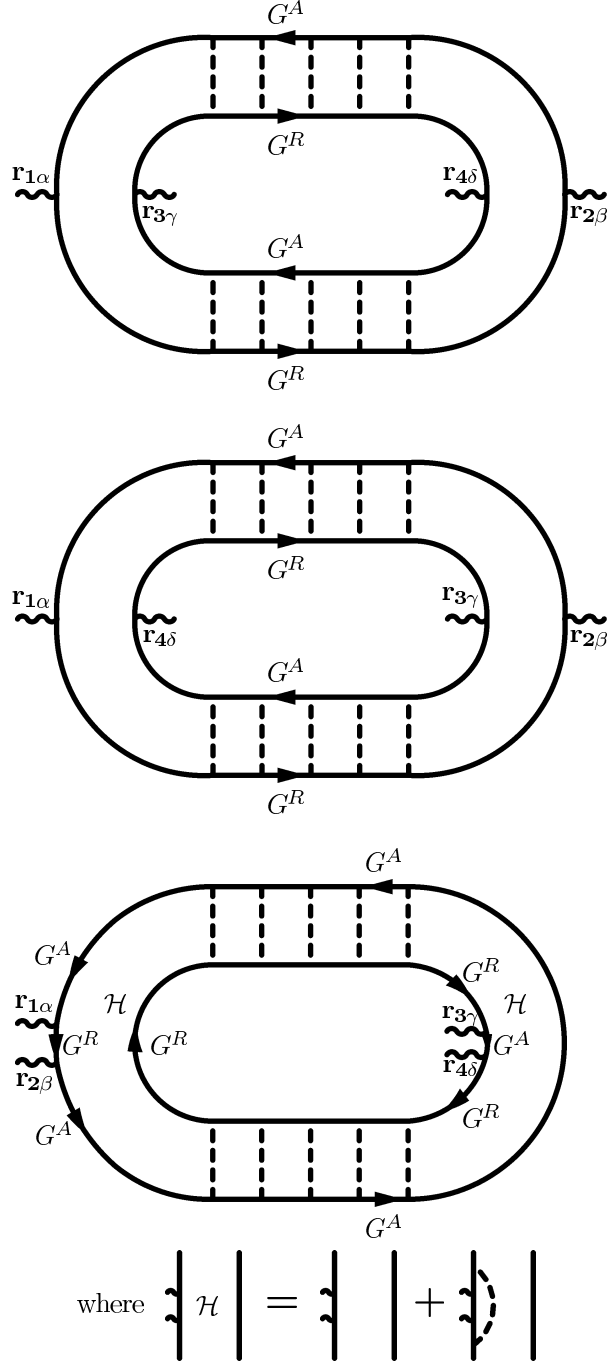


Figure 1.4: Diffuson diagrams contributing to the correlation of conductivity components $\langle \delta\sigma_{\alpha\beta}(\mathbf{r}_1, \mathbf{r}_2) \delta\sigma_{\gamma\delta}(\mathbf{r}_3, \mathbf{r}_4) \rangle$ resulting in Eq. (1.12). The wiggly lines denote external velocity vertices, G^R and G^A the retarded and advanced Green's functions, respectively, and the dashed lines the impurity potential correlator. The impurity ladders (diffusons) are given by Eq. (1.13).

This value is in equal parts due to diffuson and Cooperon contributions. The diffuson diagrams are shown in Fig. 1.4. For broken time-reversal symmetry, the Cooperon contribution is suppressed and Eqs. (1.15), (1.12) should be multiplied with $1/2$. In the case of strong spin-orbit coupling, spin-rotation symmetry is broken and the singlet and (three) triplet contributions to the diffuson and the Cooperon should be treated separately. The triplet propagators acquire a mass due to the spin-orbit coupling, so that only the singlet contributions survive over long distances. As a result, the variance of the conductance is suppressed by another factor of 4.

Experimentally, the ensemble average is replaced by an average over a range of magnetic fields. Changing the interference pattern by sweeping the magnetic field over a sufficiently wide range, the statistical properties extracted from the magnetofingerprint are equivalent to the properties of the ensemble average. The condition for this can be expressed as the condition that the range of magnetic fields swept through should be much larger than the correlation field (which is given by one flux quantum $\Phi_0 = h/e$ being added to a region of the length scale of the phase-breaking length L_φ), meaning that the scattering pattern should be completely rearranged many times for the equivalence to be valid. This is widely referred to as the ergodic hypothesis, for a careful discussion see Ref. [91].

At nonzero temperature, mesoscopic conductance fluctuations are suppressed by thermal averaging: Since each individual sample from the disorder ensemble is averaged over a range of energies available for conduction, the variance of the conductance over the disorder ensemble decreases because the phase distribution becomes thermally broadened on the lengthscale of the thermal length $L_T = (D/T)^{1/2}$. In addition to thermal smearing, the conductance fluctuations are suppressed by phase-breaking processes like scattering off magnetic impurities or inelastic electron-electron collisions. As a result, a characteristic length scale L_φ arises beyond which the phase of a conduction electron is randomized. The fluctuations of the conductance of a wire of length $L \gg L_\varphi$ can be understood as the result of L/L_φ fluctuating resistances which add up incoherently. The fluctuations thus partially average out.

For the wire geometry at finite temperature, the amplitude of mesoscopic conductance fluctuations depends on the thermal length L_T and the phase-breaking length L_φ given by (1.11) in the following way [27, 36],

$$\langle \delta g^2 \rangle \sim \left(\frac{L_T}{L} \right)^2 \frac{L_\varphi}{L} , \quad L_T \ll L_\varphi \ll L . \quad (1.16)$$

Recently, in Ref. [85] it has been demonstrated that the amplitude of mesoscopic conductance fluctuations and the weak localization correction are suppressed by dephasing effects originating from inelastic electron-electron collisions *in precisely the same way*, allowing to establish a formal relation between the two quantities without specifying their values. This can serve as a tool to examine the nature of dephasing effects. In Section 2.3 this relation is re-examined and derived in a more fundamental way, allowing for

a straightforward generalization to a similar relation between h/e and $h/2e$ Aharonov-Bohm oscillations (see Section 1.1.3 for an introduction). In Section 4.3 this relation is further generalized to the case of interaction through a transverse gauge field.

As the voltage difference of the reservoirs the sample is connected to is increased beyond the linear-response regime, the amplitude of mesoscopic conductance fluctuations becomes a nontrivial function of the voltage [34, 60, 78, 79, 86, 87]. This is examined in Chapter 3.

1.1.3 Aharonov-Bohm oscillations of conductance

In a multiply-connected geometry (a ring), electrons acquire topological phase factors (Aharonov-Bohm phases) when encircling the ring enclosing a vector potential [5]. As a result, quantum interference of paths encircling the ring in different directions becomes a function of the flux of vector potential enclosed by the ring (for reviews, see Refs. [38, 48, 64]). Two types of Aharonov-Bohm effects in metallic rings have to be distinguished: the weak-localization Aharonov-Bohm effect ($h/2e$ effect) and the mesoscopic Aharonov-Bohm effect (h/e effect).

The $h/2e$ effect is closely related to weak localization: It is the result of Cooperon paths encircling the ring. While in the bulk material the weak localization effect is destroyed by an applied magnetic field due to paths enclosing different areas and acquiring different phases, in a narrow ring all Cooperons with winding number one acquire the same phase. Therefore the weak localization effect is recovered if an integer number of magnetic flux quanta is threading the ring, and the conductance of the ring becomes a periodic function of the flux, with the fundamental period of $h/2e$ due to the Cooperon coupling to the magnetic field with the charge $2e$. Higher harmonics of this effect exist due to Cooperons with winding numbers greater than one. The $h/2e$ effect, like weak localization in bulk, is insensitive to ensemble averaging because it is symmetric in the flux, rather than featuring a sample-specific phase. Similar to the bulk weak localization effect, the $h/2e$ Aharonov-Bohm effect is suppressed when a magnetic flux of the order of the flux quantum Φ_0 threads the *wires* forming the sample, as opposed to the area *enclosed* by the ring. At this scale of magnetic field, which for narrow rings is a much larger scale than the one related to the oscillations, the phase differences between different Cooperon paths of winding number one become appreciable, resulting in cancellation of interference amplitudes similar to the suppression of the bulk weak-localization effect. Since the $h/2e$ effect survives ensemble averaging, oscillations with the fundamental period of $h/2e$ also occur in hollow metal cylinders threaded by an axial magnetic field [17], the cylinder representing an average over rings of small thickness, and in networks of rings [95, 104].

The h/e effect, on the other hand, arises in a similar fashion as mesoscopic conductance fluctuations in a singly-connected geometry: Due to sample-specific microscopic impurity configurations, the interference of trajectories with a relative winding number one acquires a sample-specific phase, which varies periodically as a function of the

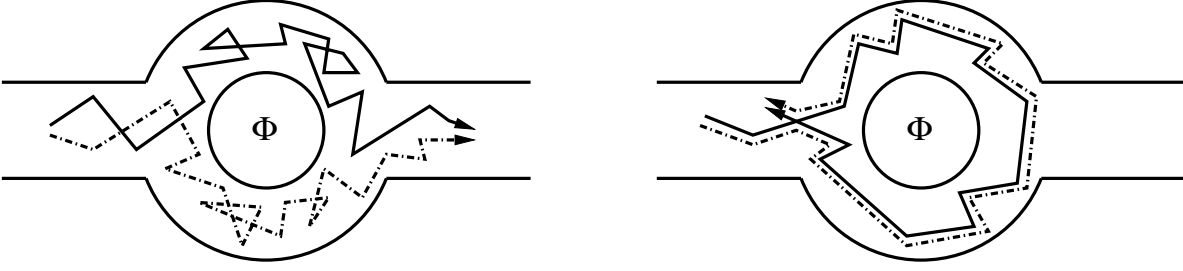


Figure 1.5: Left: the analog of Fig. 1.3 in the ring geometry. Paths encircling the ring in opposite directions give rise to conductance oscillations as a function of the magnetic flux Φ with a fundamental period of h/e with a sample-specific amplitude and phase. Taken over a large range of magnetic fields, these oscillations are ensemble-averaged. Right: A trajectory encircling the ring interferes constructively with the one visiting the same impurities in reversed order, similar to the interference shown in the right part of Fig. 1.1. As a result, at zero flux the probability of the particle to diffuse through the ring is diminished, reducing the conductance. When the ring is threaded by a magnetic flux Φ , the interference is modulated with a fundamental period of $h/2e$ due to the two trajectories accumulating opposite phase factors.

magnetic flux enclosed by the sample, with a fundamental period of h/e . On ensemble averaging this phase averages to zero. However, the harmonics of the variance of the conductance over the ensemble take characteristic values which depends on some details of the geometry [89, 94]. On the field scale of a flux quantum threading the *metal*, the sample-specific phase gets randomized relative to its value at zero field due to the magnetic field altering the interference pattern *within* the sample, as opposed to the topological Aharonov-Bohm phase acquired upon encircling the ring.

The h/e oscillations, including higher harmonics due to paths with relative winding numbers greater than one, can be written as

$$\delta g(\Phi) = \delta g_0 + 2 \sum_{n=1}^{\infty} \delta g_n \cos \left(\frac{2\pi n \Phi}{\Phi_0} + \theta_n \right) , \quad (1.17)$$

with the sample-specific amplitudes δg_n and phases θ_n , the flux enclosed by the ring Φ and the flux quantum $\Phi_0 = h/e$. Eq. (1.17) is valid over a not too large range of magnetic fields where θ_n can be regarded as constant, i.e. over a range corresponding to the flux through the wires changing by less than a flux quantum.³ The amplitudes δg_n

³The condition that the phases θ_n remain constant over a large enough range of magnetic field is that the area enclosed by the ring is much larger than the area of the metal itself, leading to well-separated scales of h/e oscillations and aperiodic fluctuations [24, 25]. For theoretical work on rings with finite linewidth see Ref. [50].

are determined by the diffuson diagrams for conductance fluctuations, while the phases θ_n are determined by the corresponding Cooperon diagrams [89, 94]. It should be emphasized that the Cooperon diagrams determine the phases *only*, not the amplitudes. It has been directly observed [30] that the mesoscopic oscillations have random phases associated, while the weak-localization oscillations do not.

When taking a magnetofingerprint of an Aharonov-Bohm sample over a large range of magnetic fields, at the same time an ensemble average over the disorder is performed (ergodic hypothesis). The peaks seen in a Fourier transformation of the magnetofingerprint therefore are the ensemble-averaged amplitudes $\langle \delta g_n^2 \rangle$. These can be evaluated by calculating Eq. (1.12) in the ring geometry with appropriate boundary conditions and extracting the Fourier components. This has been performed in Refs. [89, 94] for the zero-temperature situation (without any dephasing) with the result

$$\langle \delta g_n^2 \rangle = \frac{1}{30} (\gamma^{1/2} - 1)^{2n} (\gamma^{1/2} + 1)^{-2n} \gamma^{1/2} (\gamma + 1) [9 - 10\gamma + 9\gamma^2 + 20n\gamma^{1/2}(\gamma + 1)] , \quad (1.18)$$

where γ is a coefficient related to the geometry⁴ of the ring and the leads, $\gamma = (\text{resistance of ring})/(\text{resistance of total sample}) = R_1/(R_1 + R_2)$ with the resistances R_1 and R_2 defined as shown in Fig. 1.6. By definition, $0 \leq \gamma \leq 1$. The coefficient

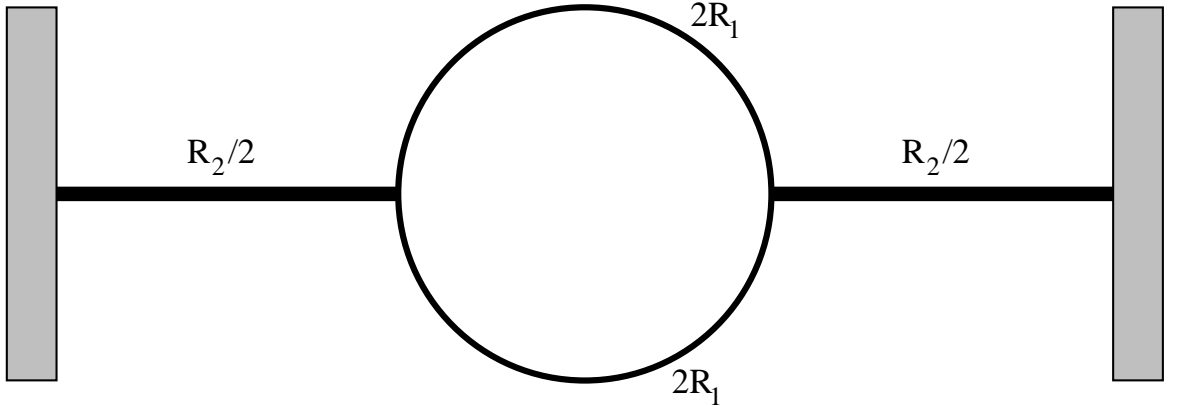


Figure 1.6: Two-terminal Aharonov-Bohm sample geometry which in the noninteracting limit shows the mesoscopic conductance oscillations (1.18). The geometrical coefficient γ is defined as $\gamma = R_1/(R_1 + R_2)$.

of Eq. (1.18) should be multiplied with an extra factor $1/4$ in the presence of strong spin-orbit interaction. The first four harmonics as given by Eq. (1.18) are plotted in Fig. 1.7. Clearly, even without dephasing the fundamental ($n = 1$) harmonic is much

⁴Eq. (1.18) is strictly valid only for a two-terminal configuration. In a four-terminal setup extra contributions appear [39, 41, 42], since the Onsager symmetries [1] allow for an antisymmetric part of the response to the magnetic flux.

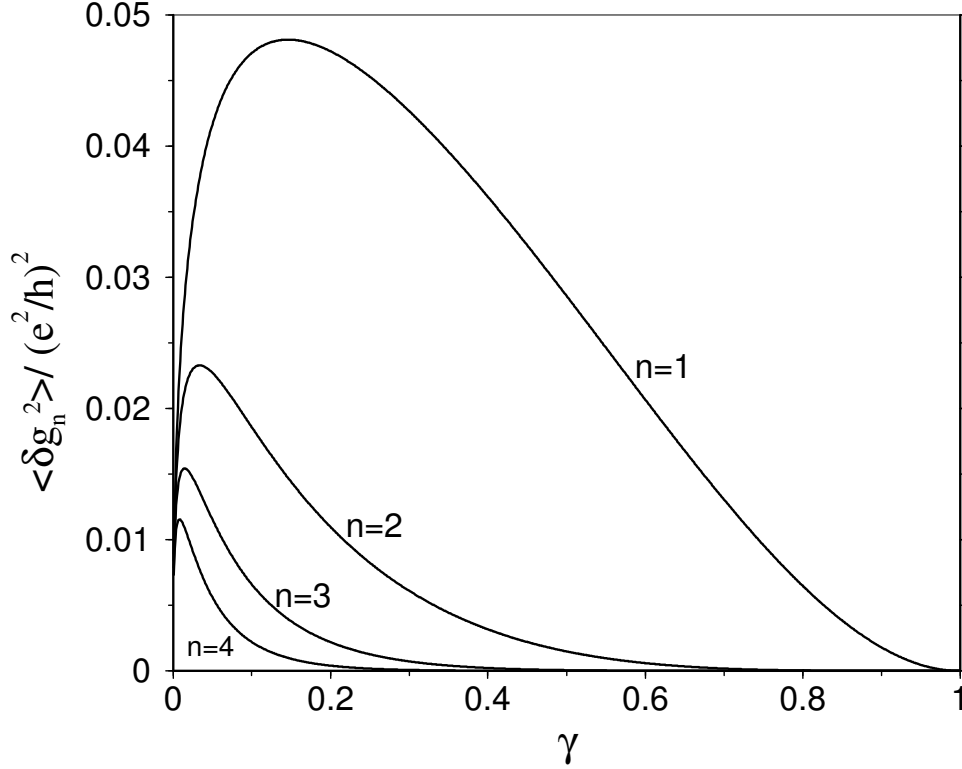


Figure 1.7: The ensemble-averaged amplitudes $\langle \delta g_n^2 \rangle$ of the first four harmonics of mesoscopic Aharonov-Bohm oscillations. The coefficient is calculated for systems without spin-orbit interaction. For systems with strong spin-orbit interaction, the $\langle \delta g_n^2 \rangle$ are reduced by an extra factor of $1/4$.

larger than the higher ones. This is due to the probability of escaping to the reservoirs if the lead lengths are finite, $\gamma > 0$. With dephasing, the higher harmonics are even more suppressed compared to the fundamental one, and for $n > 2$ are hardly ever observed in disordered metallic samples.⁵ In the limit of short leads ($\gamma \rightarrow 1$), Eq. (1.18) agrees with the results of Ref. [49] (where the leads were modelled by introducing an escape probability at two opposite points of the ring) in the absence of spin-flip scattering.

Superimposed onto the mesoscopic oscillations are also the aperiodic mesoscopic fluctuations of the wires forming the ring. Early experiments [21], which used rather small rings, could not resolve the h/e oscillations from the aperiodic background since the field scales for a flux quantum threading the ring and for a flux quantum penetrating

⁵It should be noted that in a ballistic high-mobility semiconductor heterostructure, harmonics up to $n = 6$ have been observed [81]. Eq. (1.18) does not apply to ballistic systems. Also, in Ref. [98] measurements on a network of metallic rings are reported which display h/e oscillations with observable harmonic content, however these systems do not compare directly to single rings [76].

the wire coincided. In larger rings composed of narrow wires [25], the aperiodic fluctuations happen on much larger field scales than the h/e oscillations, making the h/e oscillations well observable.

Experimentally [25, 28, 40, 30, 37, 78, 79, 82, 88, 95], h/e Aharonov-Bohm oscillations of conductance have the advantage that they are not sensitive to breaking of time-reversal symmetry by a strong magnetic field penetrating the wires, and can therefore be used to analyse quantum-coherent transport in situations not accessible to weak-localization measurements. A beautiful example is the demonstration that even concentrations of magnetic impurities as low as 1 ppm can have a considerable impact on quantum coherence [88]. When those impurities are aligned by a strong magnetic field, spin-flip scattering is suppressed, greatly enhancing coherence. The sample and a magnetofingerprint from Ref. [88] are shown in Fig. 1.8. For a theoretical treatment of the effect of magnetic impurities see Ref. [100]. When the magnetic impurities are aligned by the magnetic field, inelastic electron-electron collisions are the dominating source of phase-breaking processes. While this regime is accessible via measurements of h/e oscillations, the weak-localization correction is suppressed already by the time-reversal breaking due to the magnetic field, prohibiting measurements of the dephasing of the weak-localization correction. The experiment reported in Ref. [88] has been performed at very low temperatures. As a result, the amplitudes of Aharonov-Bohm oscillations at high magnetic fields approach the maximum values (Eq. (1.18), multiplied by 1/4 to account for strong spin-orbit interaction) expected from perfectly coherent samples [89, 94]. Chapter 2 of this thesis considers the opposite limit, when dephasing due to Coulomb interaction between conduction electrons is strong. It is found that the dephasing of Aharonov-Bohm oscillations differs from the dephasing of weak localization and mesoscopic fluctuations in singly-connected geometries in a remarkable way.

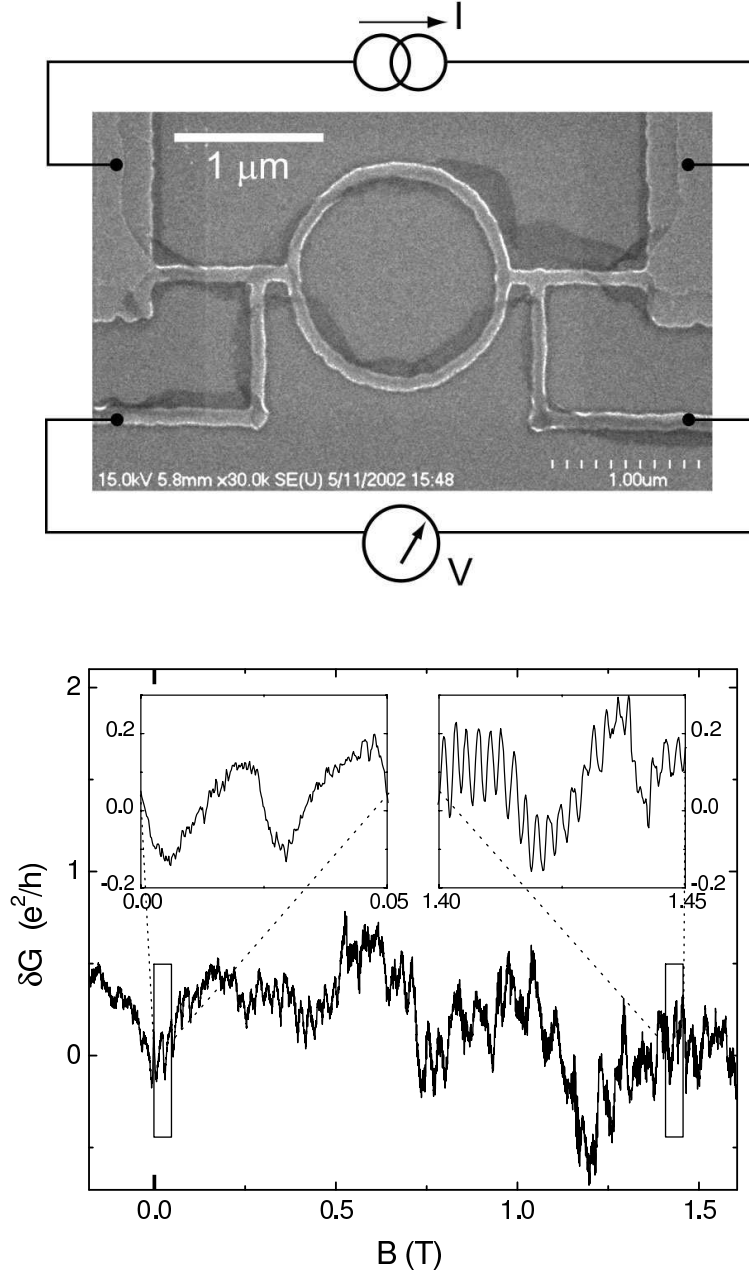


Figure 1.8: Image of an Aharonov-Bohm ring and a magnetofingerprint of this sample, both taken with kind permission from Pierre and Birge [88]. The raw data clearly show Aharonov-Bohm oscillations of the conductance (right inset), superimposed by aperiodic mesoscopic fluctuations on larger field scales. It is also immediately visible from the raw data that at high magnetic fields (right inset) the Aharonov-Bohm oscillations are much stronger than at low magnetic fields (left inset).

2 Effect of Coulomb interaction on Aharonov-Bohm oscillations

2.1 Dephasing on a phenomenological level

The following formula has been given in Refs. [17, 38] for the weak localization correction ($h/2e$ amplitude) to the conductance of a ring,

$$\Delta G = -\frac{e^2}{h} L_\varphi \frac{\sinh \frac{2\pi R}{L_\varphi}}{\cosh \frac{2\pi R}{L_\varphi} - \cos \frac{4\pi \Phi}{\Phi_0}} , \quad (2.1)$$

where G is the conductance per unit length, R is the ring circumference, Φ is the magnetic flux threading the ring, and $\Phi_0 = h/e$ is the magnetic flux quantum. The dephasing length L_φ is here a phenomenological parameter without a microscopic derivation, introduced via a mass of the Cooperon given by the (constant) dephasing rate $1/\tau_\varphi$,

$$\left\{ -D\nabla^2 - i\omega + \frac{1}{\tau_\varphi} \right\} \mathcal{C}_\omega(\mathbf{r}, \mathbf{r}') = \delta(\mathbf{r} - \mathbf{r}') \quad (2.2)$$

and using $L_\varphi = (D\tau_\varphi)^{1/2}$. For dephasing by electron-electron interaction, usually the dephasing length (1.11) is inserted into Eq. (2.1), however no microscopic derivation exists which would justify this. However, due to lack of a better theory, Eq. (2.1) together with (1.11) has been widely used to describe experimental data [37, 88].

In this chapter it is shown that in fact a more sophisticated treatment of inelastic collisions is necessary. Following the ideas of Refs. [18, 29, 85], a microscopic theory of inelastic collisions with small energy transfers in the Aharonov-Bohm geometry is developed. This is performed for mesoscopic (h/e) oscillations first. Later it is shown in Section 2.3 that the result can be directly transferred to weak-localization ($h/2e$) oscillations too. It is shown that the amplitude of $h/2e$ oscillations in the strong-dephasing regime can be written in a form similar to Eq. (2.1), but with a dephasing length that is parametrically different from Eq. (1.11).

2.2 Dephasing of h/e Aharonov-Bohm oscillations by Coulomb interaction

2.2.1 Screened Coulomb interaction in real space

In low dimensions ($d = 1, 2$), phase relaxation is dominated by electron-electron collisions with small ($\omega \ll T$) energy transfers [18, 29]. Therefore, the effective electron-electron interaction can be conveniently represented [18, 29, 72, 85] by a time-dependent random *classical* potential $\varphi(\mathbf{r}, t)$, with the correlator $\langle \varphi(\mathbf{r}, t) \varphi(\mathbf{r}', t') \rangle$ given by the fluctuation-dissipation theorem [6]:

$$\langle \varphi^\alpha(\mathbf{r}, t) \varphi^\beta(\mathbf{r}', t') \rangle_\omega = -\text{Im } U(\mathbf{r}, \mathbf{r}'; \omega) \delta_{\alpha\beta} \delta(t - t') \coth \frac{\omega}{2T} , \quad (2.3)$$

where the indices α, β denote different measurements taken. The dynamically screened Coulomb interaction U is given in the random-phase approximation [2, 29] (RPA, see Fig. 2.1) by

$$\begin{aligned} \text{wavy line } U &= \text{wavy line } U_0 + \text{wavy line } U_0 \text{ --- } \text{bubble } -\Pi \text{ --- } \text{wavy line } U_0 + \text{wavy line } U_0 \text{ --- } \text{bubble } -\Pi \text{ --- } \text{wavy line } U_0 \text{ --- } \text{bubble } -\Pi \text{ --- } \text{wavy line } U_0 + \dots \\ &= \text{wavy line } U_0 \text{ --- } \text{bubble } -\Pi \text{ --- } \text{wavy line } U \end{aligned}$$

Figure 2.1: Random-phase approximation for the screened Coulomb interaction. Summing up the series results in Eq. (2.4).

$$U(q, \omega) = \frac{1}{U_0^{-1}(q) + \Pi(q, \omega)} \simeq \Pi^{-1}(q, \omega) , \quad (2.4)$$

where $U_0(q)$ is the bare Coulomb interaction,

$$\Pi(q, \omega) = \frac{\nu D q^2}{D q^2 - i\omega} \quad (2.5)$$

is the polarization operator due to diffusive motion of the conduction electrons and coincides with the density-density correlation function [29], and ν is the density of states at the Fermi energy. In a diffusive system, the screening length (which is of the order of the Fermi wavelength) is much smaller than typical diffusive length scales (for an Aharonov-Bohm ring set by the ring diameter). This allows one to neglect the bare Coulomb interaction compared to the polarization, resulting in the last approximate equality in Eq. (2.4). The interaction is thus entirely dominated by the diffusive dynamics of the conduction electrons.

Since small momentum transfers (of the order of the inverse system size, as will be seen later) are the important ones, the nontrivial geometry of the Aharonov-Bohm ring is best treated in a real-space calculation. To generalize Eqs. (2.3), (2.4) to real space, consider first the eigenfunctions Ψ_i of the Laplace operator, $\Delta\Psi_i = \epsilon_i\Psi_i$. These eigenfunctions satisfy the completeness relation $\sum_i |\Psi_i\rangle\langle\Psi_i| = 1$. Therefore the polarization is given by

$$\begin{aligned}\Pi &= \nu \sum_i \frac{|\Psi_i\rangle\langle\Psi_i|}{\epsilon_i - i\omega} \\ &= \nu \left[\mathbb{I} + i\omega \sum_i \frac{|\Psi_i\rangle\langle\Psi_i|}{\epsilon_i - i\omega} \right] \\ &= \nu \sum_i |\Psi_i\rangle\langle\Psi_i| \frac{\epsilon_i}{\epsilon_i - i\omega},\end{aligned}\tag{2.6}$$

which in momentum space is just Eq. (2.5). In real-space notation the inverse Π^{-1} is equal to

$$\begin{aligned}\Pi^{-1} &= \frac{1}{\nu} \sum_i |\Psi_i\rangle\langle\Psi_i| \frac{\epsilon_i - i\omega}{\epsilon_i}, \\ \text{Im } \Pi^{-1}(\mathbf{r}, \mathbf{r}') &= -\frac{\omega}{\nu} \sum_i \frac{\Psi_i(\mathbf{r})\Psi_i(\mathbf{r}')}{\epsilon_i} \\ &= -\frac{\omega}{D\nu} \mathcal{D}(\mathbf{r}, \mathbf{r}')\end{aligned}\tag{2.7}$$

(note that the Ψ_i are real), where \mathcal{D} is the solution of the Laplace equation, $-\Delta\mathcal{D}(\mathbf{r}, \mathbf{r}') = \delta(\mathbf{r} - \mathbf{r}')$, with zero boundary conditions at the contacts with the bulk electrodes. As a result, the generalization of Eq. (2.4) to real space reads, as might be naively expected,

$$\text{Im } U(\mathbf{r}, \mathbf{r}'; \omega) \simeq \text{Im } \Pi^{-1}(\mathbf{r}, \mathbf{r}'; \omega) = -\frac{\omega}{\nu D} \mathcal{D}(\mathbf{r}, \mathbf{r}') ,\tag{2.8}$$

For relevant frequencies $\omega \ll T$, the approximation $\coth \frac{\omega}{2T} \simeq \frac{2T}{\omega}$ may be used, and the correlator of the random potential is therefore

$$\langle \varphi^\alpha(\mathbf{r}, t) \varphi^\beta(\mathbf{r}', t') \rangle = \frac{2T}{\nu D} \mathcal{D}(\mathbf{r}, \mathbf{r}') \delta_{\alpha\beta} \delta(t - t') ,\tag{2.9}$$

requiring in particular knowledge of the Laplace propagator $\mathcal{D}(\mathbf{r}, \mathbf{r}')$ in the ring geometry with the appropriate boundary conditions.

2.2.2 Effect of Coulomb interaction on Aharonov-Bohm interference

In the presence of a fluctuating potential $\varphi(x, t)$ the diffuson propagator \mathcal{D} satisfies in each quasi-one-dimensional wire the equation

$$\left\{ \frac{\partial}{\partial t} - D \frac{\partial}{\partial x^2} + i [\varphi^\alpha(x, t) - \varphi^\beta(x, t)] \right\} \mathcal{D}_{\delta\Phi}^{\alpha\beta}(x, t; x', t') = \delta(x - x') \delta(t - t') , \quad (2.10)$$

supplemented by appropriate matching conditions at the junctions of the ring and leads. Here $\delta\Phi = \Phi_1 - \Phi_2$ is the difference in the magnetic flux between the two measurements, which is incorporated in the matching conditions via a phase factor $\exp\{2\pi i \Phi / \Phi_0\}$ which is acquired upon encircling the ring.

When inelastic processes are taken into account, a difference arises between “true” diffusons and the impurity ladders in Fig. 2.2, which have been named “CF diffusons” in Ref. [85]. In the diagrams describing mesoscopic conductance fluctuations, the impurity ladders connect Green’s functions corresponding to *two different measurements*. While the impurity configuration of a specific sample remains the same for both measurements, the configurations of the fluctuating electric potential for the two measurements are uncorrelated. Therefore, interaction lines may not connect Green’s functions corresponding to different measurements [85]. As a result, the CF diffuson is sensitive to electron-electron interaction, unlike the “true” diffuson, for which particle number conservation ensures that self-energy and vertex corrections exactly cancel. At high temperatures $T \gg E_c$, where $E_c = D/L^2$ is the Thouless energy and L is the system size, the variance of the conductance can be written [85] as¹

$$\langle \delta G(\Phi_1) \delta G(\Phi_2) \rangle = \frac{4e^4 D^2}{3\pi T L^4} \int_{\text{sample}} d\mathbf{r}_1 d\mathbf{r}_2 \int dt dt' \tilde{\delta}(t - t') \left\langle \mathcal{D}_{\delta\Phi}^{12}(\mathbf{r}_1, \mathbf{r}_2, t) \mathcal{D}_{\delta\Phi}^{21}(\mathbf{r}_2, \mathbf{r}_1, t') \right\rangle , \quad (2.11)$$

where the angular brackets denote averaging over the fluctuating fields φ . The function $\tilde{\delta}(t - t')$ arises from thermal smearing of the distribution functions and is explicitly given by

$$\begin{aligned} \tilde{\delta}(t - t') &= 12\pi T \int \frac{d\epsilon_1}{2\pi} \frac{d\epsilon_2}{2\pi} f'(\epsilon_1) f'(\epsilon_2) \exp\left\{ i(\epsilon_1 - \epsilon_2)(t - t') \right\} \\ &= 3\pi T^3 (t - t')^2 \sinh^{-2} [\pi T(t - t')] . \end{aligned} \quad (2.12)$$

The function $\tilde{\delta}(t - t')$ is peaked around $t - t' = 0$ and has a width of $1/T$. In the following it will be replaced by the true delta function $\delta(t - t')$, neglecting dephasing during the

¹The Cooperon contribution to the correlation function is discarded, since it does not influence the variance $\langle g_n^2 \rangle$ of harmonics of the AB oscillations but only the statistics of the oscillation phase, see Refs. [89, 94].

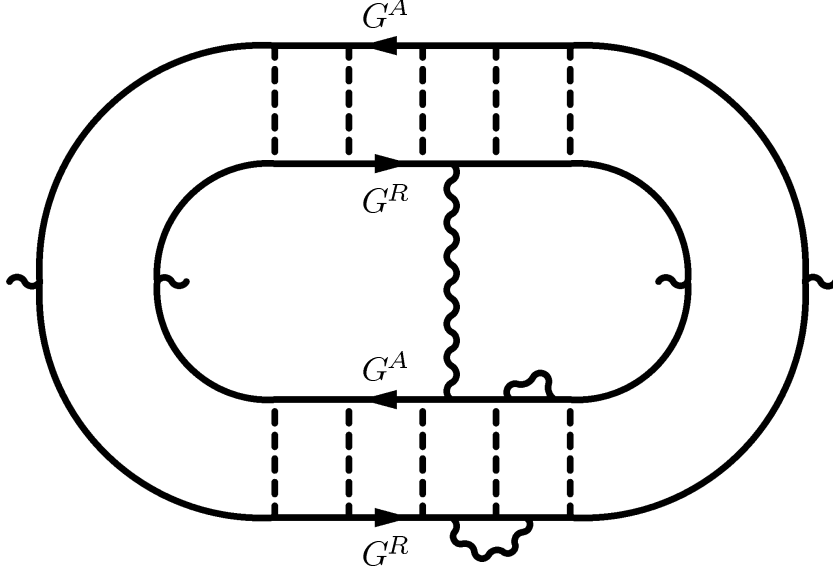


Figure 2.2: Diagrammatic representation of Eq. (2.11). The wiggly lines represent the RPA-screened Coulomb interaction. Since two separate measurements are involved, interaction lines only connect Green's functions corresponding to the same measurement.

time difference $t - t' \sim 1/T$. To justify this, consider two paths with durations t and t' , respectively. During the time difference $t - t'$ there will be a strong effect of bare fluctuations $\sim \exp\{-\langle[\varphi^\alpha(\mathbf{r}_1)]^2\rangle/T\}$ (as opposed to the cancellation in Eq. (2.15)). The resulting suppression factor (which should be negligible for the two paths of slightly unequal durations to contribute) can be estimated² as

$$\exp\left\{-\frac{\langle[\varphi^\alpha(\theta_1)]^2\rangle}{T}\right\} \sim \exp\left\{-\frac{2TL}{\nu DT}\right\} \sim \exp\left\{-\frac{L}{\xi}\right\}, \quad (2.13)$$

where ξ is the localization length of the system. When the conductance of the system is large compared to the conductance quantum $e^2/h \simeq (25\text{ k}\Omega)^{-1}$ (the sample is well into the metallic state), the localization length is much larger than the system size and the suppression factor (2.13) can be replaced by 1. This condition is well satisfied in typical experiments, therefore allowing to replace $\tilde{\delta}(t - t') \rightarrow \delta(t - t')$. The diagram corresponding to Eq. (2.11) is shown in Fig. 2.2. However, the diagrammatic technique suffers from divergences due to the infrared behaviour of the screened Coulomb interaction and is not convenient to use in the present situation.

²This estimate gives an upper boundary on the dephasing during the time difference $t - t'$. Due to gauge invariance requirements, the dephasing is even weaker than this estimate. For example, fluctuations with zero wavenumber (a uniform change of the background potential, not leading to any electric field) should not result in extra dephasing.

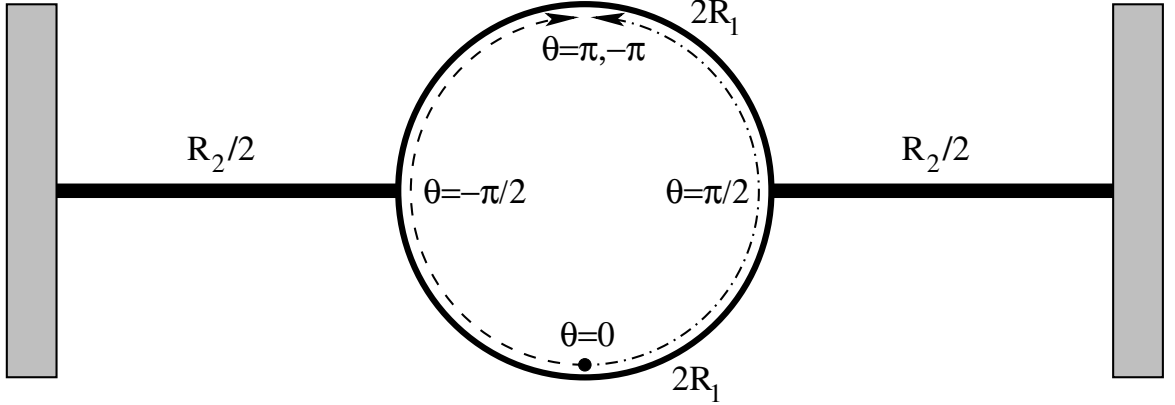


Figure 2.3: The sample geometry and the angular coordinate θ suitable to describe the motion along the ring. The paths representing the saddle-point solution derived in Section 2.2.3 are shown. The geometric parameter γ is defined as the ratio of the resistance of the ring without the leads to the resistance of the total sample, $\gamma = R_1/(R_1 + R_2)$.

A more suitable method is to express Eq. (2.11) with the help of path integrals. It is convenient to introduce an angular coordinate θ describing the location on the ring as shown in Fig. 2.3. The leads will not need detailed description since, as will be discussed below, in the regime of strong dephasing the important paths do not extend into the leads.

Expressing the CF diffuson propagator \mathcal{D}^{12} as a path integral,

$$\mathcal{D}^{12}(\theta_1, \theta_2) = \int_0^\infty dt \int_{\theta_2}^{\theta_1} \mathcal{D}[\theta(t)] \exp \left\{ - \int_0^t dt' \left[\frac{R^2 \dot{\theta}^2(t')}{4D} + i [\varphi_1[\theta(t'), t'] - \varphi_2[\theta(t'), t']] \right] \right\}, \quad (2.14)$$

the n th harmonic δg_n of the conductance variance $\langle \delta g(\Phi) \delta g(\Phi) \rangle$ with respect to the flux Φ is then given, up to a geometrical coefficient, by

$$\begin{aligned} \langle \delta g_n^2 \rangle \sim & \frac{D^2}{T R^4} \int_{-\pi}^{\pi} d\Theta_1 \int_{-\pi}^{\pi} d\Theta_2 \int_0^\infty dt \int_{\Theta_2}^{\Theta_1} \mathcal{D}[\theta_1(t)] \int_{\Theta_2}^{\Theta_1} \mathcal{D}[\theta_2(t)] \\ & \times \exp \left\{ - \int_0^t dt' \left[\frac{R^2 \dot{\theta}_1^2}{4D} + \frac{R^2 \dot{\theta}_2^2}{4D} + V(\theta_1, \theta_2) \right] \right\}, \end{aligned} \quad (2.15)$$

where the path integral goes over pairs of paths $\theta_1(t)$, $\theta_2(t)$ which have a relative winding

number n , and the “potential” $V(\theta_1, \theta_2)$ is given by

$$V(\theta_1, \theta_2) = \left\langle [\varphi^\alpha(\theta_1) - \varphi^\alpha(\theta_2)]^2 \right\rangle, \quad (2.16)$$

where the formula $\langle \exp\{i\varphi\} \rangle = \exp\{-\langle \varphi^2 \rangle / 2\}$ for Gaussian variables φ has been used. To explicitly calculate the “potential” $V(\theta_1, \theta_2)$, the solution $\mathcal{D}(\mathbf{r}, \mathbf{r}')$ of the Laplace equation in the ring is required, which is [89]

$$\mathcal{D}(\theta_1, \theta_2) = \frac{R}{8\pi\gamma} (1 - \gamma) [\pi^2 + 4\gamma \theta_1 (\pi - \theta_2)] \quad (2.17)$$

for $|\theta_1| \leq \pi/2$, $\pi/2 \leq \theta_2 \leq \pi$ (coordinates in different arms of the ring) and

$$\mathcal{D}(\theta_1, \theta_2) = \frac{R}{8\pi\gamma} [\pi^2 (1 + \gamma) - 4\gamma (1 + \gamma) \theta_1 \theta_2 + 4\pi\gamma |\theta_1 - \theta_2|] \quad (2.18)$$

for $-\pi/2 \leq \theta_i \leq \pi/2$ (both coordinates in the same arm of the ring). The geometrical coefficient γ is defined in the same way as in Section 1.1.3 and shown again in Fig. 2.3. The expression for the ranges of θ_i not stated follow from symmetry considerations. Using the correlator (2.9), the “potential” $V(\theta_1, \theta_2)$ is

$$V(\theta_1, \theta_2) = \frac{2TR}{\nu D} \left[\frac{\pi}{2} - \frac{1 + \gamma}{2\pi} \theta_1^2 - \frac{1 + \gamma}{2\pi} (\pi - \theta_2)^2 - \frac{1 - \gamma}{\pi} \theta_1 (\pi - \theta_2) \right] \quad (2.19)$$

for coordinates in different arms of the ring, $|\theta_1| \leq \pi/2$, $\pi/2 \leq \theta_2 \leq \pi$, and

$$V(\theta_1, \theta_2) = \frac{2TR}{\nu D} \left[|\theta_1 - \theta_2| - \frac{1 + \gamma}{2\pi} (\theta_1 - \theta_2)^2 \right], \quad (2.20)$$

for coordinates in the same arm of the ring, $|\theta_i| \leq \pi/2$.

The amplitude $\langle \delta g_n^2 \rangle$ is now mapped to the problem of a particle of mass $R^2/2D$ moving in the twodimensional potential $V(\theta_1, \theta_2)$ (or, equivalently, two particles with the coordinates θ_1 and θ_2 moving in one dimension and interacting via the potential $V(\theta_1, \theta_2)$). The solution of the full twodimensional problem is not attempted here, however is considerably simplified at high temperatures, when the potential $V(\theta_1, \theta_2)$ is high, $TR/\nu D \gg 1$, and dephasing is strong.

2.2.3 Analytic solution of the strong-dephasing case

Consider first the fundamental harmonic of the Aharonov-Bohm oscillations, which is due to pairs of paths half-encircling the ring in opposite directions. At high enough temperature, when the dephasing effect is strong, the path integral in Eq. (2.15) can be evaluated with the help of the saddle-point method.

The saddle-point (instanton) method [19] is valid in the regime of strong dephasing (when the tunnelling amplitude of the fictitious particle is strongly suppressed). In this

case, since the action [22] of every path is large, the path integral Eq. (2.15) is dominated by paths with actions close to the minimal action only. The leading exponential factor is then given by the action of the optimal path.

The optimal pair of paths can be identified in the following way: First, the paths do not extend into the leads since exploring part of a lead and returning into the ring to complete the path would only increase the action of that part. Moreover, the optimal configuration will be a pair of paths with a maximum amount of symmetry, with the common start- and endpoints located either at the junction of the ring with the leads, $\theta_1(t) - \pi/2 = -(\theta_2(t) - \pi/2) \equiv \tilde{\theta}$, or on the ring at the points with maximal distance from the leads, $\theta_1(t) = -\theta_2(t) \equiv \theta$. Within the saddle-point approximation (within exponential accuracy), the problem then reduces to the description of a quantum particle moving in a *onedimensional* potential.

The optimal path configuration can be easily found from Eqs. (2.19), (2.20): For the situation with the start- and endpoints located at the junctions of the ring with the leads, the leading contribution to the result is given by a one-dimensional Schrödinger-type equation,

$$\langle \delta g_n^2 \rangle \sim \frac{D^2}{TR^4} \int_0^\infty dt \int_0^\pi \mathcal{D}[\tilde{\theta}(t)] \exp \left\{ - \int_0^t dt' \left[\frac{R^2 \dot{\tilde{\theta}}^2}{2D} + \tilde{V}(\tilde{\theta}) \right] \right\}, \quad (2.21)$$

with the potential

$$\tilde{V}(\tilde{\theta}) = \frac{4TR}{\nu D} \times \begin{cases} \left[\begin{array}{cc} \tilde{\theta} & - \\ & \frac{1}{\pi} \tilde{\theta}^2 \end{array} \right], & 0 \leq \tilde{\theta} \leq \frac{\pi}{2} \\ \left[\begin{array}{cc} (\pi - \tilde{\theta}) & - \\ & \frac{1}{\pi} (\pi - \tilde{\theta})^2 \end{array} \right], & \frac{\pi}{2} \leq \tilde{\theta} \leq \pi \end{cases} \quad (2.22)$$

while for paths $\theta_1(t) = -\theta_2(t)$ the motion is described by

$$\langle \delta g_n^2 \rangle \sim \frac{D^2}{TR^4} \int_0^\infty dt \int_0^\pi \mathcal{D}[\theta(t)] \exp \left\{ - \int_0^t dt' \left[\frac{R^2 \dot{\theta}^2}{2D} + V(\theta) \right] \right\}, \quad (2.23)$$

and the potential (see Fig. 2.4)

$$V(\theta) = \frac{4TR}{\nu D} \times \begin{cases} \left[\begin{array}{cc} \theta & - \\ & \frac{\gamma+1}{\pi} \theta^2 \end{array} \right], & 0 \leq \theta \leq \frac{\pi}{2} \\ \left[\begin{array}{cc} (\pi - \theta) & - \\ & \frac{\gamma+1}{\pi} (\pi - \theta)^2 \end{array} \right], & \frac{\pi}{2} \leq \theta \leq \pi \end{cases}. \quad (2.24)$$

This potential is composed of two quadratic parts, and for finite lead length is always lower than the potential $\tilde{V}(\tilde{\theta})$, Eq. (2.22). As a result, the optimal paths are characterized by $\theta_1(t) = -\theta_2(t) \equiv \theta$, where θ is the coordinate of a quantum particle of mass R^2/D moving from $\theta = 0$ to $\theta = \pi$ in the potential (2.24).

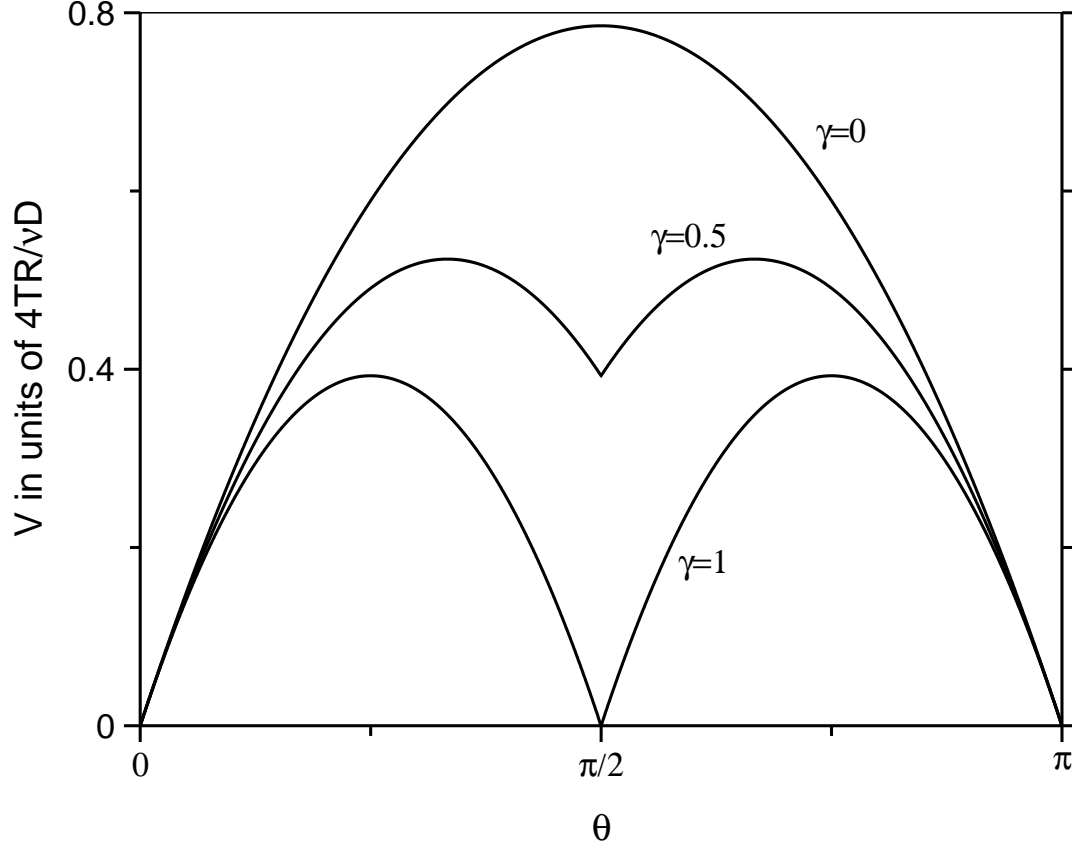


Figure 2.4: The potential $V(\theta)$ of the tunnelling problem, Eq. (2.24), plotted in units of $4TR/\nu D$ for different values of the geometrical coefficient γ . The leads attached to the perfect reservoirs result in a suppression of the field fluctuations in the vicinity of the junctions, resulting in the dip in the potential.

Performing a Wick rotation to the imaginary time domain,

$$t \equiv -i\tau \ , \quad (2.25)$$

the optimal path now is the solution of the classical equation of motion describing a particle with zero energy in the potential *minus* Eq. (2.24), the sign arising from the

rotation to imaginary time. The classical action S_{cl} is easily calculated from Eq. (2.24):

$$\begin{aligned}
 S_{\text{cl}} &= 2 \int_0^{\pi/2} d\theta p(\theta) , \quad \frac{p^2}{2m} = \frac{4TR}{D\nu} \left[\theta - \frac{\gamma+1}{\pi} \theta^2 \right] , \quad m = \frac{R^2}{D} \\
 &= 2 \sqrt{\frac{2R^2}{D}} \sqrt{\frac{4TR}{D\nu}} \int_0^{\pi/2} d\theta \sqrt{\theta - \frac{\gamma+1}{\pi} \theta^2} \\
 &= 2 \sqrt{\frac{2R^2}{D}} \sqrt{\frac{4TR}{D\nu}} \frac{\pi^{3/2} \left[2\gamma \sqrt{1-\gamma^2} + \pi + 2 \arcsin \gamma \right]}{16(\gamma+1)^{3/2}} \\
 &= C_\gamma \frac{T^{1/2} R^{3/2}}{\nu^{1/2} D}
 \end{aligned} \tag{2.26}$$

where it is convenient to introduce C_γ as a geometry-dependent coefficient of order unity,

$$C_\gamma = \left[\frac{\pi}{2(\gamma+1)} \right]^{3/2} \left[2\gamma (1-\gamma^2)^{1/2} + \pi + 2 \arcsin \gamma \right] , \tag{2.27}$$

which increases monotonically with increasing length of the leads (lowering γ). In the limits of long leads ($\gamma \rightarrow 0$) or short leads ($\gamma \rightarrow 1$), this expression takes the values

$$C_\gamma = \begin{cases} \frac{\pi^{5/2}}{2^{3/2}} , & \gamma \rightarrow 0 \\ \frac{\pi^{5/2}}{4} , & \gamma \rightarrow 1 \end{cases} \tag{2.28}$$

The result for the lowest harmonic of the h/e Aharonov-Bohm oscillations therefore is

$$\langle \delta g_1^2 \rangle \propto \exp\{-S\} \tag{2.29}$$

with the instanton action

$$S = C_\gamma \frac{T^{1/2} R^{3/2}}{\nu^{1/2} D} . \tag{2.30}$$

The dependence of the action on the type of the leads via the coefficient C_γ arises since short leads let the optimal paths come very close to the perfect reservoirs when the paths are separated the most, therefore diminishing the impact of the fluctuations on coherence. A somewhat related dependence of the dephasing rate on the lead configuration in a *ballistic* Aharonov-Bohm interferometer has been found in Ref. [92]. The influence of the leads is also visible in the shape of the instanton solution, Fig. 2.5. The classical motion in the potential (2.24) satisfies

$$\dot{\theta}^2 = \frac{8T}{\nu R} \left(\theta - \frac{\gamma+1}{\pi} \theta^2 \right) , \quad 0 \leq \theta \leq \pi/2 , \tag{2.31}$$

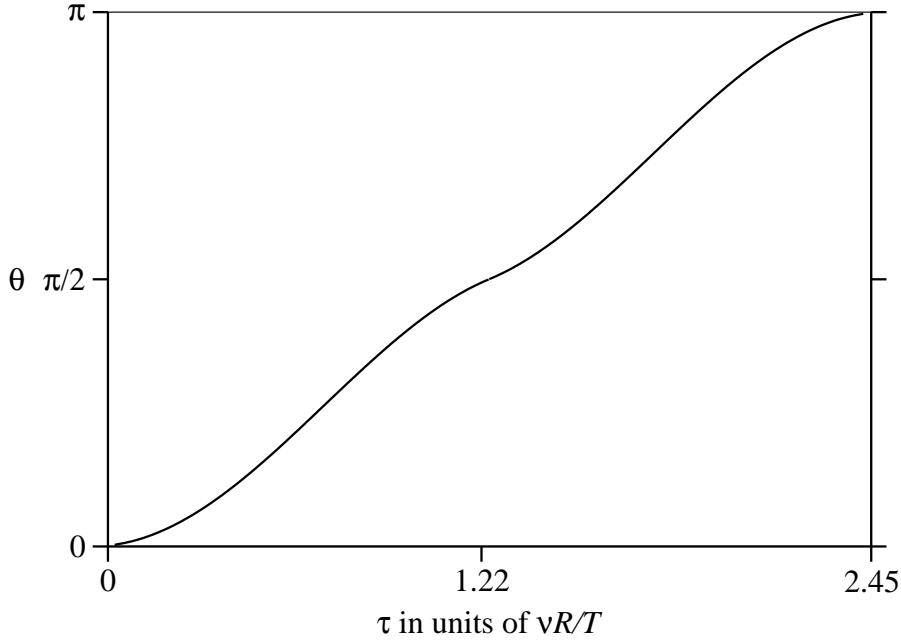


Figure 2.5: The shape of the instanton solution in the potential (2.24), Fig. 2.4, plotted for short leads ($\gamma = 0.9$). The effect of the proximity of the reservoirs on the solution is clearly visible from the instanton solution slowing down in the vicinity of the junction (located at $\theta = \pi/2$).

and is completed in the time (see Appendix A)

$$\tau_{\text{opt}} = \left(\frac{\nu R}{8T} \right)^{1/2} \frac{\pi^{1/2} (\pi - \arccos \gamma)}{(\gamma + 1)^{1/2}}, \quad (2.32)$$

The generalization to higher harmonics (with period h/ne) of the Aharonov-Bohm oscillations is straightforward: The optimal paths for odd n still begin at $\theta_{1,2} = 0$ and end at $\theta_{1,2} = \pi$ for odd harmonics, while the optimal paths for even n begin and end at $\theta_{1,2} = 0$ for even harmonics. They perform $n/2$ windings each to give a relative winding number of n . The corresponding instanton action is just the action of tunnelling through the potential landscape shown in Fig. 2.4 n times, yielding the action $S_n = nS$ (the instantons do not interact for strong dephasing).

To find the preexponential factor in (2.30) for the variance of the amplitude of the AB oscillations, it is necessary to perform several Gaussian integrations over small deviations from the instanton solution in the path integral (2.15). This is performed in Appendix A. The final result for the variance of the harmonics of the mesoscopic Aharonov-Bohm

oscillations reads, up to a numerical prefactor,

$$\langle \delta g_n^2 \rangle \sim \left(\frac{L_T}{R} \right)^{7/2} \left(\frac{\nu D}{R} \right)^{3/4} \exp\{-nS\} , \quad (2.33)$$

where $n = 1, 2, \dots$, and the action S is given by Eq. (2.30). Numerical prefactors, including powers of n , are not calculated explicitly here.

Very recently, Texier and Montambaux [102] presented results for both strong and weak dephasing, which also allow to include another dephasing mechanism (e.g. spin-flip scattering) in addition to electron-electron interaction. In the case of strong dephasing by electron-electron interaction and negligible other dephasing effects, the results of Ref. [102] reproduce the exponential behaviour of Eqs. (2.33), (2.30), Ref. [93].

2.2.4 Aharonov-Bohm dephasing time and dephasing length

Some physical insight can be obtained from the action (2.30) by defining the system-size dependent Aharonov-Bohm dephasing length

$$L_\varphi^{\text{AB}} = \frac{2\pi}{C_\gamma} \frac{\nu^{1/2} D}{T^{1/2} R^{1/2}} \quad (2.34)$$

which, by the absorption of a factor $R^{1/2}$, allows to rewrite the suppression factor in a simple exponential form,

$$\langle \delta g_n^2 \rangle \sim \left(\frac{L_T}{R} \right)^2 \left(\frac{L_\varphi^{\text{AB}}}{R} \right)^{3/2} \exp\left\{ -\frac{2\pi n R}{L_\varphi^{\text{AB}}} \right\} , \quad (2.35)$$

compatible with the phenomenological formula (2.1), although the definition of L_φ^{AB} , not being independent of R , may at first sight seem unusual.

The Aharonov-Bohm dephasing length (2.34) corresponds to an Aharonov-Bohm dephasing rate $1/\tau_\varphi^{\text{AB}} = D / (L_\varphi^{\text{AB}})^2$ which is given by

$$\frac{1}{\tau_\varphi^{\text{AB}}} = \left(\frac{C_\gamma}{2\pi} \right)^2 \frac{TR}{\nu D} , \quad (2.36)$$

which is parametrically different from the well-known result [29] for a quasi-one-dimensional wire. The difference arises from a different type of low-momentum cut-off: Calculating perturbatively the dephasing rate in a diffusive system with screened Coulomb interaction,

$$\frac{1}{\tau_\varphi} = \int \frac{dq}{2\pi} \frac{T}{\nu D q^2} . \quad (2.37)$$

For mesoscopic (universal) conductance fluctuations in a simple wire or in a twodimensional sheet [29, 72, 85], the infrared divergence is cut off self-consistently, since only

processes with energy transfers larger than the inverse dephasing time, $\omega \gtrsim \tau_\varphi^{-1}$, contribute. Therefore the lower cutoff in Eq. (2.37) is of the order of L_φ^{-1} , resulting in the well-known result (1.11). The situation is different in the case of Aharonov-Bohm oscillations because paths contributing to the lowest (or n th) harmonic must encircle the ring once (or n times), irrespective of how short the “conventional” dephasing length L_φ may be. Since shorter paths simply cannot contribute at all to the effect of interest, path with lengths of at least the circumference of the ring have to be kept. The phase coherence of those paths is affected by momentum transfers which are larger than the path length, therefore the low-momentum cutoff in Eq. (2.37) is set by the inverse system size when considering Aharonov-Bohm oscillations. This estimate results, up to the numerical coefficient, in the dephasing rate $1/\tau_\varphi^{\text{AB}} \sim TR/\nu D$, reproducing Eq. (2.36). So the fact that Aharonov-Bohm oscillations are due to coherent paths extending over a finite minimum distance (unlike universal conductance fluctuations or weak localization) is responsible for the difference between the conventional dephasing length (1.11) and the Aharonov-Bohm dephasing length (2.34), which is the one to be used in Eq. (2.1).

In a naive calculation, inserting τ_φ^{-1} as a (constant) mass into the denominator of the CF diffusion propagator, one could also expect from the relation $L_\varphi^2 = D\tau_\varphi$ a suppression factor of the form $\exp\{-S\} = \exp\{-(R/L_\varphi)^2\}$. However, typical paths contributing to Aharonov-Bohm-oscillations are not typical diffusive ones with a displacement growing as the square root of the elapsed time. Indeed, due to the fixed minimum path length of half the circumference of the ring, as the dephasing length gets much smaller than the circumference, $S \gg 1$, extraordinary straight and direct paths (as shown in Fig. 2.5) give the main contribution to the surviving Aharonov-Bohm signal: The instanton has the duration given by Eq. (2.32), much faster than a typical diffusive path. As dephasing becomes stronger (when increasing the temperature or the ring radius), the instanton solution changes its character, becoming even faster and thus leading to the suppression factor governed by (2.34).

The definition (2.34) of a system-size dependent dephasing length may seem counter-intuitive at first sight.³ The reason for this is that for the simple wire geometry it is difficult to distinguish between the length of the wire and the direction of propagation of the electron trajectories. In particular, due to the self-consistent cutoff in Eq. (2.37) for the wire geometry, a wire of length $L \gg L_\varphi$ can often be thought of as being composed of a number of similar but shorter wires which are simply concatenated. This is not possible for the ring which features a nontrivial geometry on the scale of the system size. The dependence of the dephasing length (2.34) on the ring circumference indicates that the content of fluctuations contained in the ring which are relevant for dephasing of Aharonov-Bohm oscillations depends on the system size.

³The reader who remains uncomfortable with this definition may choose to rewrite the action (2.30) as $\exp\{-S\} = \exp\{-(R/L_\varphi)^{3/2}\}$. Using this definition, it is seen that $L_\varphi = D^{2/3}\nu^{1/3}/C_\gamma^{2/3}T^{1/3}$, which is parametrically just the result (1.11) for the quasi-onedimensional case.

2.2.5 Relation to experiments

Some experiments on ring samples similar to the geometry calculated here have been performed by groups in Saclay/Michigan [88, 90], in Basel [86, 87], and in Karlsruhe [78, 79]. A similar experiment on a network of rings has been set up in Paris [95]. Since the optimal paths do not extend into the leads, the differences between the two-terminal and the four-terminal geometry do not enter the exponential suppression factor, so a comparison to the four-terminal measurements of the Saclay/Michigan and Basel groups is justified in the strong-dephasing regime. However it should be noted that the no-dephasing limit (1.18) as well as the geometrical coefficient C_γ are calculated exactly only for the two-terminal setup, while the Saclay-Michigan experiment and the Basel experiment were performed in the four-terminal configuration.

The Saclay-Michigan experiment was done with the goal of demonstrating the effect of dilute magnetic impurities, and therefore performed on a high-purity copper ring of radius $R = 0.75 \mu\text{m}$ at temperatures down to $T = 40 \text{ mK}$. It is no surprise that at this temperature with the given sample data dephasing is weak and the instanton action (2.30) evaluates to⁴

$$S \approx 0.05 C_\gamma \approx 0.3 \text{ ,} \quad (2.38)$$

where $C_\gamma \approx 5.5 \dots 6$ has been estimated using Eq. (2.28) and the sample geometry shown in Ref. [88]. In other words, the sample of the Saclay-Michigan experiment has been taken to a high level of coherence when the magnetic impurities were frozen out, and the saddle-point calculations of Section 2.2.3 cannot be applied. On the contrary, a comparison with the zero-temperature calculations [89] shows that at $T = 40 \text{ mK}$ the observed Aharonov-Bohm amplitudes are close to the maximum ones (1.18) to be expected. The difference of the observed Aharonov-Bohm amplitudes at $T = 40 \text{ mK}$ and $T = 100 \text{ mK}$ is to a large extent due to thermal averaging rather than true dephasing, since the thermal length was $L_T \approx 1 \mu\text{m}$, of the same order as the ring radius. A detailed treatment of the weak-dephasing regime can be found in Ref. [102].

The Experiment of the Basel group was done in the context of the voltage-dependence of quantum interference effects (related to the calculations presented in Chapter 3), and therefore, due to the high applied voltages, performed at a higher temperature of $T = 0.3 \text{ K}$ on a gold ring with a radius of $R = 0.5 \mu\text{m}$. For this configuration the action (2.30) is estimated as

$$S \approx 0.08 C_\gamma \approx 0.45 \text{ .} \quad (2.39)$$

The thermal length of the Basel sample was $L_T \approx 0.5 \mu\text{m}$. The calculated results (2.33), (2.30) are well compatible with the measured Aharonov-Bohm amplitudes in the low-voltage limit, which were lower by a factor ~ 2.5 compared to the Saclay/Michigan experiment.

⁴In calculating the values given in this section, the threedimensional densities of states $\nu_3^{\text{Au}} = 1.14 \cdot 10^{47} \text{ J}^{-1} \text{ m}^{-3}$ and $\nu_3^{\text{Cu}} = 1.56 \cdot 10^{47} \text{ J}^{-1} \text{ m}^{-3}$ from Ref. [90] have been used.

The Karlsruhe group performed their measurements on several samples, where their Sample 3 was a copper sample in two-terminal configuration with very similar dimensions as the gold sample of the Basel group, but with a higher resistance and at a temperature of $T = 90$ mK. From the given parameters, a diffusion constant $D \approx 43$ cm²/s and a thermal length $L_T \approx 0.6$ μ m can be extracted, resulting in

$$S \approx 0.064 C_\gamma \approx 0.33 , \quad (2.40)$$

where $C_\gamma = 5.2$ has been calculated from the resistances given in Ref. [82]. The reported Aharonov-Bohm amplitudes, which are lower by a factor ~ 3 than those seen in the Basel experiment, and lower by a factor ~ 7 than those of the Saclay/Michigan experiment, do not agree with this, but correspond to much stronger dephasing. However, the authors themselves have extracted a dephasing length of $L_\varphi = 0.8$ μ m from the correlation field of universal conductance fluctuations. This indicates that another dephasing mechanism than electron-electron interaction probably dominates, possibly magnetic impurities included in the copper, as the authors of Refs. [88, 90] have shown.

The temperature-dependence of Aharonov-Bohm oscillations has been studied in a series of experiments in Paris [95]. It has first been reported that the temperature dependence of Eq. (2.34) has not been observed in a network of 10^6 semiconductor rings. Instead, comparing the first two harmonics of Aharonov-Bohm oscillations, a ratio $\sim \exp\{-T^{1/3}\}$ was measured instead of the ratio $\sim \exp\{-T^{1/2}\}$ which would follow from Eq. (2.30). These experiments were mostly performed at temperatures below the strong-dephasing regime $L_\varphi^{\text{AB}} \ll R$, for which Eq. (2.30) is written. More recent measurements [104] from the same samples have recently confirmed that the dephasing length for the lowest harmonic of Altshuler-Aronov-Spivak ($h/2e$) oscillations indeed crosses over from a $T^{-1/3}$ dependence to a $T^{-1/2}$ dependence as the temperature range where L_φ given by Eq. (1.11) is shorter than the periodicity of the network is entered. This temperature dependence is at variance with the dephasing length extracted from the magnetoresistance envelope (weak localization) and confirms the result (2.34).

2.3 Relation of h/e oscillations and $h/2e$ oscillations

It has been shown in Ref. [85] that the dephasing rate for mesoscopic conductance fluctuations is precisely the same as for weak localization. Moreover, in Ref. [85] the following relation was established for quasi-onedimensional⁵ geometry:

$$\langle \delta G(H_1) \delta G(H_2) \rangle = \frac{e^2 D}{3 T L^2} \left| \delta G_{\text{WL}} \left(\frac{H_1 - H_2}{2} \right) + \delta G_{\text{WL}} \left(\frac{H_1 + H_2}{2} \right) \right| , \quad (2.41)$$

assuming that the temperature is larger than the Thouless energy D/L^2 and spin-orbit interaction is absent. In the rest of this section, the second term of Eq. (2.41) will be

⁵In two dimensions the relation (2.41) becomes more complicated due to logarithmic dependencies on the short-scale physics; this is discussed at the end of this section.

discarded, corresponding to measuring mesoscopic conductance fluctuations in a high magnetic field where many flux quanta are threading the body of the sample.⁶ However, the presented derivation can be straightforwardly generalized to the case of weaker magnetic field, the result acquiring a form analogous to Eq. (2.41).

As demonstrated below in this section, Eq. (2.41) can be obtained from the path integral representations of both phenomena. It is shown within this framework that a relation analogous to Eq. (2.41) exists between the h/e (mesoscopic) Aharonov-Bohm oscillations and the $h/2e$ (weak-localization) Aharonov-Bohm oscillations. These arise from mesoscopic conductance fluctuations and weak localization, respectively, when the path integral is restricted to the ring geometry and only pairs of paths with relative winding number one or Cooperon paths with winding number one, respectively, are taken into account. For convenience of notation, the derivation of the connection between the two phenomena is carried out for the quasi-onedimensional Aharonov-Bohm situation, it can, however, be directly transferred to the twodimensional singly-connected geometry and therefore serve as an alternative proof of Eq. (38) of Ref. [85].

As has been discussed before, for mesoscopic Aharonov-Bohm oscillations only interaction lines within the same measurement are to be drawn. Furthermore, the correlator $\langle \varphi \varphi \rangle$ is local in time, so the interaction lines connect points on the two paths corresponding to the same time. This results in the structure shown in Fig. 2.6. For weak localization, the path interferes with its time-reversed version. Therefore the local-in-time interaction lines always connect a point on the positive-time part of the path with its corresponding image for negative time.

The path integral for the fundamental harmonic of the mesoscopic (h/e) Aharonov-Bohm oscillations can be written in the absence of spin-orbit interaction as (see Eqs. (2.11), (2.14))

$$\begin{aligned} \langle \delta G_{h/e}^2 \rangle = & \frac{4e^4 D^2}{3\pi T (2\pi R)^4} \int d\Theta_1 \int d\Theta_2 \int_0^\infty dt \int_{\theta_1(0)=\Theta_2}^{\theta_1(t)=\Theta_1} \mathcal{D}[\theta_1(t)] \int_{\theta_2(0)=\Theta_2}^{\theta_2(t)=\Theta_1} \mathcal{D}[\theta_2(t)] \\ & \times \left\langle \exp \left\{ \int_0^t dt' \left[-\frac{R^2 \dot{\theta}_1^2(t')}{4D} + i\varphi_1[\theta_1(t'), t'] - i\varphi_2[\theta_1(t'), t'] \right] \right. \right. \\ & \left. \left. + \int_0^t dt' \left[-\frac{R^2 \dot{\theta}_2^2(t')}{4D} - i\varphi_1[\theta_2(t'), t'] + i\varphi_2[\theta_2(t'), t'] \right] \right\} \right\rangle \quad (2.42) \end{aligned}$$

(Performing the Gaussian averaging over the fields φ , one finds Eq. (2.15)).

⁶When Aharonov-Bohm oscillations are considered, the Cooperon contribution only affects the phases of mesoscopic Aharonov-Bohm oscillations, not the amplitudes [89]. For $h/2e$ oscillations, the low-field amplitudes are considered. In the bulk geometry, at low magnetic field the second term in Eq. (2.41) is equal to the first one, and the Cooperon contribution enhances the conductance fluctuations by a factor of 2.

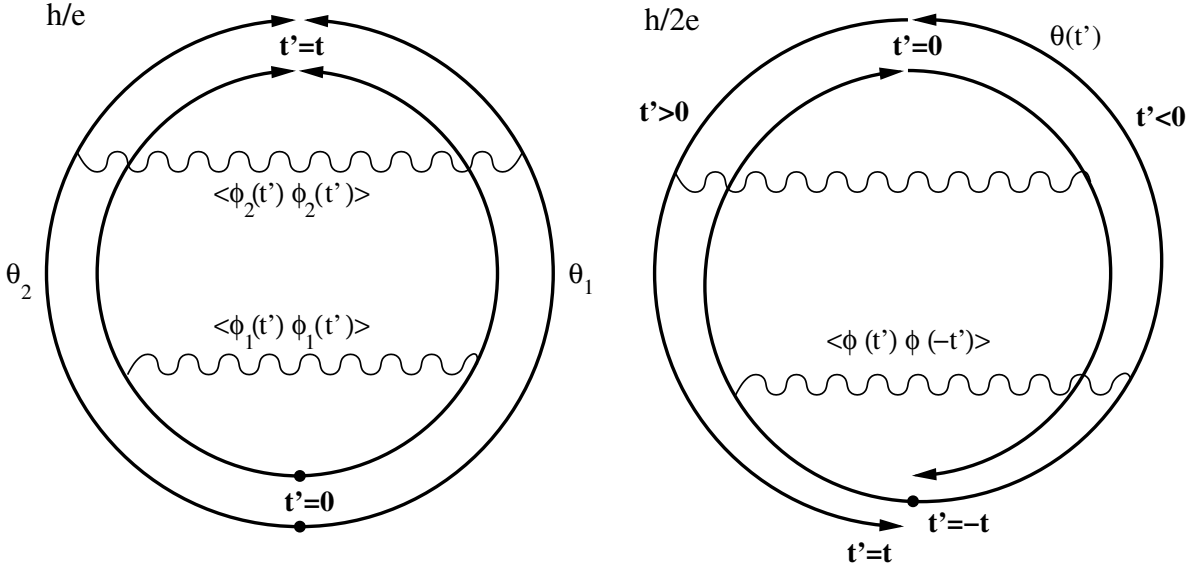


Figure 2.6: Comparison of the pairs of paths contributing to mesoscopic (h/e) Aharonov-Bohm oscillations to the closed paths contributing to weak-localization ($h/2e$) Aharonov-Bohm oscillations. For the h/e Aharonov-Bohm effect (mesoscopic conductance fluctuations), the correlator of the scalar potential is local in time and only connects diffusion paths corresponding to the same measurement. Two copies of the paths, corresponding to the two measurements, are shown. For the $h/2e$ Aharonov-Bohm effect (weak localization), the correlator connects points with opposite time coordinates on the closed path and its time-reversed version. These properties of the allowed interaction lines have the effect that the path integral expressions can be transformed into each other by re-parametrizing the path segments, combining the pair of paths into one closed loop.

It is now demonstrated that the path integral (2.42) describing the mesoscopic oscillations can be mapped to the path integral describing the $h/2e$ Aharonov-Bohm oscillations (in the general case: weak localization) by the parametrization

$$\theta(t') = \begin{cases} \theta_1(t + t') , & -t \leq t' \leq 0 \\ \theta_2(t - t') , & 0 \leq t' \leq t \end{cases} \quad (2.43)$$

(see Fig. 2.6), which joins the two separate paths into a single one of the double length by parametrizing one path in reversed direction. Strictly speaking, this transformation is only valid up to an accuracy L_T , since the durations of the two paths in a pair may differ up to an amount of the order of $1/T$, during which the length L_T is travelled. However, since for quasi-one-dimensional systems the expressions for both weak localization

and conductance fluctuations are entirely dominated by the low-momentum behaviour, this has no effect on the result for the quasi-one-dimensional case. Performing the transformation (2.43), the details are as follows: Starting from the expression (2.42) for h/e oscillations, the action may be rewritten using Eq. (2.43) in the following way:

$$\begin{aligned} \langle \delta G_{h/e}^2 \rangle &= \frac{4e^4 D^2}{3\pi T (2\pi R)^4} \int d\Theta \int_0^\infty dt \int_{\theta(-t)=\Theta}^{\theta(t)=\Theta} \mathcal{D}[\theta(t)] \\ &\times \left\langle \exp \left\{ \int_0^t dt' \left[-\frac{R^2 \dot{\theta}^2(t')}{4D} - \frac{R^2 \dot{\theta}^2(-t')}{4D} \right. \right. \right. \\ &\quad \left. \left. + i\varphi_1[\theta(-t'), t-t'] - i\varphi_1[\theta(t'), t-t'] \right. \right. \\ &\quad \left. \left. - i\varphi_2[\theta(-t'), t-t'] + i\varphi_2[\theta(t'), t-t'] \right] \right\} \right\rangle. \quad (2.44) \end{aligned}$$

Keeping only field correlators for the same measurement and dropping the corresponding indices, performing the average over Gaussian variables φ results in

$$\begin{aligned} \langle \delta G_{h/e}^2 \rangle &= \frac{4e^4 D^2}{3\pi T (2\pi R)^4} \int d\Theta \int_0^\infty dt \int_{\theta(-t)=\Theta}^{\theta(t)=\Theta} \mathcal{D}[\theta(t)] \\ &\times \exp \left\{ - \int_0^t dt' \left[\frac{R^2 \dot{\theta}^2(t')}{4D} + \frac{R^2 \dot{\theta}^2(-t')}{4D} \right] \right. \\ &\quad \left. - \int_0^t dt' dt'' \left\langle \left(\varphi[\theta(-t'), t-t'] - \varphi[\theta(t'), t-t'] \right) \right. \right. \\ &\quad \left. \left. \left(\varphi[\theta(-t''), t-t''] - \varphi[\theta(t''), t-t''] \right) \right\rangle \right\}, \quad (2.45) \end{aligned}$$

where two equal fluctuation terms have been added up. Since the correlator $\langle \varphi \varphi \rangle$ is local in time,⁷ only correlators connecting time coordinates with opposite signs on the

⁷local in the time parametrizing the *original* paths in Eq. (2.42).

original two paths should be kept, and therefore it may be written equivalently as

$$\begin{aligned}
 \langle \delta G_{h/e}^2 \rangle &= \frac{4e^4 D^2}{3\pi T (2\pi R)^4} \int d\Theta \int_0^\infty dt \int_{\theta(-t)=\Theta}^{\theta(t)=\Theta} \mathcal{D}[\theta(t)] \\
 &\quad \times \exp \left\{ - \int_{-t}^t dt' \frac{R^2 \dot{\theta}^2(t')}{4D} \right. \\
 &\quad \left. - \int_0^t dt' dt'' \left\langle \left(\varphi[\theta(-t'), t-t'] - \varphi[\theta(t''), t-t''] \right)^2 \right\rangle \right\} \\
 &= \frac{4e^4 D^2}{3\pi T (2\pi R)^4} \int d\Theta \int_0^\infty dt \int_{\theta(-t)=\Theta}^{\theta(t)=\Theta} \mathcal{D}[\theta(t)] \\
 &\quad \times \exp \left\{ - \int_{-t}^t dt' \frac{R^2 \dot{\theta}^2(t')}{4D} \right. \\
 &\quad \left. - \int_{-t/2}^{t/2} dt' dt'' \left\langle \left(\varphi \left[\theta \left(\frac{t}{2} - t' \right), \frac{3t}{2} - t' \right] - \varphi \left[\theta \left(\frac{t}{2} + t'' \right), \frac{3t}{2} - t'' \right] \right)^2 \right\rangle \right\},
 \end{aligned} \tag{2.46}$$

where the last transformation is just a shift of the variables. Performing the change of variables $t - t' \equiv t/2 + \eta/2$, $t - t'' \equiv t/2 - \eta'/2$, this expression simplifies to

$$\begin{aligned}
 \langle \delta G_{h/e}^2 \rangle &= \frac{4e^4 D^2}{3\pi T (2\pi R)^4} \int d\Theta \int_0^\infty dt \int_{\theta(-t)=\Theta}^{\theta(t)=\Theta} \mathcal{D}[\theta(t)] \\
 &\quad \times \exp \left\{ - \int_{-t}^t d\eta \frac{R^2 \dot{\theta}^2(\eta)}{4D} \right. \\
 &\quad \left. - \frac{1}{2} \int_{-t}^t d\eta d\eta' \left\langle \left(\varphi[\theta(\eta/2), t + \eta/2] - \varphi[\theta(\eta'/2), t - \eta'/2] \right)^2 \right\rangle \right\}.
 \end{aligned} \tag{2.47}$$

The factor $1/2$ in front of the fluctuation term is the combination of a factor $1/4$ arising from the Jacobian of the transformation to the new time coordinates and a factor 2 from rescaling the field correlator in time. Shifting the time arguments of the random fields

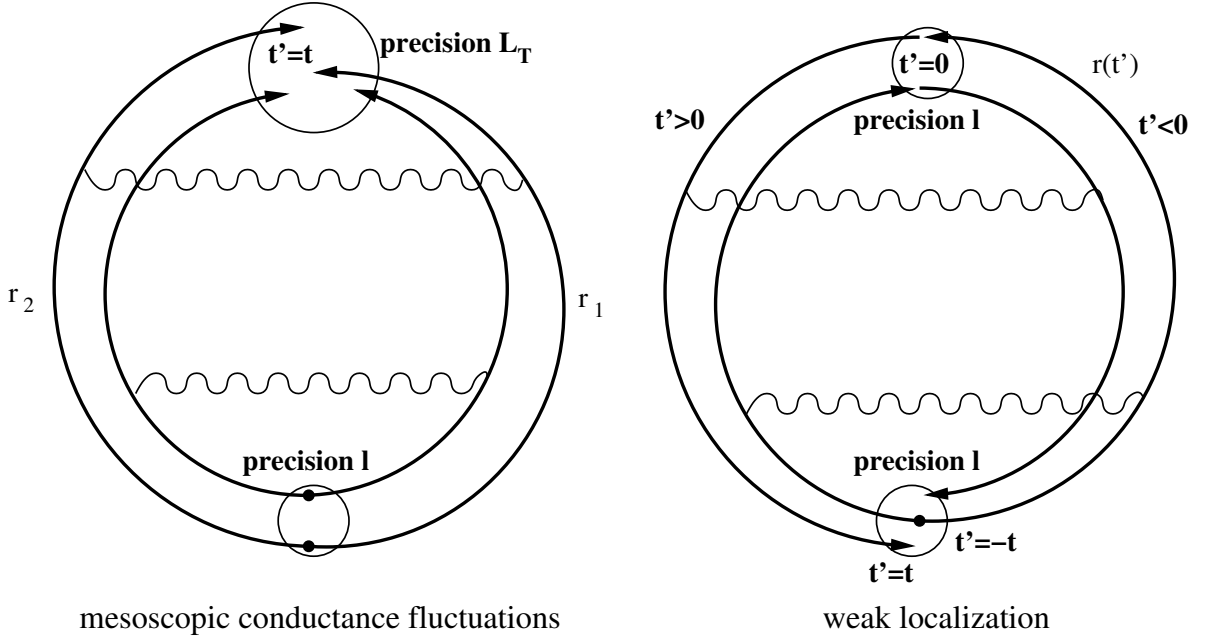


Figure 2.7: Unlike in the quasi-onedimensional case (see Fig. 2.6), in two dimensions mesoscopic conductance fluctuations and weak localization depend logarithmically on the short-scale physics. The respective cutoffs are different: For conductance fluctuations, the thermal factor arising from the distribution functions imposes the condition that the two paths have to reach the common endpoint after times t_1, t_2 differing by no more than $t_1 - t_2 \sim 1/T$, meaning that after the same time $t = \min(t_1, t_2)$ both paths should end at coordinates within a distance $L_T = (D/T)^{1/2}$. For weak localization, the short-distance cutoff is given by the elastic mean free path l , since one continuous path is considered.

by t , Eq. (2.47) can be identified with the path integral representation of the Cooperon in a fluctuating external field [18, 29]. As a result, the fundamental harmonics of h/e and $h/2e$ Aharonov-Bohm oscillations are related by

$$\langle \delta G_{h/e}^2 \rangle = \frac{e^2 D}{3T (2\pi R)^2} |\delta G_{h/2e}^{WL}|. \quad (2.48)$$

Eq. (2.48) is the equivalent to Eq. (38) of Ref. [85], without the need to actually carry out any of the path integrals or assuming a specific form of the correlator $\langle \varphi^\alpha \varphi^\beta \rangle$ other than being local in time.

The generalization to higher harmonics of both effects is obvious: Pairs of paths with relative winding number n are related to weak localization paths with winding number

n by

$$\langle \delta G_{h/ne}^2 \rangle = \frac{e^2 D}{3T (2\pi R)^2} |\delta G_{h/2ne}^{\text{WL}}|, \quad (2.49)$$

connecting the n th harmonic of the mesoscopic Aharonov-Bohm effect with the n th harmonic of the $h/2e$ Aharonov-Bohm effect, measured in low magnetic fields.

It immediately follows from the relation between h/e and $h/2e$ oscillations that also the dephasing length must be the same for both effects.

The presented arguments for the ring geometry can be directly used in the bulk geometry too, proving the relation (2.41) on a more fundamental level. While this is straightforward in the quasi-onedimensional situation, a little extra care is needed in the twodimensional case since in two dimensions at finite temperature $T \gg E_c$ both the weak localization correction and mesoscopic conductance fluctuations depend logarithmically on the short-scale cutoff, $\delta g_{\text{WL}} \sim \ln(L_\varphi/l)$ [85] and $\langle \delta g^2 \rangle \sim \ln(L_\varphi/L_T)$ [36], where $L_T = (D/T)^{1/2}$ and l is the elastic mean free path. The transformation (2.43) joining the two paths is not applicable below a length scale of L_T : The pairs of paths contributing to conductance fluctuations are only required by the thermal factor to have durations which differ by no more than the order of the inverse temperature [85]. Equivalently, after the same duration the two paths only end within a distance of L_T , not l , of each other. The condition for a closed loop contributing to weak localization is stronger since it must be continuous down to the scale of the elastic mean free path l . This can be written as

$$\langle \delta G^2 \rangle = \frac{e^2 D}{3T L^2} |\delta G_{\text{WL}}(H=0)|_{l \rightarrow L_T}, \quad d=1,2, \quad (2.50)$$

meaning that the elastic mean free path l in the result for the weak localization amplitude is to be substituted by L_T ; this only changes the result in two dimensions.

2.4 Summary

In this chapter, the theory of inelastic electron-electron collisions in low dimensions from Refs. [18, 29] has been generalized to the case of Aharonov-Bohm interference in multiply-connected metallic samples (metallic rings). Using a real-space version of the formalism, the result in the strong-dephasing regime given by Eqs. (2.33), (2.30) has been derived. The corresponding dephasing length (2.34) differs from the one for the singly-connected (wire) geometry in a remarkable way: Although the Aharonov-Bohm dephasing length (2.34) is much shorter than the system size in the regime of interest, it is determined by inelastic processes with momentum transfers of the order of the inverse system size (instead of the inverse dephasing length). This leads to the temperature dependence $L_\varphi^{\text{AB}} \sim T^{-1/2}$ instead of the usual $L_\varphi \sim T^{-1/3}$ behaviour.

This can be understood from the properties of the contributing paths, which have a fixed minimum length given by the ring circumference, while paths contributing to

the weak localization amplitude or mesoscopic conductance fluctuations in a singly-connected geometry are not restricted in this way and may be arbitrarily short. Therefore, the low-momentum cutoff for inelastic processes contributing to the dephasing of the paths relevant for the Aharonov-Bohm effect is set by *their* inverse length, i.e. the system size, while for weak localization and conductance fluctuations it is set by the inverse of their *typical* length, i.e. selfconsistently by the inverse of the dephasing length itself.

As a result, typical electron trajectories contributing to the Aharonov-Bohm interference are of special character. Since their minimum length is fixed, as the dephasing length L_φ^{AB} decreases the class of typical contributing paths changes, narrowing down to paths which feature a more directed motion than average diffusive trajectories.

The close relation between weak localization and mesoscopic conductance fluctuations first demonstrated in Ref. [85] has been proven above on a more fundamental level. The path-integral formulation makes it possible to express the relation between the two quantities without specifying the geometry, allowing a straightforward generalization to the similar relation (2.48) between the amplitudes of h/e (mesoscopic) and $h/2e$ (weak-localization) Aharonov-Bohm oscillations as well.

The obtained results (2.33), (2.30) for the dephasing of Aharonov-Bohm oscillations have been confirmed by recent experimental data [104].

3 Nonequilibrium mesoscopic conductance fluctuations

3.1 Overview of previous results and available experimental data

When the regime of linear response is left, the voltage dependence of mesoscopic conductance fluctuations exhibits a rich behaviour. In an early theoretical paper, Larkin and Khmelnitskii [34] predicted an enhancement of the fluctuations of the differential conductance g with the voltage. Specifically, they found the asymptotically linear enhancement of the variance of the differential conductance $g = dI/dV$,

$$\langle \delta g^2 \rangle \sim \frac{V}{V_c} , \quad V \gg V_c . \quad (3.1)$$

Here $eV_c = D/L^2$ is the Thouless energy, D the diffusion constant, and L the system size. Eq. (3.1) is valid in any geometry as long as inelastic processes are negligible. The coefficient of Eq. (3.1) is geometry-dependent and was not calculated in Ref. [34]. Eq. (3.1) in particular implies that, if inelastic processes remain negligible, the fluctuations of the differential conductance will be of the order of the conductance itself at a voltage $V \sim g^2 V_c$, leading to the appearance of regions of negative differential conductance in the IV -characteristics.

As is discussed in more detail in Section 3.2.2, the enhancement of conductance fluctuations given by Eq. (3.1) is due to the fact that fluctuations of the electrochemical potential affect all electrons in the energy window contributing to transport. As a result, the voltage has a different effect than just a finite temperature in the way that an applied voltage changes the (position-dependent) electrochemical potential in the sample in addition to making an energy window of width eV available for transmission, while the temperature just averages over an energy range of width T while leaving the potential profile in the sample unchanged.

Early measurements [40, 43, 51] could not reliably confirm the prediction (3.1), however more recent experiments [60, 78, 79, 86, 87] did observe a nontrivial voltage dependence of both mesoscopic fluctuations and Aharonov-Bohm oscillations of the differential conductance. A common observation in all experiments was that at sufficiently high voltages the amplitude of the conductance fluctuations decreases again. In particular,

negative differential conductance has not been observed experimentally. Clearly, the assumption entering Eq. (3.1) that inelastic scattering can be neglected is not valid above a certain voltage, since the phase space available for inelastic processes increases with the voltage. However, a quantitative theory of inelastic electron-electron scattering has not been developed before. Larkin and Khmelnitskii [34] introduced a phenomenological inelastic out-scattering time τ_{in} and out-scattering length $L_{\text{in}} = \sqrt{D\tau_{\text{in}}}$, but no theory for the voltage dependence of τ_{in} was given. The authors of Refs. [86, 87] estimated the effect of inelastic processes by using the equilibrium dephasing length $L_{\varphi}(T)$ given by Eq. (1.11) and replacing the temperature with the voltage, $T \rightarrow eV$, however the result they obtained was inconsistent with the observed behaviour, $\langle \delta g^2 \rangle \propto V^{-1.28}$ for a quasi-one-dimensional wire at high voltages. The authors of Refs. [86, 87] therefore concluded that electron-phonon scattering should lead to the observed suppression of conductance fluctuations.

In this chapter a systematic theory of the voltage dependence of conductance fluctuations of mesoscopic wires is presented. After a brief recapitulation of the Keldysh formalism for disordered systems, in Section 3.2.2 the behaviour of the fluctuations of the differential conductance $\langle \delta g^2 \rangle (V/V_c)$ as a function of the applied voltage is calculated quantitatively over the entire voltage range from the linear-response limit to the asymptotic behaviour (3.1) of the noninteracting system. The coefficient of Eq. (3.1), which has not been evaluated before, is calculated for the wire geometry. It is found that in addition to the linear asymptotic behaviour a nontrivial crossover regime occurs. In Section 3.2.3, the effect of a finite temperature on the results of Section 3.2.3 is considered. As may be naively expected, the finite temperature does not have a strong influence on the high-voltage behaviour of the conductance fluctuations. An evaluation of the effect of inelastic processes is performed in Section 3.3. The results are in reasonable agreement with the available experimental data at high voltages [86, 87], and explain them without the need to include electron-phonon scattering.

3.2 Voltage dependence of conductance fluctuations in a noninteracting system

3.2.1 Keldysh diagrammatic method for disordered systems

This section briefly reviews the Keldysh formalism [8] (see Refs. [35, 99] for extended reviews) applied to disordered systems for later reference.

To describe nonequilibrium processes, Green's functions are used which describe expectation values that are averaged over arbitrary states (not necessarily equilibrium states):

$$iG_{12} = \langle n | \hat{T} \Psi_1 \Psi_2^\dagger | n \rangle , \quad (3.2)$$

where $\Psi_i \equiv \Psi(\mathbf{r}_i, t_i)$ are the field operators, \hat{T} is the time-ordering operator, and $|n\rangle$ is an arbitrary state. Using the notation $\langle n | \cdots | n \rangle \equiv \langle \cdots \rangle$, the following four Green's functions can be defined:

$$iG_{12}^{--} = \langle \hat{T} \Psi_1 \Psi_2^\dagger \rangle \quad (3.3)$$

$$iG_{12}^{+-} = \langle \Psi_1 \Psi_2^\dagger \rangle \quad (3.4)$$

$$iG_{12}^{-+} = \mp \langle \Psi_2^\dagger \Psi_1 \rangle \quad (3.5)$$

$$iG_{12}^{++} = \langle \hat{\bar{T}} \Psi_1 \Psi_2^\dagger \rangle , \quad (3.6)$$

where $\hat{\bar{T}}$ is the anti-timeordering operator, and the upper/lower sign is for Fermi/Bose operators respectively. Note that G^{--} is equal to the “usual” zero-temperature Green's function. For equal time arguments $t_1 = t_2 \equiv t$, the function G^{-+} is related to the one-particle density matrix by

$$G^{-+}(\mathbf{r}_1, t; \mathbf{r}_2, t) = \pm iN\rho(\mathbf{r}_1, \mathbf{r}_2, t) , \quad (3.7)$$

where N is the particle number. By definition the four functions defined above are not independent, but satisfy

$$i(G_{12}^{+-} - G_{12}^{-+})_{t_1=t_2} = \delta(\mathbf{r}_1 - \mathbf{r}_2) \quad (3.8)$$

$$G_{12}^{--} + G_{12}^{++} = G_{12}^{-+} + G_{12}^{+-} \quad (3.9)$$

$$G_{12}^{--} = -(G_{21}^{++})^* \quad (3.10)$$

$$G_{12}^{-+} = -(G_{21}^{+-})^* \quad (3.11)$$

$$G_{12}^{+-} = -(G_{21}^{-+})^* . \quad (3.12)$$

The retarded and advanced Green's functions are given by

$$G^R = G^{--} - G^{-+} = G^{+-} - G^{++} \quad (3.13)$$

$$G^A = G^{--} - G^{+-} = G^{-+} - G^{++} . \quad (3.14)$$

In Fourier space, the field operators can be written as

$$\Psi = \frac{1}{\sqrt{V}} \sum_{\mathbf{p}} \hat{a}_{\mathbf{p}} \exp\left\{i[\mathbf{p}\mathbf{r} - (\varepsilon - \mu)t]\right\} , \quad (3.15)$$

where the annihilation and creation operators \hat{a} , \hat{a}^\dagger are related to the distribution function n by

$$\langle \hat{a}_{\mathbf{p}}^\dagger \hat{a}_{\mathbf{p}} \rangle = n_{\mathbf{p}} , \quad \langle \hat{a}_{\mathbf{p}} \hat{a}_{\mathbf{p}}^\dagger \rangle = 1 \mp n_{\mathbf{p}} . \quad (3.16)$$

As a result [12],

$$G^{+-}(\omega, \mathbf{p}) = -2\pi i (1 \mp n_{\mathbf{p}}) \delta(\omega - \varepsilon + \mu) \quad (3.17)$$

$$G^{-+}(\omega, \mathbf{p}) = \pm 2\pi i n_{\mathbf{p}} \delta(\omega - \varepsilon + \mu) \quad (3.18)$$

$$G^R(\omega, \mathbf{p}) = (\omega - \varepsilon + \mu + i0)^{-1} \quad (3.19)$$

$$G^A(\omega, \mathbf{p}) = (\omega - \varepsilon + \mu - i0)^{-1} \quad (3.20)$$

$$G^{--}(\omega, \mathbf{p}) = \mathcal{P}\left\{\frac{1}{\omega - \varepsilon + \mu}\right\} + i\pi (\pm 2n_{\mathbf{p}} - 1) \delta(\omega - \varepsilon + \mu) , \quad (3.21)$$

where \mathcal{P} denotes the operation of taking the principal value. For an ideal gas, the unperturbed Green's functions $G^{(0)}$ satisfy the equations of motion [12]

$$\left(i\frac{\partial}{\partial t} + \frac{\nabla^2}{2m} + \mu\right) G_{12}^{(0) --} = \delta(\mathbf{r}_1 - \mathbf{r}_2) \delta(t_1 - t_2) \quad (3.22)$$

$$\left(i\frac{\partial}{\partial t} + \frac{\nabla^2}{2m} + \mu\right) G_{12}^{(0) ++} = -\delta(\mathbf{r}_1 - \mathbf{r}_2) \delta(t_1 - t_2) \quad (3.23)$$

$$\left(i\frac{\partial}{\partial t} + \frac{\nabla^2}{2m} + \mu\right) G_{12}^{(0) +-} = 0 \quad (3.24)$$

$$\left(i\frac{\partial}{\partial t} + \frac{\nabla^2}{2m} + \mu\right) G_{12}^{(0) -+} = 0 . \quad (3.25)$$

For the Hamiltonian $H = H_0 + V$ with the perturbation V , a perturbation series can be constructed [12] in complete analogy to the standard Green's function formalism. Consider the Green's function

$$iG_{12}^{--} = \left\langle \hat{S}^{-1} \hat{T} [\Psi_1 \Psi_2^\dagger \hat{S}] \right\rangle \quad (3.26)$$

with the evolution operator

$$\hat{S} = \hat{T} \exp \left\{ -i \int_{-\infty}^{\infty} dt V(t) \right\} \quad (3.27)$$

and Ψ and V taken in the interaction representation. Expanding \hat{S} and \hat{S}^\dagger and using Wick's theorem, the averaging over an *arbitrary* state also leads to contractions involving

field operators from \hat{S}^{-1} appearing, at variance with the standard Green's function formalism, which averages over the ground state. This structure can be accounted for using a 2×2 matrix notation for the Green's function and self-energy,

$$\hat{G} = \begin{pmatrix} G^{--} & G^{+-} \\ G^{+-} & G^{++} \end{pmatrix}, \quad \hat{\Sigma} = \begin{pmatrix} \Sigma^{--} & \Sigma^{+-} \\ \Sigma^{+-} & \Sigma^{++} \end{pmatrix}, \quad (3.28)$$

leading to the self-energy equation

$$\hat{G}_{12} = \hat{G}_{12}^{(0)} + \int d^4 3 d^4 4 \hat{G}_{14}^{(0)} \hat{\Sigma}_{43} \hat{G}_{32}. \quad (3.29)$$

and the equation of motion

$$\left\{ i \frac{\partial}{\partial t} + \frac{\nabla^2}{2m} + \mu \right\} \hat{G}_{12}^{(0)} = \hat{\tau}_z \delta(\mathbf{r}_1 - \mathbf{r}_2) \delta(t_1 - t_2) \quad (3.30)$$

with $\hat{\tau}_z \equiv \begin{pmatrix} 1 & 0 \\ 0 & -1 \end{pmatrix}$. Combining these two equations, the equation of motion for the full Green's function reads

$$\left\{ i \frac{\partial}{\partial t} + \frac{\nabla^2}{2m} + \mu \right\} \hat{G}_{12} = \hat{\tau}_z \delta(\mathbf{r}_1 - \mathbf{r}_2) \delta(t_1 - t_2) + \int d^4 3 \hat{\tau}_z \hat{\Sigma}_{13} \hat{G}_{32}. \quad (3.31)$$

Due to Eqs. (3.17), (3.18), the matrix equations reduce to the $(--)$ component and therefore to the usual zero-temperature diagrammatic technique when a Fermi system in equilibrium is considered (when n is replaced by the zero-temperature Fermi distribution function).

Exploiting the relations between the various Green's functions, one component of the Green's function matrix can be made equal to zero. Different conventions exist [8, 12, 35, 99], the Larkin-Ovchinnikov one [10, 35] being

$$\hat{G} = \begin{pmatrix} G^R & G^K \\ 0 & G^A \end{pmatrix} \quad (3.32)$$

with the Keldysh Green's function $G^K = G^{--} + G^{++} = G^{-+} + G^{+-}$. The notation (3.32) has the property that \hat{G} satisfies the equation of motion

$$\left\{ \epsilon + \frac{1}{2m} \nabla^2 - U(\mathbf{r}) - e\phi(\mathbf{r}) \right\} \hat{G}_\epsilon(\mathbf{r}, \mathbf{r}') = \mathbb{I} \delta(\mathbf{r} - \mathbf{r}') , \quad (3.33)$$

where the disorder potential U and the electrochemical potential ϕ couple via a unit matrix in Keldysh space.

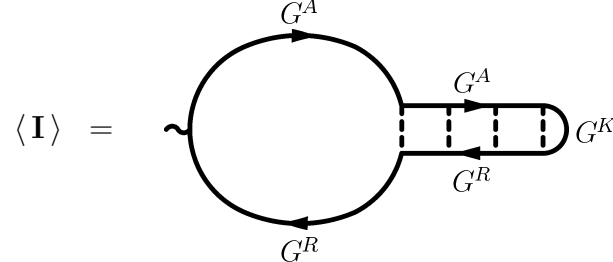
It is seen from Eqs. (3.17), (3.18) that the disorder averaged *diagonal* Keldysh function $G^K(\mathbf{r}) \equiv G^K(\mathbf{r}, \mathbf{r})$ is related to the distribution function by

$$G^K(\mathbf{r}, \mathbf{r}) = 2\pi i \nu [2n(\mathbf{r}) - 1] \quad (3.34)$$

and satisfies the kinetic equation (see Appendix B) [34]

$$\nabla^2 \langle G_\epsilon^K(\mathbf{r}) \rangle = 0 . \quad (3.35)$$

Moreover, the average current can be expressed by the disorder averaged diagonal Keldysh function in the following way,

$$\begin{aligned} \langle \mathbf{I} \rangle &= \text{Diagram} \\ &= \frac{e}{4\pi i} D \nabla \int d\epsilon \langle G_\epsilon^K(\mathbf{r}) \rangle . \end{aligned} \quad (3.36)$$


Here D is the diffusion constant, ν is the density of states, G^R , G^A , and G^K denote the retarded, advanced, and Keldysh Green's functions respectively, and the wiggly line denotes the external current vertex, with which an operator $(-e)\hat{\mathbf{v}}$ is associated.

3.2.2 Voltage-induced enhancement of conductance fluctuations in a quasi-onedimensional wire

In this section, a quasi-onedimensional metallic sample (a wire) of length L attached to two reservoirs which are at a finite voltage difference V is considered.

The diagrams for current fluctuations can be obtained from Eq. (3.36) by connecting two current diagrams by impurity ladders (diffusons or Cooperons, assuming unbroken time-reversal symmetry) in all possible ways, leading to the six¹ diagrams shown in Figs. 3.1, 3.2. Similar to the standard impurity diagram technique, the diagrams consist of (short-ranged) electronic vertices (Hikami boxes) which are connected by (long-ranged) diffuson and Cooperon ladders. The Hikami boxes take into account the possibility of inserting additional impurity lines connecting electronic Green functions of the same type (retarded with retarded, or advanced with advanced) without crossings. For the hexagonal vertices of the diagrams c-diff and c-coop, only the insertions contributing to the leading (zeroth) order in the external momenta are shown. Due to the different number of impurity ladders (the diagrams c-diff and c-coop contain only one), all diagrams are thus evaluated to the same order of the diffuson/Cooperon momenta. The vertex factors may be evaluated in momentum space, since they decay exponentially on the scale of the mean free path l , and thus are of much shorter range than

¹Note that the diagrams c-diff and c-coop, as well as some possibilities of inserting additional impurity lines in the Hikami boxes, are missing in Fig. 1 of Ref. [34]. However, the expression given in Ref. [34] correctly states the sum of all diagrams, Eq. (3.37).

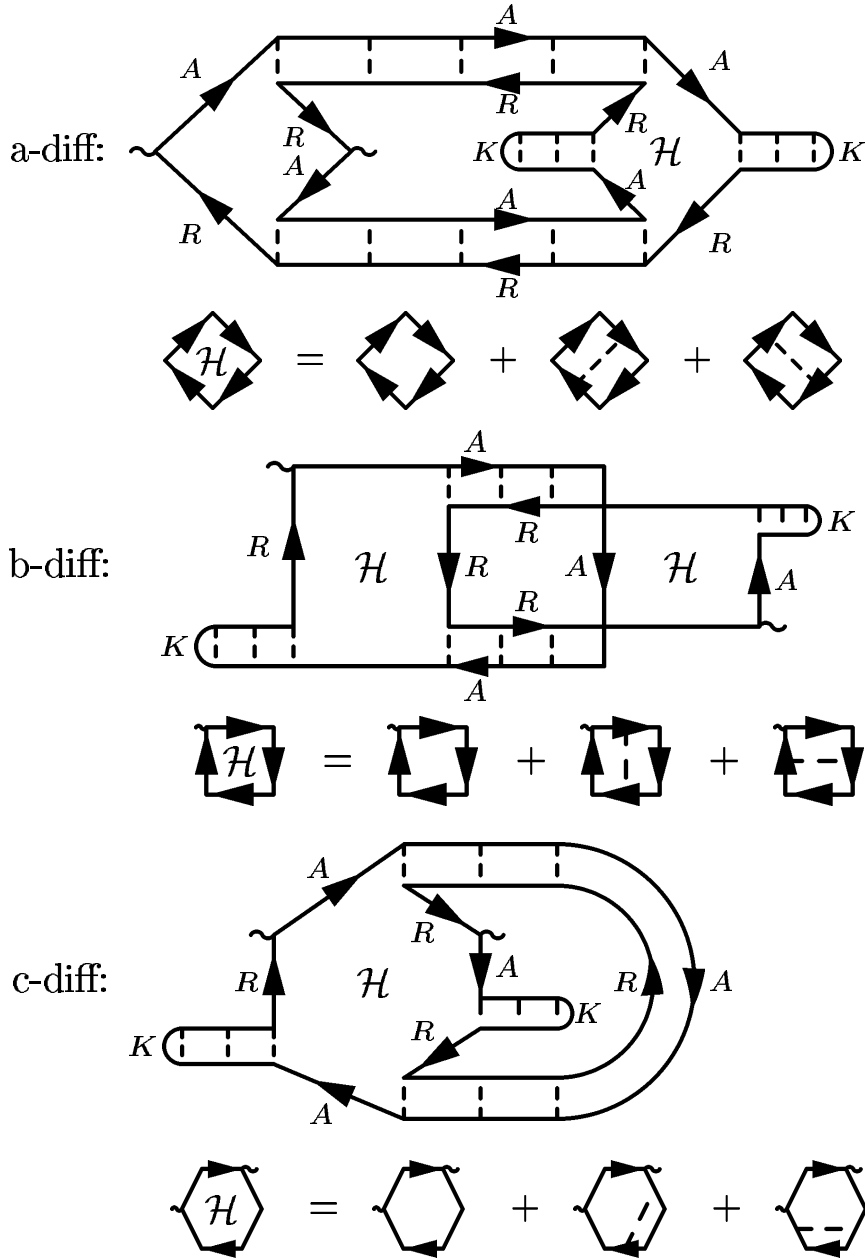


Figure 3.1: The diagrams describing conductance fluctuations are obtained by connecting two diagrams of the type shown in Eq. (3.36) by impurity ladders. With diffuson ladders, these three diagrams can be constructed. R , A , and K denote the retarded, advanced, and Keldysh Green's function respectively, while the wiggly lines denote the external current vertex. The vertex factors are presented in Appendix C. The three diffuson diagrams sum up to half of Eq. (3.37).

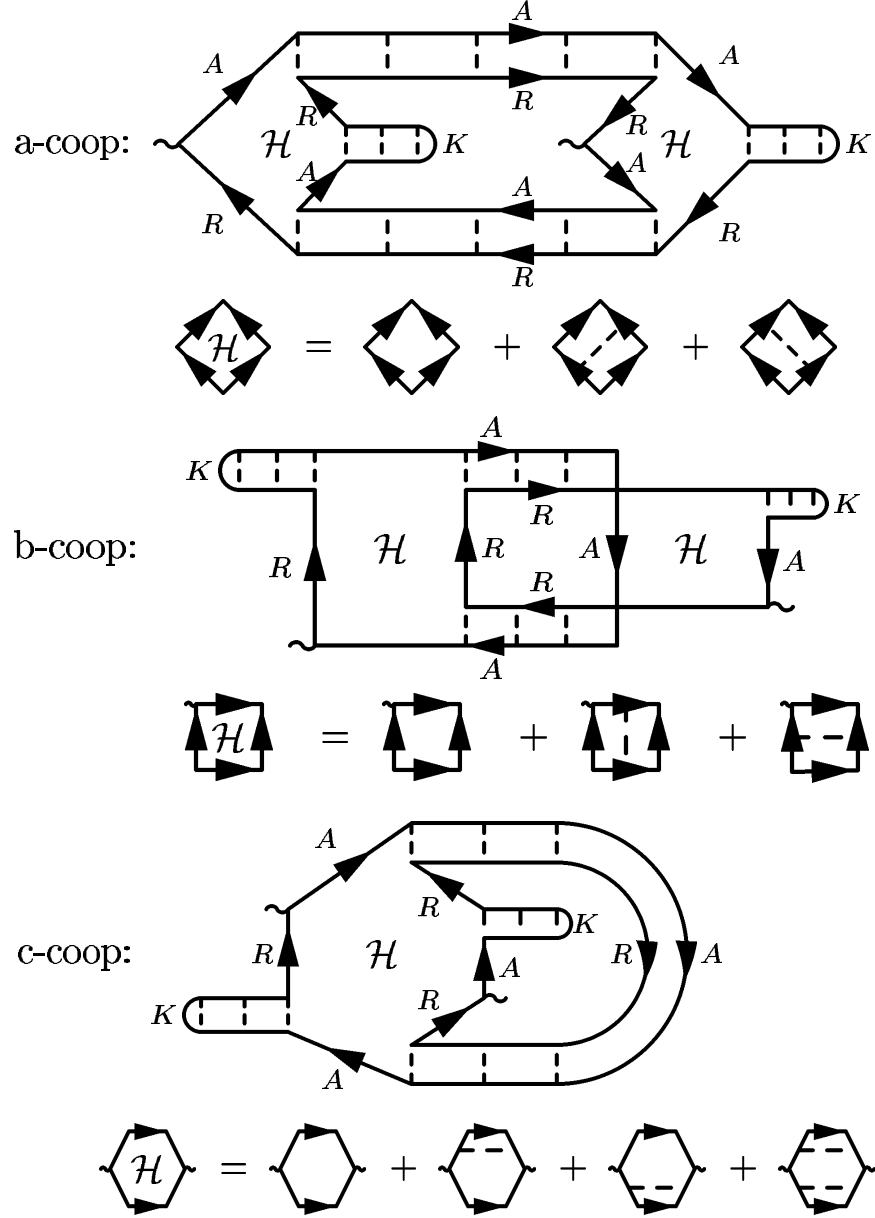


Figure 3.2: In analogy to the diffuson diagrams shown in Fig. 3.1, these three Cooperon diagrams can be constructed. All diffuson and Cooperon diagrams add up to Eq. (3.37). Note that, while diagram c-diff of Fig. 3.1 evaluates to zero in the leading order, diagram c-coop gives a nonzero contribution.

the diffuson/Cooperon ladders. The technical details of the calculation are presented in Appendix C. The result for the sum of all contributions to the variance of the current is as follows,

$$\begin{aligned} \langle \delta I(V_1) \delta I(V_2) \rangle &= -\frac{e^2}{(2\pi)^2} \left(\frac{1}{2\pi\nu} \right)^2 \int d\epsilon_1 d\epsilon_2 \int \frac{dx_1 dx_2}{L^2} \frac{\partial}{\partial x_1} \langle G_{\epsilon_1}^K(x_1) \rangle \frac{\partial}{\partial x_2} \langle G_{\epsilon_2}^K(x_2) \rangle \\ &\quad \times [2 |\mathcal{D}_{\epsilon_1 - \epsilon_2}(x_1, x_2)|^2 + \text{Re } \mathcal{D}_{\epsilon_1 - \epsilon_2}^2(x_1, x_2)] \quad , \quad (3.37) \end{aligned}$$

where \mathcal{D} is a rescaled diffusion propagator satisfying the equation

$$\left\{ \frac{\partial^2}{\partial x^2} + \frac{i\omega}{D} + \frac{ie}{D} [\phi_1(x) - \phi_2(x)] \right\} \mathcal{D}_\omega(x, x') = -\delta(x - x') \quad (3.38)$$

with the potential profiles $\phi_{1,2}(x) = (x/L)V_{1,2}$ corresponding to the voltage differences $V_{1,2}$ between the reservoirs. The boundary conditions for Eq. (3.38) are that $\mathcal{D} = 0$ if one of the coordinates x, x' lies at one of the reservoirs at 0 or L .

The prefactor of Equation (3.37) is written for spinless electrons and unbroken time-reversal symmetry, or alternatively, for spinful electrons in the limit of strong spin-orbit interaction, when only the spin-singlet channel contributes. If the spin rotation symmetry is preserved, Eq. (3.37) should be multiplied by a factor 4 to account for the spin. If time-reversal symmetry is broken, Eq. (3.37) should be multiplied by an extra factor of 1/2 because the Cooperon contribution is absent.

Although the individual diagrams do not feature this property, when the complete set of diffuson/Cooperon diagrams (including c-diff and c-coop) is taken into account they combine so that only the spatial derivative of the Keldysh function enters the result (3.37). This could be expected because only the electrons in the energy window of width V contribute to the transport, and the result should not depend on an overall offset of the energy scale.

In this section it is assumed that the temperature of the reservoirs is sufficiently low, $T \ll eV_c$ (the thermal diffusion length $L_T = (D/T)^{1/2}$ is much larger than the system size). This allows to set $T = 0$ for the rest of this section. At low voltage the system is therefore in the regime of universal conductance fluctuations. The behaviour with increasing voltage at $T = 0$ is the subject of the rest of this section, while the effect of a finite temperature, $T \gg eV_c$, will be analyzed in Section 3.2.3.

When the wire is connected to two perfect reservoirs with different Fermi energies, the distribution function of *noninteracting* electrons in the wire is not a Fermi function, but has a double-step shape [65, 96], since there is no energy exchange between the electrons originating from the two reservoirs. A plot of the distribution function for different positions on the wire is shown in Fig. 3.3. In the Keldysh formalism, this can be easily obtained from the kinetic equation for the averaged diagonal Keldysh function (3.35) with the boundary conditions that the distribution function assumes a zero-temperature Fermi shape with the respective Fermi levels at each of the two reservoirs,

$$\langle G_\epsilon^K(x) \rangle = -2\pi i\nu \times \begin{cases} 1 - 2f(\epsilon) , & x = 0 \\ 1 - 2f(\epsilon - eV) , & x = L , \end{cases} \quad (3.39)$$

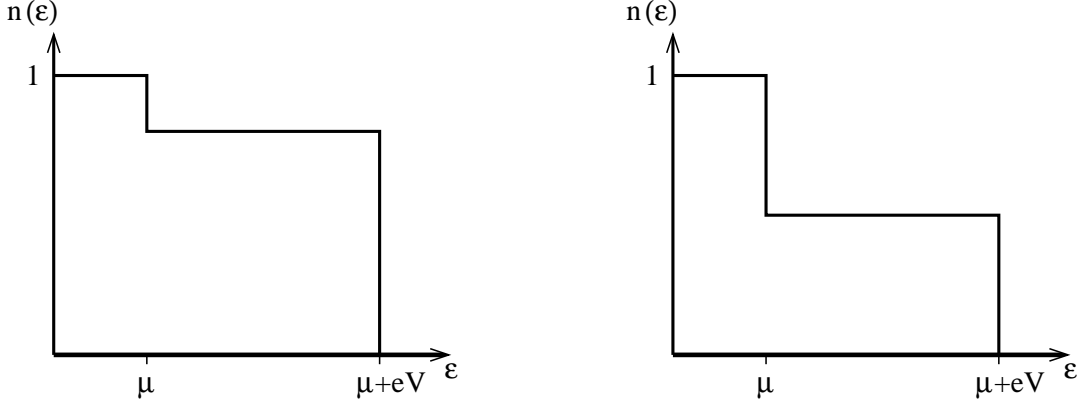


Figure 3.3: The electron distribution function of a wire with negligible energy exchange connected to two reservoirs with electrochemical potentials μ and $\mu + eV$ takes a double-step shape, with the height of the intermediate plateau depending on the position. Left: The distribution function at a position close to the reservoir which is at $\mu + eV$. Right: distribution function of the same wire taken at equal distances to the reservoirs.

where f is the Fermi function. As a result, the Keldysh function is a linear function of the spatial coordinate,

$$\langle G_\epsilon^K(x) \rangle = -2\pi i\nu \left\{ 1 - 2f(\epsilon) + 2\frac{x}{L} [f(\epsilon) - f(\epsilon - eV)] \right\} . \quad (3.40)$$

This yields (now including a factor 4 to account for the spin)

$$\langle \delta I(V_1) \delta I(V_2) \rangle = 16 V_c^2 \int_0^{V_1/V_c} dz_1 \int_0^{V_2/V_c} dz_2 \Xi_{z_1 - z_2}(V_1 - V_2) , \quad (3.41)$$

where

$$\Xi_z(V_1 - V_2) = \int_0^1 dy_1 dy_2 [2 |\Pi_z(y_1, y_2)|^2 + \text{Re} \Pi_z^2(y_1, y_2)] \equiv \text{Tr} [2 |\Pi_z|^2 + \text{Re} \Pi_z^2] \quad (3.42)$$

with

$$\left\{ \frac{\partial^2}{\partial y^2} + iz + i\alpha y \right\} \Pi_z(y, y') = -\delta(y - y') , \quad (3.43)$$

now written in dimensionless variables $y = x/L$, $z = \omega/eV_c$, and $\alpha = (V_1 - V_2)/V_c$.

To get the fluctuations of the differential conductance $\langle \delta g(V) \delta g(V) \rangle$, Eq. (3.41) is differentiated with respect to both voltages before setting $V_1 = V_2 \equiv V$. The result has

the form

$$\langle \delta g^2 \rangle = \langle \delta g^2 \rangle_0 + \langle \delta g^2 \rangle_1 + \langle \delta g^2 \rangle_2 , \quad (3.44)$$

where

$$\langle \delta g^2 \rangle_0 = 16 \Xi_0|_{\alpha=0} = \frac{8}{15} , \quad (3.45)$$

$$\langle \delta g^2 \rangle_1 = 32 \int_0^{V/V_c} dz \frac{\partial}{\partial \alpha} \Xi_{z-V/V_c} \Big|_{\alpha=0} , \quad (3.46)$$

$$\langle \delta g^2 \rangle_2 = -16 \int_0^{V/V_c} dz_1 dz_2 \frac{\partial^2}{\partial \alpha^2} \Xi_{z_1-z_2} \Big|_{\alpha=0} . \quad (3.47)$$

The three contributions (3.45), (3.46), and (3.47) to the variance of the differential conductance arise from two physically different mechanisms: In the low-voltage (linear-response) regime $V \ll V_c$, the effect of a voltage increment dV is to change the electrochemical potential in the reservoirs, making the states with energies in the window dV available for electron transmission. The corresponding conductance fluctuations are given by the term (3.45), reproducing the well-known UCF result [36], $\langle \delta g^2 \rangle = 8/15$, which is due to the fact that at a different electrochemical potential the conduction electrons explore a different realization of disorder. The two other terms (vanishing at low voltages) describe true non-equilibrium effects. Out of equilibrium the effect of the applied voltage is not only to change the chemical potential in the reservoirs, but also to alter the (position-dependent) electrochemical potential $\phi(x)$ in the sample. The shift dV of the voltage induces the variation $d\phi(x) = (x/L)dV$ of the potential, and this variation affects *all* the electrons in the energy window of width eV by changing the disorder realization explored by them. However, electrons at different energies move in different disorder realizations which are essentially uncorrelated if the energies differ by more than the Thouless energy eV_c , and also fluctuate independently, with the fluctuations adding up incoherently. This is the mechanism responsible for the third term, Eq. (3.47). The second term, Eq. (3.46), is a cross-term due to correlations between the above two random contributions to dI/dV .

To evaluate the derivatives in Eqs. (3.46) and (3.47), the diffusion propagator Π can be expanded up to second order in the dimensionless voltage difference α ,

$$\Pi_z = \Pi_z^{(0)} + i\alpha \Pi_z^{(0)} y \Pi_z^{(0)} - \alpha^2 \Pi_z^{(0)} y \Pi_z^{(0)} y \Pi_z^{(0)} + \mathcal{O}(\alpha^3) , \quad (3.48)$$

where $\Pi_z^{(0)} \equiv (-\partial_y^2 - iz)^{-1}$. This expression can be evaluated using the representation diagonalizing $\Pi_z^{(0)}$,

$$\left(-\frac{\partial^2}{\partial y^2} - iz \right) = \sum_{n>0} \lambda_n |n\rangle \langle n| , \quad |n\rangle = \sqrt{2} \sin(n\pi y) , \quad \lambda_n = (n\pi)^2 - iz . \quad (3.49)$$

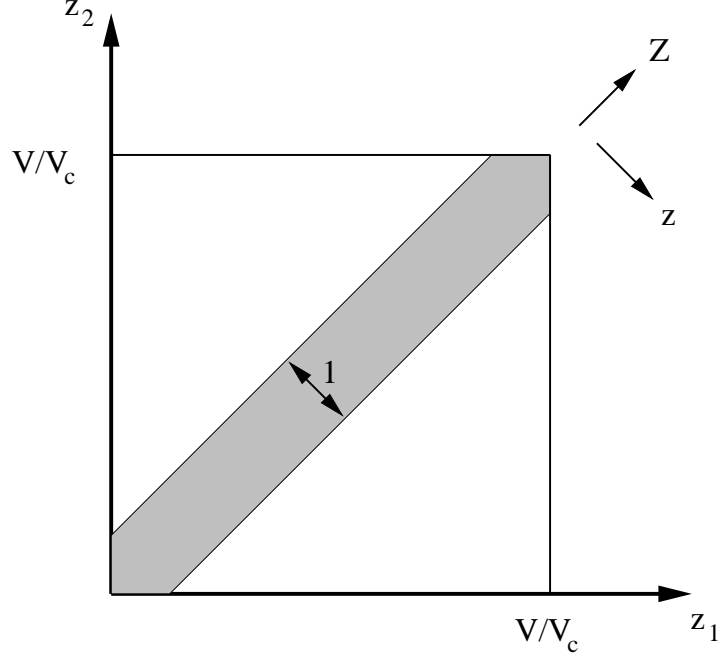


Figure 3.4: The relevant range of voltages for Eq. (3.47). The integrand is of appreciable magnitude in the shaded area $z_1 - z_2 \lesssim 1$ only. For $V/V_c \gg 1$, the integration over the dimensionless energy difference z may be extended to infinity, while the integration over the sum Z gives just an overall factor V/V_c .

The matrix elements of the position operator y in this representation are given by

$$\begin{aligned} \langle n|y|m\rangle &= \frac{4 [(-1)^{m+n} - 1] m n}{(m-n)^2 (m+n)^2 \pi^2}, \quad n \neq m, \\ \langle n|y|n\rangle &= \frac{1}{2}. \end{aligned} \quad (3.50)$$

Consider first the asymptotic behaviour of $\langle \delta g^2 \rangle$ in the limit $V \gg V_c$. Only the term proportional to $|\Pi|^2$ needs to be kept in Eq. (3.42) to find the asymptotics, since the poles of $\text{Re } \Pi_z^2$ are in the same half of the complex z -plane. It is then easy to see that the leading contribution (proportional to V/V_c) is due only to Eq. (3.47) with the term second order in α of Eq. (3.48). Changing the variables z_1, z_2 to $Z \equiv (z_1 + z_2)/\sqrt{2}$, $z \equiv (z_1 - z_2)/\sqrt{2}$, the integration over Z gives just a factor V/V_c since the integrand of Eq. (3.47) only depends on z (see Fig. 3.4). Using the expansion (3.48), the term second

order in α is

$$\begin{aligned} \text{Tr } |\Pi_z|^2 \Big|_{\text{order } \alpha^2} &= \alpha^2 \sum_{m,n>0} \left[\frac{1}{|(n\pi)^2 - iz|^2} \langle n|y|m \rangle \frac{1}{|(m\pi)^2 - iz|^2} \langle m|y|n \rangle \right. \\ &\quad - \frac{1}{|(n\pi)^2 - iz|^2} \frac{1}{(n\pi)^2 + iz} \langle n|y|m \rangle \frac{1}{(m\pi)^2 + iz} \langle m|y|n \rangle \\ &\quad \left. - \frac{1}{|(n\pi)^2 - iz|^2} \frac{1}{(n\pi)^2 - iz} \langle n|y|m \rangle \frac{1}{(m\pi)^2 - iz} \langle m|y|n \rangle \right]. \end{aligned} \quad (3.51)$$

The integration over z may be extended to infinity. Evaluating the z -integrals via the residue theorem, the result is

$$\begin{aligned} \langle \delta g^2 \rangle_{V \gg V_c} &= -32 \frac{V}{V_c} \int_{-\infty}^{\infty} dz \frac{\partial^2}{\partial \alpha^2} \text{Tr } |\Pi_z|^2 \Big|_{\alpha=0} \\ &= c_1 \frac{V}{V_c}, \end{aligned} \quad (3.52)$$

with the coefficient

$$\begin{aligned} c_1 &= 64 \sum_{m,n>0} \frac{1}{\pi^5} \left[\frac{1}{n^4 (m^2 + n^2)} - \frac{1}{m^2 n^2 (m^2 + n^2)} \right] \langle n|y|m \rangle^2 \\ &= 7.785 \cdot 10^{-4}. \end{aligned} \quad (3.53)$$

Although the large- V asymptotics is in principle indeed of the form $\sim V/V_c$ obtained by Larkin and Khmel'nitskii, the corresponding numerical coefficient c_1 for the quasi-one-dimensional wire (which was not evaluated in Ref. [34]) is extremely small.

The evaluation of the full crossover behaviour of $\langle \delta g^2 \rangle$ as a function of (arbitrary) V/V_c can be done in a similar way, although the evaluations turn out to be more complicated. First, also the contribution of Eq. (3.46) must be taken into account. Second, in both Eqs. (3.46) and (3.47) the part $\sim \text{Re } \Pi_z^2$ cannot be neglected. All these contributions saturate towards constants as $V/V_c \rightarrow \infty$, but give nontrivial results in the crossover range. Finally, all the z -integrals in Eqs. (3.47) and (3.46) must be evaluated for finite (not infinite) voltage V . The detailed calculations are presented in Appendix D. The result is shown in Figs. 3.5 and 3.6.

As is seen from these plots, the linear behaviour (3.52) predicted by Larkin and Khmel'nitskii only emerges at very high voltages, $V/V_c \gtrsim 50$. Moreover, the corresponding coefficient c_1 is so small that the linear behaviour dominates the other terms only at $V/V_c \gtrsim 1000$. For $V/V_c \gtrsim 50$ the subleading contributions saturate but still numerically dominate the result for $\langle \delta g^2 \rangle$, which is well described by the following formula including a constant term in addition to the one linear in V ,

$$\langle \delta g^2 \rangle = \frac{8}{15} + c_0 + c_1 \frac{V}{V_c}, \quad V \gg V_c, \quad (3.54)$$

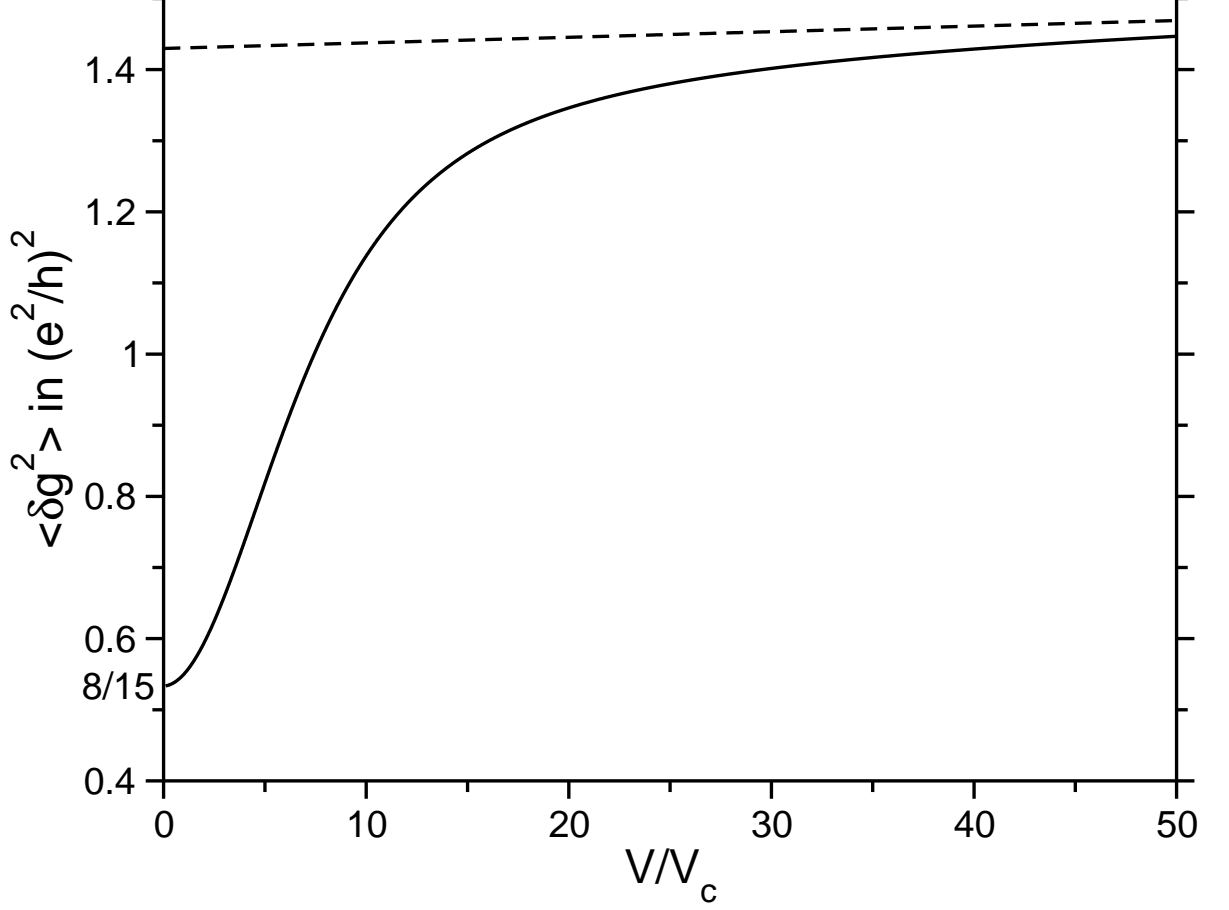


Figure 3.5: Variance of the differential conductance, $\langle \delta g^2 \rangle$, as a function of the applied voltage V normalized to the Thouless energy $eV_c = D/L^2$. The dashed line represents the high-voltage asymptotic behaviour, $\langle \delta g^2 \rangle = 8/15 + c_0 + c_1 V/V_c$ with $c_0 = 0.8964$ and $c_1 = 7.785 \cdot 10^{-4}$, see Eq. (3.54).

with c_1 given by Eq. (3.53) and $c_0 = 0.8964$. In other words, the extremely weak linear behaviour of $\langle \delta g^2 \rangle$ is almost indistinguishable from a saturation, while the crossover regime is very broad and features an increase of the conductance fluctuations by roughly a factor of 3.

Experimentally [86, 87] an increase of $\langle \delta g^2 \rangle$ has been observed in the range $V/V_c \lesssim 200$, followed by a decrease at higher voltages. The observed enhancement is clearly on a voltage scale too low for the asymptotic slope to be present and is due to

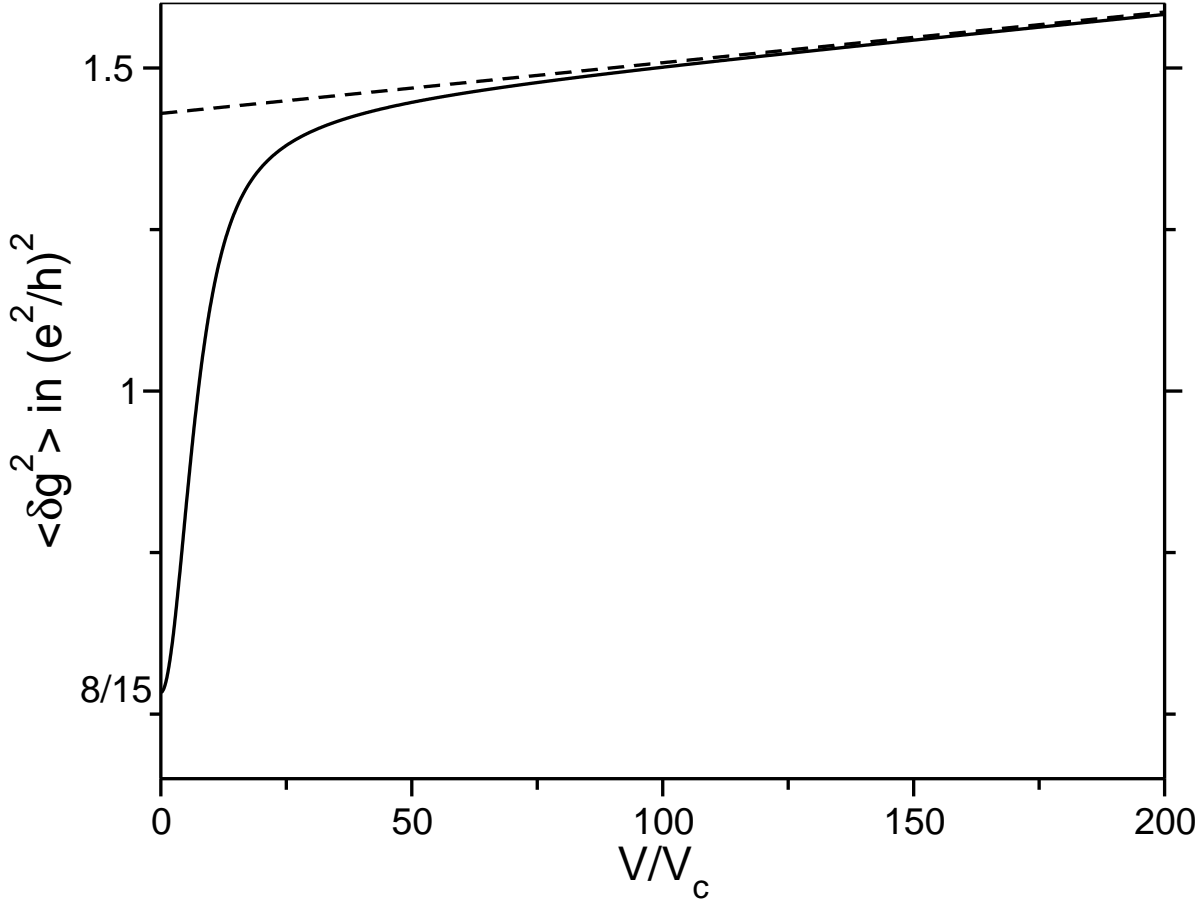


Figure 3.6: The same as Fig. 3.5, but plotted on a voltage scale where the convergence towards the asymptotic behaviour, Eq. (3.54), is clearly visible. Note the very large voltage scale on which this occurs.

the crossover contributions which have not been considered in Ref. [34]. As is shown in Section 3.2.3, in the intermediate-voltage range the result is slightly modified by finite temperature, further broadening the crossover and leading to an approximately linear behaviour over a certain voltage range before the asymptotic slope is realized. On the other hand, as will be discussed in Section 3.3, inelastic scattering processes limit the voltage range showing the linear behaviour (3.54) from above, potentially eliminating it entirely. The comparison with experiment is repeated in detail in Section 3.3.3, after the effects of temperature and of inelastic scattering have been discussed.

It is important to note that, although the calculation seems to be performed within a noninteracting picture, electron-electron interaction is contained implicitly in the def-

initiation of the electrochemical potential, which ultimately is a result of the screened Coulomb interaction. An evaluation of the conductance variance in the framework of scattering theory, using noninteracting electrons with different concentrations entering the sample from the left and right reservoirs, would miss the contributions (3.46) and (3.47) which give the voltage-dependent enhancement. The reason is that the system size is much larger than the screening length, and therefore the effect of changing the electrochemical potential in the reservoirs is to alter the potential profile in the wire rather than changing the concentration of electrons. A change of the electrochemical potential implies that all electrons in the relevant energy window of width V are affected and will explore different disorder realizations, leading to the enhancement of conductance fluctuations given by Eq. (3.54).

3.2.3 Effect of finite temperature

In this section, the effect of finite temperature on the nonequilibrium conductance fluctuations is considered. Throughout this section it is assumed that the temperature is not too high, so that at low voltages the inelastic scattering can be neglected (the dephasing length $L_\varphi(T)$ is large compared to the system size). The temperature however influences the result via the change of the electron distribution function in the reservoirs. At a finite temperature, Eqs. (3.45)–(3.47) are modified in the following way (now written in dimensionful voltages for clarity),

$$\langle \delta g^2 \rangle_0 = \frac{16}{e^2} \int d\epsilon_1 d\epsilon_2 \Delta f'_1 \Delta f'_2 \Xi_{\epsilon_1 - \epsilon_2} , \quad (3.55)$$

$$\begin{aligned} \langle \delta g^2 \rangle_1 &= \frac{16}{e^2} \int d\epsilon_1 d\epsilon_2 \Delta f'_1 \Delta f_2 \frac{\partial}{\partial V_2} \Xi_{\epsilon_1 - \epsilon_2} \\ &\quad + \frac{16}{e^2} \int d\epsilon_1 d\epsilon_2 \Delta f_1 \Delta f'_2 \frac{\partial}{\partial V_1} \Xi_{\epsilon_1 - \epsilon_2} , \end{aligned} \quad (3.56)$$

$$\langle \delta g^2 \rangle_2 = \frac{16}{e^2} \int d\epsilon_1 d\epsilon_2 \Delta f_1 \Delta f_2 \frac{\partial^2}{\partial V_1 \partial V_2} \Xi_{\epsilon_1 - \epsilon_2} , \quad (3.57)$$

where $\Delta f_i = f(\epsilon_i) - f(\epsilon_i + eV_i)$ (f is the Fermi function) and $\Delta f'_i = \frac{\partial}{\partial V_i} \Delta f_i$. Again the derivatives are taken at $V_1 = V_2 = V$.

Evaluation of the full crossover (i.e. the conductance fluctuations at arbitrary V/V_c and T/eV_c) is too cumbersome. Therefore this section deals with the limit $T \gg eV_c$, when the temperature strongly affects the conductance fluctuations at low voltages (in the opposite limit, $T \ll eV_c$, the temperature is irrelevant for all voltages, so that the results of Section 3.2.2 apply). This condition is reasonably fulfilled in most of relevant experiments, where the temperature is usually several times higher than the Thouless energy.

Further distinction is necessary between the two limits of low ($V \ll V_c$) and high ($V \gg V_c$) bias voltages. In the first case, $V/V_c \rightarrow 0$, only the voltage-independent contribution $\langle \delta g^2 \rangle_0$ survives. For $T \gg eV_c$ the thermal smearing strongly suppresses this

contribution compared to its zero-temperature (UCF) value. Eq. (1.12) is then modified to

$$\langle \delta g^2 \rangle_0 = 16 \int d\epsilon_1 d\epsilon_2 f'(\epsilon_1) f'(\epsilon_2) \frac{1}{L^4} \sum_n 2 \frac{1}{\left| q_n^2 - i \frac{(\epsilon_1 - \epsilon_2)}{D} \right|^2}, \quad (3.58)$$

where for the wire geometry $q_n = n\pi/L$, and only the leading contribution has been kept. Changing to the variables $\epsilon = (\epsilon_1 + \epsilon_2)/2D$, $\omega = (\epsilon_1 - \epsilon_2)/D$, the arguments of the Fermi distributions can be set to ϵ , since typical ω are of the order $eV_c \ll T$. The result then is

$$\begin{aligned} \langle \delta g^2 \rangle_0 &= 16 \frac{1}{6T} \frac{1}{L^4} \sum_n 2 \int d\omega \frac{1}{\left(\frac{\omega}{D} - iq_n^2 \right) \left(\frac{\omega}{D} + iq_n^2 \right)} \\ &= 16 \frac{1}{6T} \frac{1}{L^4} \sum_n 2 \frac{\pi D}{q_n^2}, \end{aligned} \quad (3.59)$$

and finally

$$\langle \delta g^2 \rangle_0 = \frac{8\pi}{9} \frac{eV_c}{T}, \quad T \gg eV_c. \quad (3.60)$$

In the opposite limit, when eV , $T \gg eV_c$ (the ratio eV/T can be arbitrary), the high-voltage behaviour (3.54) is modified by thermal smearing of the distribution function in the following way,

$$\langle \delta g^2 \rangle = a \left(\frac{eV}{T} \right) \cdot c_0 + b \left(\frac{eV}{T} \right) \cdot c_1 \frac{V}{V_c}, \quad V \gg V_c \quad (3.61)$$

where c_1 is given by Eq. (3.53) and the functions $a(eV/T)$ and $b(eV/T)$ have the form

$$a \left(\frac{eV}{T} \right) = 2 \int d\epsilon \left[f(\epsilon) - f(\epsilon + eV) \right] \left(-\frac{\partial f}{\partial \epsilon} \right) = \frac{\sinh \frac{eV}{T} - \frac{eV}{T}}{\cosh \frac{eV}{T} - 1}, \quad (3.62)$$

$$b \left(\frac{eV}{T} \right) = \frac{1}{eV} \int d\epsilon \left[f(\epsilon) - f(\epsilon + eV) \right]^2 = \coth \frac{eV}{2T} - \frac{2T}{eV}. \quad (3.63)$$

It is worth emphasizing that for any T at sufficiently high bias voltages the $T = 0$ result is recovered up to the missing offset of 8/15. The characteristic feature of the distribution function at high voltage is the double-step shape with a width eV of the intermediate step. This shape is responsible for the enhancement (3.54) of conductance fluctuations. In contrast to the zero-voltage (UCF) limit, the high-voltage contributions (3.56), (3.57) are only affected by high temperatures $T \sim eV$. In other words, in the noninteracting picture the enhancement of conductance fluctuations at high voltage is quite robust against thermal smearing and the variance of the differential conductance always increases monotonically.

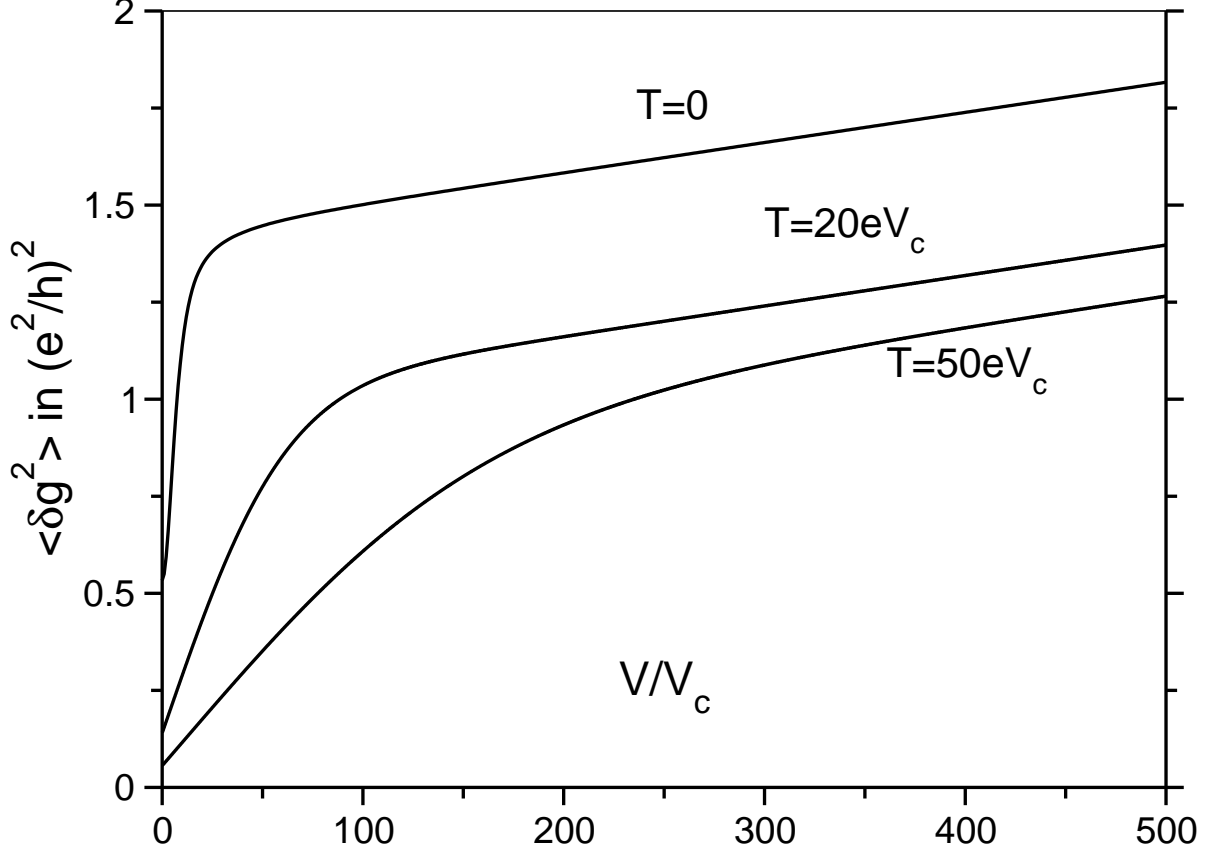


Figure 3.7: The voltage dependence of the conductance fluctuations as given by the interpolation formula (3.64), for the temperatures $T = 20eV_c$ and $T = 50eV_c$. The $T = 0$ result (see Figs. 3.5, 3.6) is also shown for comparison. It is clearly seen that only the offset (3.45), but not the slope of the asymptotic linear behaviour (3.53) is changed by the temperature, and the crossover towards the linear asymptotics is broadened on a voltage scale of the order of the temperature.

Adding the term $\langle \delta g^2 \rangle_0$, Eq. (3.60), to (3.61) results in the following interpolation formula, which is parametrically justified in the regime $V \gg V_c$ and has the correct limit at $V/V_c \rightarrow 0$:

$$\langle \delta g^2 \rangle = \frac{8\pi}{9} \frac{eV_c}{T} + \frac{\sinh \frac{eV}{T} - \frac{eV}{T}}{\cosh \frac{eV}{T} - 1} \cdot 0.8964 + \left[\coth \frac{eV}{2T} - \frac{2T}{eV} \right] \cdot 7.785 \cdot 10^{-4} \frac{V}{V_c} . \quad (3.64)$$

This formula can thus be used as a convenient approximation for $\langle \delta g^2 \rangle$ in the full range of voltages at $T \gg eV_c$. The resulting voltage dependence of the conductance fluctuations is shown in Fig. 3.7 for the temperatures $T = 20 \text{ eV}_c$ and $T = 50 \text{ eV}_c$. These theoretical results are compared with experimental data in Section 3.3.3 below.

3.3 Effect of Coulomb interaction at high voltage

3.3.1 Nonequilibrium noise: Boltzmann-Langevin approach

In quasi-onedimensional diffusive systems, dephasing is dominated by scattering processes with small energy transfers ($\omega \ll T$ in the case of temperature-driven fluctuations, and therefore $\omega \ll eV$ for high voltages $eV \gtrsim T$). This allows to replace the dynamically screened Coulomb interaction by a fluctuating classical potential acting on the electrons. At a high bias voltage, the fluctuations of the electric field can be described by an effective temperature $T_{\text{eff}}(V)$ which is defined below. Since the problem has a semiclassical character, it is feasible to use the Boltzmann-Langevin approach [9, 62, 68] to describe the field fluctuations. The fluctuations of the local current density \mathbf{j} can be expressed in the following way:

$$\delta \mathbf{j} = -iD\mathbf{q} \delta \rho + \sigma \delta \mathbf{E} + \delta \mathbf{j}^{\text{ext}} . \quad (3.65)$$

Here the first term on the right hand side of the equation is of diffusive origin and due to density fluctuations $\delta \rho$ and the second term is driven by fluctuations of the electric field $\delta \mathbf{E}$ via the conductivity $\sigma = e^2 \nu D$. The last term is due to elastic scattering from impurities. These Langevin fluctuations can be obtained from the fluctuation-dissipation theorem in equilibrium, while out of equilibrium they are known from shot noise theory [74]. The correlator of the Langevin current fluctuations in a wire is²

$$\langle \delta j_x^{\text{ext}}(x, t) \delta j_x^{\text{ext}}(x', t') \rangle = 2\sigma T_{\text{eff}} \delta(x - x') \delta(t - t') , \quad (3.66)$$

with the effective temperature $T_{\text{eff}}(x, V)$ given by

$$T_{\text{eff}} = \int d\epsilon n_\epsilon(x) [1 - n_\epsilon(x)] . \quad (3.67)$$

Here $n_\epsilon(x)$ is the electron distribution function which can (and in the present case will) be a nonequilibrium distribution. The shape of this function in the strong-dephasing regime addressed in this chapter deserves some additional thoughts.

It has been shown [29, 72] that in low dimensions the phase relaxation rate arising from electron-electron interaction greatly exceeds the energy relaxation rate. Therefore, in the regime of strong dephasing energy relaxation is still weak, $L_\varphi \ll L \ll L_\epsilon$. So to treat the regime of strong dephasing, in this section a sample with weak energy exchange

²The indices α, β denoting the measurements are suppressed. It is understood that $\delta_{\alpha\beta}$ should be inserted when two measurements are considered, which see independent configurations.

will be considered, which in a parametrically broad range of voltages features a double-step distribution function which is essentially identical to the noninteracting one. In Section 3.3.3 it is discussed how this assumption can be relaxed, based on the results from the calculation using the double-step distribution function which are performed in Section 3.3.2.

Using the double-step distribution function with Eq. (3.67), the effective temperature in the wire is found to be

$$T_{\text{eff}}(x) = eV \frac{x}{L} \left(1 - \frac{x}{L}\right) . \quad (3.68)$$

The effective temperature is position-dependent, taking its maximum in the middle of the wire and approaching zero at the contacts with the reservoirs.

The density fluctuations $\delta\rho$ can be expressed by the current fluctuations via the continuity equation,

$$\delta\rho = \frac{\mathbf{q}}{\omega} \delta\mathbf{j} . \quad (3.69)$$

The current fluctuations $\delta\mathbf{j}$ can be expressed by $\delta\mathbf{j}^{\text{ext}}$ in the following way: The potential fluctuations $\delta\phi$, which satisfy $\delta\mathbf{E} = -\nabla\phi$, are determined by the density fluctuations,

$$e^2 \delta\phi(\mathbf{q}) = \delta\rho(\mathbf{q}) U^{(0)}(q) , \quad (3.70)$$

where $U^{(0)}(|\mathbf{r} - \mathbf{r}'|) = e^2/|\mathbf{r} - \mathbf{r}'|$ is the bare Coulomb interaction. Substituting $\delta\rho$ and $\delta\mathbf{E}$ in Eq. (3.65) gives

$$\delta j_x = \frac{-i\omega}{-i\omega + Dq^2 [1 + \nu U^{(0)}(q)]} \delta j_x^{\text{ext}} . \quad (3.71)$$

For the metallic samples under consideration, $\nu U^{(0)}(q) \gg 1$ is satisfied. As a result, the field fluctuations δE_x are determined by the Langevin current fluctuations:

$$\sigma \delta E_x(q) = -\delta j_x^{\text{ext}}(q) , \quad q \neq 0 , \quad (3.72)$$

while the $q = 0$ component of δE_x is determined by the boundary conditions: At $T = 0$ there are no potential fluctuations at the contacts to the perfect reservoirs, and therefore the $q = 0$ -component of δE_x must vanish. At $T \ll eV$, the voltage-induced fluctuations dominate over the temperature-induced ones everywhere except in a very close vicinity of the reservoirs, which still allows to neglect thermal fluctuations in the calculation of the voltage-driven fluctuations. The electric field fluctuations in real space, taking the absence of the $q = 0$ component correctly into account, are therefore given by

$$\delta E_x(x) = -\frac{1}{\sigma} \left[\delta j_x^{\text{ext}}(x) - \frac{1}{L} \int dx \delta j_x^{\text{ext}}(x) \right] . \quad (3.73)$$

Using Eq. (3.66), the electric field correlator can now be obtained,

$$\langle \delta E_x(x) \delta E_x(x') \rangle = \frac{2}{\sigma} \left[T_{\text{eff}}(x) \delta(x - x') - \frac{1}{L} T_{\text{eff}}(x) - \frac{1}{L} T_{\text{eff}}(x') + \int \frac{d\tilde{x}}{L^2} T_{\text{eff}}(\tilde{x}) \right] , \quad (3.74)$$

(for convenience the factors $\delta_{\alpha\beta} \delta(t - t')$ are suppressed from now on), and the corresponding potential correlator $\langle \varphi \varphi \rangle$ is explicitly found by spatial integration after the insertion of the effective temperature.

3.3.2 Strong-dephasing limit

Inserting the effective temperature (3.68) into Eq. (3.74) and integrating over the spatial coordinates, the correlator of quasiclassical potential fluctuations is

$$\begin{aligned} \langle \varphi(x) \varphi(x') \rangle &= \frac{2}{\sigma} \left[\int_0^{x_<} d\tilde{x} T_{\text{eff}}(\tilde{x}) - \frac{x_<}{L} \int_0^{x_>} d\tilde{x} T_{\text{eff}}(\tilde{x}) \right. \\ &\quad \left. - \frac{x_>}{L} \int_0^{x_<} d\tilde{x} T_{\text{eff}}(\tilde{x}) + \frac{x_< x_>}{L^2} \int_0^1 d\tilde{x} T_{\text{eff}}(\tilde{x}) \right] \\ &= \frac{2}{\sigma} eV \frac{x_< (L - x_>)}{3L^3} \\ &\quad \times \left[x_< (L - x_<) + x_> (L - x_>) - \frac{L}{2} (x_> - x_<) \right], \quad (3.75) \end{aligned}$$

where $x_< = \min(x, x')$ and $x_> = \max(x, x')$. At this point it is convenient to switch to dimensionless variables $\theta = \varphi/eV_c$, $y = x/L$, $\tau = eV_c t$ (remember the suppressed $\delta(t - t')$). The correlator of the dimensionless potential θ is

$$\langle \theta(y) \theta(y') \rangle = \frac{2V}{3gV_c} y_< (1 - y_>) \left[y_< (1 - y_<) + y_> (1 - y_>) - \frac{(y_> - y_<)}{2} \right], \quad (3.76)$$

It is seen that the dimensionless parameter V/gV_c describes the strength of the inelastic processes. The results of Sections 3.2.2 and 3.2.3 are valid at voltages $V \lesssim gV_c$. In particular, voltages of order $V \sim g^2 V_c$ are excluded by this condition and cannot be treated in the noninteracting picture. These voltages would be required, as has been discussed in Section 3.1, to make conductance fluctuations exceed the conductance and thus result in appearance of regions with negative differential resistance in the IV characteristics. A preliminary conclusion therefore is that for voltages $V \gtrsim gV_c$, well below the range required for negative differential conductance, the enhancement discussed in Section 3.2.2 begins to compete with dephasing effects. A detailed analysis is needed to investigate whether the dephasing effects from electron-electron interaction alone can lead to the observed nonmonotonic behaviour of the conductance fluctuations as a function of the voltage. In the rest of this section the case of strong dephasing, $V \gg gV_c$, is considered.

As described in Section 3.2.2, at high voltages only the contribution $\sim |\Pi|^2$ of Eq. 3.42 gives the asymptotic behaviour. The CF diffusion propagator Π may be expressed as a path integral in the dimensionless variables $y = x/L$, $\tau = eV_c t$, $\theta = \phi/eV_c$ introduced

in the previous section,

$$\begin{aligned}
 \text{Tr } |\Pi_z|^2 &= \int_0^1 dy_1 dy_2 \int_0^\infty d\tau_1 d\tau_2 \exp\{iz(\tau_1 - \tau_2)\} \int_{\xi_1(0)=y_2}^{\xi_1(\tau_1)=y_1} \mathcal{D}[\xi_1(t_1)] \int_{\xi_2(0)=y_2}^{\xi_2(\tau_2)=y_1} \mathcal{D}[\xi_2(t_2)] \\
 &\times \exp \left\{ \int_0^{\tau_1} dt_1 \left[-\frac{\dot{\xi}_1^2}{4} - \frac{i(V_1 - V_2)}{V_c} \xi_1(t_1) - i\theta[\xi_1(t_1), t_1] \right] \right. \\
 &\quad \left. + \int_0^{\tau_2} dt_2 \left[-\frac{\dot{\xi}_2^2}{4} + \frac{i(V_1 - V_2)}{V_c} \xi_2(t_2) + i\theta[\xi_2(t_2), t_2] \right] \right\} . \quad (3.77)
 \end{aligned}$$

At sufficiently high voltage $V \gg gV_c$, this path integral is dominated by pairs of paths which stay close to each other, $|\xi_1(t) - \xi_2(t)| \ll 1$, allowing to expand the dephasing terms in the action in $|\xi_1(t) - \xi_2(t)|$. In this regime the averaging over Gaussian fluctuations using Eq. (3.76) and $\langle \exp\{i\theta\} \rangle = \exp\{-\langle \theta^2 \rangle / 2\}$ results in

$$\begin{aligned}
 \langle \text{Tr } |\Pi_z|^2 \rangle &= \int_0^1 dy_1 dy_2 \int_0^\infty d\tau_1 d\tau_2 \exp\{iz(\tau_1 - \tau_2)\} \int_{\xi_1(0)=y_2}^{\xi_1(\tau_1)=y_1} \mathcal{D}[\xi_1(t_1)] \int_{\xi_2(0)=y_2}^{\xi_2(\tau_2)=y_1} \mathcal{D}[\xi_2(t_2)] \\
 &\times \exp \left\{ \int_0^{\tau_1} dt_1 \left[-\frac{\dot{\xi}_1^2}{4} - \frac{i(V_1 - V_2)}{V_c} \xi_1(t_1) \right] \right. \\
 &\quad + \int_0^{\tau_2} dt_2 \left[-\frac{\dot{\xi}_2^2}{4} + \frac{i(V_1 - V_2)}{V_c} \xi_2(t_2) \right] \\
 &\quad - \frac{2V}{gV_c} F(y_2) |\tau_1 - \tau_2| \\
 &\quad \left. - \frac{2V}{gV_c} \int_0^{\min(\tau_1, \tau_2)} dt |\xi_1(t) - \xi_2(t)| f(y_2) \right\} , \quad (3.78)
 \end{aligned}$$

where

$$F(y) = \langle \theta(y)^2 \rangle = \frac{2}{3} [y_2(1 - y_2)]^2 \quad (3.79)$$

and

$$f(y) = \left. \frac{\partial \langle [\theta(y) - \theta(y + \xi)]^2 \rangle}{\partial \xi} \right|_{\xi=0} = y(1 - y) . \quad (3.80)$$

Note that, within the high-voltage approximation of expanding in the separation of the paths, the factors $F(y_2)$ and $f(y_2)$ in the dephasing terms could be equally well written

as $F(y_1)$ and $f(y_1)$, respectively. The last two terms in the exponent of Eq. (3.78) represent the dephasing effects induced by the applied voltage. Clearly, paths ξ_1, ξ_2 which experience large separations $|\xi_1(t) - \xi_2(t)| \sim 1$ cannot contribute significantly to the path integral since their action, due to the last term representing dephasing during the propagation of both diffusons, is large in the parameter $V/gV_c \gg 1$. The next to last term represents the dephasing during a small time difference $|\tau_1 - \tau_2|$ between the durations of the two diffuson trajectories and is of order $1/g$, since after the integration over the dimensionless frequency z the characteristic values of $|\tau_1 - \tau_2|$ are of order V_c/V , cancelling the voltages from the prefactor of this term. It is therefore justified to keep only the second dephasing term in Eq. (3.78).

Instead of calculating Ξ_z , Eq. (3.77), it is convenient to take advantage of the Fourier transformation

$$\Xi_z = 2 \int_0^\infty d\tau \exp\{iz\tau\} \tilde{\Xi}(\tau) . \quad \int_{-\infty}^\infty dz \Xi_z = 2\pi \tilde{\Xi}(0) \quad (3.81)$$

The leading high-voltage contribution (3.47) to the conductance variance,

$$\langle \delta g^2 \rangle_2 = 16 V_c^2 \frac{\partial^2}{\partial V_1 \partial V_2} \Big|_{V_1=V_2=V} \int_0^{V/V_c} dz_1 dz_2 \Xi_{z_1-z_2}(V_1, V_2) \quad (3.82)$$

can be written as (using $z = z_1$ and $\epsilon = z_1 - z_2$)

$$\begin{aligned} \langle \delta g^2 \rangle_2 &= 16 V_c^2 \frac{\partial^2}{\partial V_1 \partial V_2} \Big|_{V_1=V_2=V} \int_0^{V/V_c} dz \int_{z-V/V_c}^z d\epsilon \Xi_\epsilon \\ &= 16 V_c^2 \frac{\partial^2}{\partial V_1 \partial V_2} \Big|_{V_1=V_2=V} \left[\int_{-V/V_c}^0 d\epsilon \left(\frac{V}{V_c} + \epsilon \right) \Xi_\epsilon + \int_0^{V/V_c} d\epsilon \left(\frac{V}{V_c} - \epsilon \right) \Xi_\epsilon \right] \\ &= 16 V_c^2 \frac{\partial^2}{\partial V_1 \partial V_2} \Big|_{V_1=V_2=V} \int_{-V/V_c}^{V/V_c} d\epsilon \left[\frac{V}{V_c} - |\epsilon| \right] \Xi_\epsilon \end{aligned} \quad (3.83)$$

Substituting the Fourier transformation (3.81) into this equation, the integration over ϵ

is easily done:

$$\begin{aligned}
 \langle \delta g^2 \rangle_2 &= 32 V_c^2 \frac{\partial^2}{\partial V_1 \partial V_2} \Big|_{V_1=V_2=V} \int d\tau \tilde{\Xi}(\tau) \\
 &\times \left[\frac{V}{V_c \tau} \sin(\epsilon \tau) \Big|_0^{V/V_c} - \left(\frac{\epsilon}{\tau} \sin(\epsilon \tau) + \frac{1}{\tau^2} \cos(\epsilon \tau) \right) \Big|_0^{V/V_c} \right] \\
 &= 64 V_c^2 \frac{\partial^2}{\partial V_1 \partial V_2} \Big|_{V_1=V_2=V} \int_{-\infty}^{\infty} d\tau \tilde{\Xi}(\tau) \frac{1}{\tau^2} \sin^2 \left(\frac{V \tau}{2 V_c} \right)
 \end{aligned} \tag{3.84}$$

For high voltages $V \gg V_c$, the approximation

$$\frac{1}{\tau^2} \sin^2 \left(\frac{V \tau}{2 V_c} \right) \simeq \frac{\pi V}{2 V_c} \delta(\tau) \tag{3.85}$$

may be made, and therefore the asymptotic behaviour of the high-voltage term³ (3.47) at $V \gg g V_c$ is given by

$$\langle \delta g^2 \rangle_2 = 32 \pi V V_c \frac{\partial^2}{\partial V_1 \partial V_2} \Big|_{V_1=V_2=V} \tilde{\Xi}(0) , \tag{3.86}$$

where $\tilde{\Xi}(0) \approx \text{Tr} [2 |\Pi_0|^2]$ (see Eq. (3.42), again as explained in Section 3.2.2 the second term does not contribute to the leading behaviour) is twice Eq. (3.78) with τ_1 set to τ_2 . Transforming to the sum and the difference of the coordinates, $\zeta_1 = (\xi_1 + \xi_2)/\sqrt{2}$ and $\zeta_2 = (\xi_1 - \xi_2)/\sqrt{2}$, it is seen that the path integral over the sum ζ_1 is not affected by the fluctuations and is equal to $\Theta(\tau)/\sqrt{2}$, while the path integral over the difference ζ_2 can be transformed back to the solution of a differential equation:

$$\langle \delta g^2 \rangle_2 = 32 \sqrt{2} \pi V V_c \frac{\partial^2}{\partial V_1 \partial V_2} \Big|_{V_1=V_2=V} \int_0^1 dy \int_0^\infty d\tau I_y(0, \tau) , \tag{3.87}$$

where $I_y(\zeta, \tau)$ obeys the equation

$$\left[\frac{\partial}{\partial \tau} - \frac{\partial^2}{\partial \zeta^2} + i \sqrt{2} \frac{(V_1 - V_2)}{V_c} \zeta + \frac{2V}{g V_c} \sqrt{2} y(1-y) |\zeta| \right] I_y(\zeta, \tau) = \delta(\zeta) \delta(\tau) . \tag{3.88}$$

The dimensions can be scaled out of the differential equation by a transformation to the variables

$$t = p^{2/3} \tau \tag{3.89}$$

$$\eta = p^{1/3} \xi \tag{3.90}$$

$$\mathcal{I} = p^{-1/3} I \tag{3.91}$$

$$v = i \sqrt{2} \frac{(V_1 - V_2)}{V_c p} , \tag{3.92}$$

³it is verified later that this term remains the dominating one at strong dephasing.

where

$$p = \frac{2V}{gV_c} \sqrt{2} y(1-y) . \quad (3.93)$$

Substituting the rescaled variables into Eq. (3.88),

$$\langle \delta g^2 \rangle_2 = 64\sqrt{2} \pi \frac{V}{V_c} \frac{\partial^2}{\partial v^2} \int_0^1 \frac{dy}{p^{7/3}} \int_0^\infty dt \mathcal{I}_y(0, t) , \quad (3.94)$$

and performing the integration over t results in

$$\langle \delta g^2 \rangle_2 = 8\pi \left(\frac{V_c}{V} \right)^{4/3} g^{7/3} \frac{\partial^2}{\partial v^2} Q(v, 0) \Big|_{v=0} \int_0^1 \frac{dy}{[y(1-y)]^{7/3}} , \quad (3.95)$$

where Q satisfies

$$\left\{ -\frac{\partial}{\partial \eta^2} + |\eta| + v\eta \right\} Q(v, \eta) = \delta(\eta) . \quad (3.96)$$

It is seen that the integral over the position y diverges in the vicinity of the reservoirs $y \rightarrow 0, 1$. This is because the expansion in small $|\xi_1 - \xi_2|$ is not valid in these regions since the effective temperature, Eq. (3.68) vanishes when the reservoirs are approached. The separation of the paths can therefore be larger in the vicinity of the reservoirs and these small regions with very weak dephasing dominate the conductance fluctuations.

An exact evaluation of the path integral (3.78) without the expansion in $|\xi_1 - \xi_2|$ would lead to the solution of a two-dimensional Schrödinger-type differential equation instead of the one-dimensional one (3.88). The result can however be obtained up to a numeric prefactor in the following way: The integral in Eq. (3.95) should be cut off at a distance Ly_c to the reservoirs, which is of the order of the local phase-breaking length corresponding to the local effective temperature at this position. This leads to the following self-consistency condition for the cutoff y_c ,

$$Ly_c \sim L_\varphi(y_c) = [D\tau_\varphi(T_{\text{eff}}(y_c))]^{1/2} , \quad (3.97)$$

where $T_{\text{eff}}(y) = eVy(1-y)$ and $\tau_\varphi(T_{\text{eff}}) \sim (D\nu^2/T_{\text{eff}}^2)^{1/3}$. The cutoff is found to be

$$y_c \sim \left(\frac{gV_c}{V} \right)^{1/4} \quad (3.98)$$

and the amplitude of conductance fluctuations, dominated by the segments of length $\sim Ly_c$ next to the contacts, is

$$\langle \delta g^2 \rangle_2 \sim g^2 \frac{V_c}{V} , \quad \frac{V}{V_c} \gg g . \quad (3.99)$$

A smooth matching of this asymptotic high-voltage behaviour and the noninteracting case (3.61) shows a maximum at $V/V_c \sim g$ before the decay towards the $1/V$ power law sets in. It is necessary to verify that the two subleading terms, $\langle \delta g^2 \rangle_0$ and $\langle \delta g^2 \rangle_1$, remain smaller than the leading term, $\langle \delta g^2 \rangle_2$, when the regime of strong dephasing is entered. This is done in Appendix E.

The result (3.99) can be understood qualitatively in the following way: Let the wire be split in incoherent segments of length L_φ , which is *not* constant along the wire. The variance of the conductance of one segment can in analogy to Eq. (3.57) be estimated as

$$\langle \delta g^2(L_\varphi) \rangle \sim \frac{1}{eV_c(L_\varphi)} \int d\epsilon [\Delta f_{L_\varphi}(\epsilon)]^2, \quad (3.100)$$

where $eV_c(L_\varphi) = D/L_\varphi^2$ is the Thouless energy corresponding to the length L_φ , and $\Delta f_{L_\varphi}(\epsilon)$ is the difference between the distribution functions at the left and right boundaries of the segment of length L_φ . For the double-step distribution function with position-dependent intermediate plateau, $\Delta f_{L_\varphi}(\epsilon)$ is equal to L_φ/L for energies ϵ in the window of width eV given by the reservoir potentials, and zero otherwise, resulting in

$$\langle \delta g^2(L_\varphi) \rangle \sim \frac{1}{eV_c(L_\varphi)} eV \left(\frac{L_\varphi}{L} \right)^2. \quad (3.101)$$

Expressing $V_c(L_\varphi)$ through the Thouless voltage of the entire sample V_c , $V_c(L_\varphi)/V_c = (L/L_\varphi)^2$, the conductance fluctuations of the single segment are given by

$$\langle \delta g^2(L_\varphi) \rangle \sim \frac{V}{V_c} \left(\frac{L_\varphi}{L} \right)^4. \quad (3.102)$$

Since the resistances of the segments are additive, a fluctuation $\delta g(L_\varphi)$ of the conductance of a single segment induces a fluctuation δg of the conductance of the whole sample given by

$$\delta g \sim \left(\frac{L_\varphi}{L} \right)^2 \delta g(L_\varphi), \quad (3.103)$$

so that

$$\langle \delta g^2 \rangle \sim \left(\frac{L_\varphi}{L} \right)^8 \frac{V}{V_c}. \quad (3.104)$$

Replacing L_φ by the local dephasing length of the segments adjacent to the reservoirs (where the dephasing is weakest), $L_\varphi = Ly_c$ with $y_c \sim (V_c/V)^{1/4}$ given by Eq. (3.98), the voltage dependence of the result (3.99) is reproduced and thus supported by a physical picture.

3.3.3 Comparison with experimental data

In this section, the results calculated in Section 3.3.2 are compared with measurements performed at the University of Basel [86, 87]. In these experiments, magnetoconductance traces of a gold wire with a length of $L = 1.5 \mu\text{m}$ and a Thouless energy of $eV_c \equiv D/L^2 = 3.4 \mu\text{eV}$ were taken at a moderately high temperature of $T = 300 \text{ mK} \simeq 7.6 eV_c$ over a voltage range up to $V \simeq 3.7 \text{ mV} \approx 1000 V_c$. The dimensionless conductance of the wire was $g \approx 1400$. Fig. 3.8 shows the theoretical results for both the non-interacting limit (3.64) at not too high voltages and the strong-dephasing limit (3.99) at very high voltages, compared with the measured data. It is seen that there is a reasonably good agreement between the theory and the experiment in the overall shape of $\langle \delta g^2 \rangle(V/V_c)$ and in the magnitude of its enhancement at the maximum. The voltage where the maximum is positioned also is of the correct order of magnitude, $V \sim gV_c$.

The main deviation is that the initial increase of the conductance variance is considerably less steep than on the theoretical curve. This may be attributed to the following factors: First, the full (low-voltage) curve in Fig. 3.8 is obtained from the formula (3.61), which takes into account the crossover at $eV \sim T$ but not the crossover at $V \sim V_c$. Although the temperature was larger than eV_c by a factor ~ 8 in the experiment, it has been calculated in Section 3.2.2 that the V/V_c crossover region is rather broad, extending up to $V/V_c \sim 50$. Thus the V/V_c crossover is expected to overlap with the eV/T crossover under the experimental conditions, making the total crossover region broader. Second, in the low-voltage region the effect of dephasing has not been taken into account (the full curve is the result for noninteracting electrons). It is easy to see from Eq. (3.78) that, as the voltage is increased and dephasing effects start to set in, this will first lead to a relative correction of order V/gV_c , which will provide a smooth matching with the strong-dephasing (high voltage) regime, Eq. (3.99).

An important conclusion is that the linear behaviour (3.52) could not be accessed reliably in this experiment, since it requires, in view of the very small value of the numerical coefficient (3.53), very large voltages $V/V_c \gtrsim 1000$, while the dephasing was setting in at voltages several times smaller. The observed strong enhancement of the conductance variance is due to the same physics as the asymptotic behaviour found by Larkin and Khmelnitskii [34], resulting from changes of the electrochemical potential affecting all electrons which contribute to conduction. However, the observed behaviour of the conductance fluctuations is not due to the high-voltage asymptotics (3.1), but rather a smeared out version of the steep theoretical increase in the crossover region preceding the linear asymptotics. A reliable observation of the linear behaviour predicted by Larkin and Khmelnitskii thus requires samples with still larger values of the dimensionless conductance g in order to better separate the crossover coming from low voltages and the crossover to the asymptotic decay.

At high voltages, the experimentally observed decay of the conductance fluctuations is consistent with the predicted $1/V$ decay (3.99). Indeed, the experimentally obtained

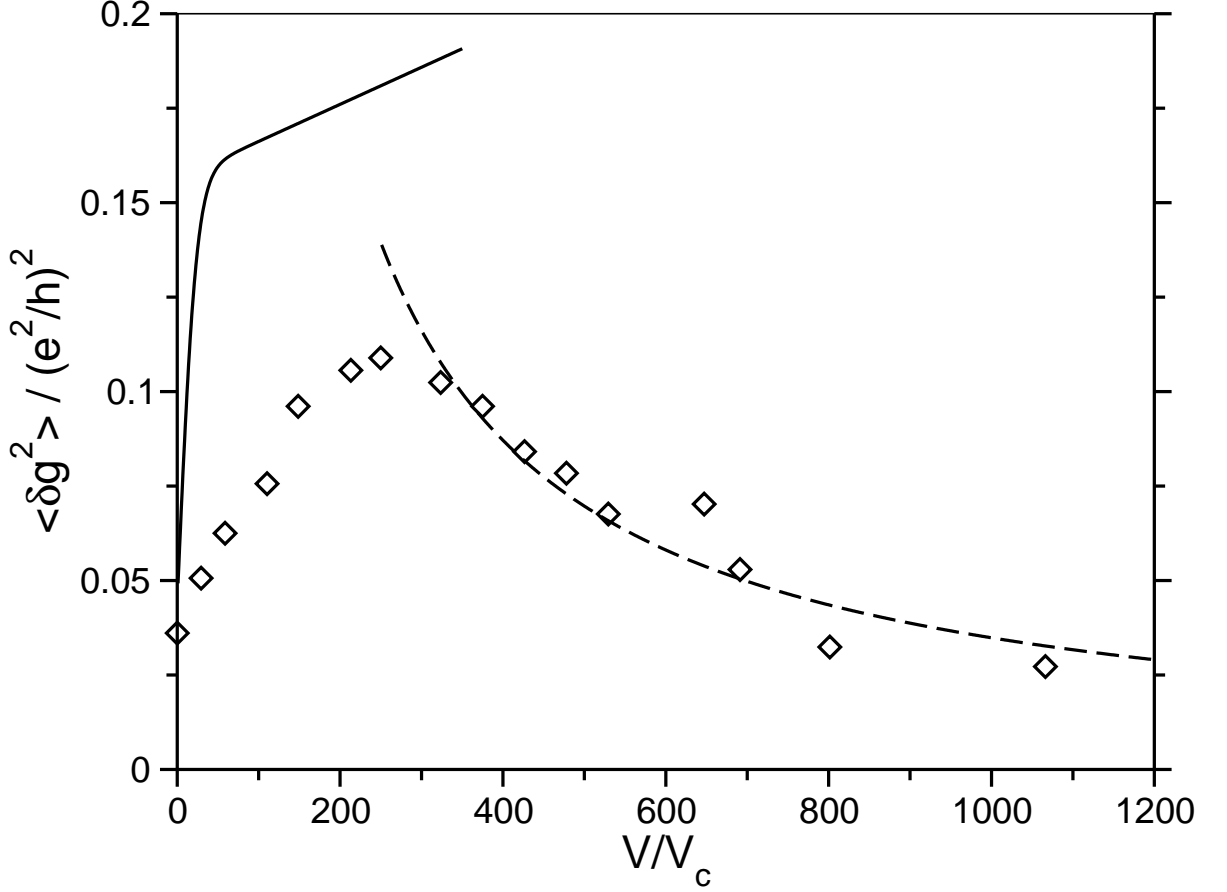


Figure 3.8: Comparison of the results of Section 3.3.2 with experimental data taken from Refs. [86, 87]. The diamonds are the data from Fig. 5.4 of Ref. [87]. The solid line represents the interpolation formula (3.64), multiplied by an overall factor of 1/8 to account for the strong spin-orbit interaction in gold and the broken time-reversal symmetry at high magnetic fields. The dashed line represents the asymptotic suppression, Eq. (3.99), with the numerical coefficient adjusted to fit the data for high voltages.

value $\gamma = 1.28 \pm 0.12$ of the exponent of the power-law decay $\langle \delta g^2 \rangle \propto V^{-\gamma}$ is in good agreement with the theoretical result $\gamma = 1$, taking into account that the measurements do not extend very far into the corresponding voltage range $V \gg V_c$ where the theoretical result is valid. The results obtained in Section 3.3.2 thus disagree with the conclusion of the authors of Ref. [86] who argued, based on a naive estimate of the dephasing effect, that the electron-electron scattering was not sufficient to suppress the

Larkin-Khmelnitskii enhancement mechanism to the observed fall-off, and concluded that this behaviour would be due to electron-phonon scattering. On the contrary, the measurements performed in the Basel group are quite well compatible with the effect of electron-electron scattering leading to the results presented in Section 3.3.2.

Seeing that the range of the asymptotic $1/V$ power law has hardly been entered, it should be noted that experiments on samples with lower conductances might give more data in the strong-dephasing range $V \gg gV_c$ and thus allow a more accurate experimental determination of the exponent of the power law.

Although throughout the calculations a sample with weak energy exchange has been considered, the results also apply to samples with a higher level of energy exchange: In the strong-dephasing limit the conductance fluctuations (3.99) are dominated by regions close to the contacts, where the distribution function is strongly influenced by the Fermi distributions in the respective nearby reservoirs [80]. So although there may be a considerable amount of energy exchange, in the regions relevant for the conductance fluctuations the distribution function retains a shape quite close to the double-step shape. Therefore the results of Section 3.3.2 remain valid even if a sample is considered which features a thermalized distribution function in its main part.

In a similar experiment performed in Karlsruhe [78], measurements on the voltage-dependence of Aharonov-Bohm oscillations are reported. The qualitative behaviour of the oscillations as a function of the current through the sample (and therefore of the voltage) is similar to the results for wire geometry. In particular, the oscillation amplitude increases towards a maximum which is located at a voltage of the order of gV_c , followed by a suppression at higher voltages. The position of the maximum at a voltage of order gV_c is confirmed by a second measurement on a sample with much longer leads. In view of the results obtained in Section 3.2.2 for the noninteracting regime, the observed increase of the oscillation amplitude should also for this experiment be attributed to the crossover regime rather than the asymptotics found by Larkin and Khmelnitskii. It should be noted that the calculations performed in the strong-dephasing regime for the wire geometry cannot be directly transferred to the ring geometry since the Aharonov-Bohm oscillations are due to the global geometry of the sample and cannot be extracted from a treatment of the regions in the proximity of the reservoirs.

3.4 Summary

In this chapter the amplitude of mesoscopic fluctuations of the differential conductance of a metallic wire has been calculated for arbitrary bias voltages.

For the noninteracting regime the variance of the conductance $\langle \delta g^2 \rangle$ increases monotonically with the applied voltage V . The origin of this behaviour is that changes of the electrochemical potential influence all electrons in the available energy window of width V . Asymptotically the linear behaviour first predicted by Larkin and Khmelnitskii is confirmed, although with a surprisingly small parameter and at very large voltages

only. Formally subleading contributions give an enhancement which dominates over the linear asymptotics up to surprisingly high voltages, covering all the range $V \lesssim gV_c$ in which inelastic effects can be neglected. The asymptotic slope is thus very difficult to access experimentally.

The existence of an electrochemical potential on diffusive length scales is assumed in the derivation of the voltage-induced enhancement. This implicitly takes into account some level of interaction, because the electrochemical potential arises from the screened Coulomb interaction on length scales much larger than the screening length. A truly noninteracting calculation in the framework of scattering theory would miss this effect.

The effect of finite temperature on the enhancement of the conductance fluctuations is quite limited. The crossover regime broadens and assumes a range $eV \sim T$ if $T \gg eV_c$. Additionally, the offset of the asymptotic linear behaviour is changed. However the asymptotic slope is not affected, since it is due to features of the distribution function on the scale V , while thermal broadening happens only on the scale T .

The effect of dephasing induced by the Coulomb interaction has been examined using a quasiclassical approach. The effect of inelastic collisions has been found to become important for voltages $V \gtrsim gV_c$, so that the regime $V \gtrsim g^2V_c$, in which negative differential conductance could be expected in the noninteracting picture, is excluded. With the effect of inelastic processes taken into account, $\langle \delta g^2 \rangle$ becomes a nonmonotonic function of V , reaching a maximum at a voltage $V \sim gV_c$ and decaying $\sim 1/V$ for $V \gg gV_c$. The effect of inelastic processes is distributed in a non-uniform way along the wire. In the strong-dephasing regime the conductance fluctuations are dominated by coherent regions of length $\sim L (gV_c/V)^{1/4}$ adjacent to the reservoirs, where the dephasing effect is small.

The calculated result are in good agreement with available experimental data, reproducing both the nonmonotonic voltage dependence and the correct scales of voltages and conductance fluctuations.

4 Effect of gauge-field interactions on quantum interference

4.1 Coupling to transverse gauge fields

In addition to electric potential fluctuations, electrons in disordered metals are subject also to transverse gauge field fluctuations. The full correlator of electromagnetic fluctuations is for $\omega \ll T$ given by [6, 18, 29, 46]¹

$$\langle a_\alpha a_\beta \rangle_{\mathbf{k},\omega} = \frac{2T}{\sigma} \frac{c^2}{\omega^2} \left[\delta_{\alpha\beta}^\perp(\mathbf{k}) \frac{1}{1 + \left(\frac{c^2 k^2}{4\pi\sigma\omega} \right)^2} + \delta_{\alpha\beta}^\parallel(\mathbf{k}) \right] , \quad (4.1)$$

with the transverse and longitudinal projectors

$$\delta_{\alpha\beta}^\perp(\mathbf{k}) = \delta_{\alpha\beta} - \frac{k_\alpha k_\beta}{k^2} \quad (4.2)$$

$$\delta_{\alpha\beta}^\parallel(\mathbf{k}) = \frac{k_\alpha k_\beta}{k^2} , \quad (4.3)$$

and the light velocity c (written for clarity in this equation only). The longitudinal part of Eq. (4.1) can be gauge transformed [72] to represent a fluctuating scalar potential φ with the correlator

$$\langle \varphi \varphi \rangle_{\mathbf{k},\omega} = \frac{2T}{\sigma} \frac{1}{q^2} \quad (4.4)$$

in momentum space, or, in real space, Eq. (2.9)². Therefore, in the following only the transverse part of the correlator (4.1) will be considered,

$$\langle a_\alpha a_\beta \rangle_{\mathbf{k},\omega} = \frac{2T}{\sigma} \frac{1}{\omega^2 + \left(\frac{k^2}{4\pi\sigma} \right)^2} \delta_{\alpha\beta}^\perp(\mathbf{k}) . \quad (4.5)$$

¹Ref. [18] contains a typographical error in this equation.

²the indices denoting the measurements in that equation should not be confused with the vector indices in Eq. (4.1).

Using the Einstein relation $\sigma = e^2 \nu D$, the transverse part of the electromagnetic correlator (4.1) is seen to be small in the parameter v_F/c relative to the longitudinal one, and usually is safe to neglect. A fluctuating gauge field with the correlator of a form similar to (4.5) also occurs in another situation: In the Composite-Fermion model of the fractional Quantum Hall effect [45], electrons are converted to so-called Composite Fermions by attachment of an even number (for half filling, two) of magnetic flux quanta. The Composite Fermions experience an average magnetic field which is reduced by the number of flux quanta attached to them, and vanishes for Composite Fermions containing two flux quanta when the external magnetic field corresponds to half filling of the lowest Landau level.

In a field-theoretical description [47], the Composite Fermions are obtained from electrons by a statistical transformation, which leads to the appearance of a fictitious Chern-Simons gauge field coupling to the Composite Fermions. Unlike the coupling of electrons to magnetic fluctuations (4.1), the coupling of composite fermions to the Chern-Simons fluctuations is not small, but of order unity. The effect of the gauge field interaction may therefore greatly exceed the effect of the Coulomb interaction.

Although the average magnetic field seen by the composite fermions is cancelled by the Chern-Simons gauge field at half filling, fluctuations of the Chern-Simons field play an important role: Impurities in the metal (which by themselves represent only scalar disorder) are screened by the composite fermions, resulting in a static random gauge field. Additionally, the random motion of the composite fermions, which carry flux quanta of the gauge field, induces dynamic fluctuations of the gauge field. A treatment of the gauge-field fluctuations in the random-phase approximation (RPA) has been developed in Ref. [52] (reviews can be found e.g. in Refs. [67, 71], for work related more closely to the current chapter see also Refs. [56, 58, 59, 61, 63, 103]). The transverse part of the gauge field correlator at RPA level has the form

$$\langle a_\alpha a_\beta \rangle_{\mathbf{k},\omega} = \frac{2T}{\sigma} \frac{1}{\omega^2 + \left(\frac{\chi(k)k^2}{\sigma} \right)^2} \delta_{\alpha\beta}^\perp(\mathbf{k}) , \quad (4.6)$$

which is of the same form as the transverse electromagnetic correlator (4.5) if a short-range interaction is considered, which leads to a constant susceptibility χ [52, 59, 63]. When the conductivity is large, Eq. (4.6) is sharply peaked around $\omega = 0$, allowing for the static approximation which collects all the weight in a δ -function. The result for the case of short-range interaction is

$$\langle a_\alpha a_\beta \rangle_{\mathbf{k},\omega} = \frac{T}{\chi k^2} \delta_{\alpha\beta}^\perp(\mathbf{k}) 2\pi\delta(\omega) . \quad (4.7)$$

This is equivalent to a static random magnetic field h with the correlator

$$\begin{aligned}\langle h h \rangle_{\mathbf{k}} &= \frac{T}{\chi} , \\ \langle h(\mathbf{r}) h(\mathbf{r}') \rangle &= \frac{T}{\chi} \delta(\mathbf{r} - \mathbf{r}') .\end{aligned}\tag{4.8}$$

The gauge field correlator (4.7) will be considered in the main calculations of this chapter. The validity of the static approximation and the possibility of relaxing it will be discussed in more detail in Sections 4.4.1 and 4.6.

4.2 Previous results on dephasing in fermion-gauge field systems

The path integral for the CF diffusion propagator in the presence of quasistatic gauge field fluctuations $\mathbf{a}(\mathbf{r}, t)$ can be written in analogy to Eq. (2.14),

$$\mathcal{D}^{12}(\mathbf{r}_1, \mathbf{r}_2) = \int_0^\infty dt \int_{\mathbf{r}_2}^{\mathbf{r}_1} \mathcal{D}[\mathbf{r}(t)] \exp \left\{ - \int_0^t dt' \left[\frac{\dot{\mathbf{r}}^2(t')}{4D} + ie \dot{\mathbf{r}} \cdot [\mathbf{a}_1[\mathbf{r}(t'), t'] - \mathbf{a}_2[\mathbf{r}(t'), t']] \right] \right\} .\tag{4.9}$$

Unlike Eq. (2.14) the action in Eq. (4.9) is nonlocal in time due to the slow dynamics of the gauge field. A treatment in the path-integral formalism thus is much less convenient than for the situation with Coulomb interaction. Examination of the path integral however shows some properties of the system: For example, a static gauge field drops out of Eq. (4.9), as expected. The two measurements may however be separated by a time which is not short on the scale of the gauge field dynamics. If the gauge field configurations \mathbf{a}_1 , \mathbf{a}_2 are completely uncorrelated, but the gauge field can be regarded as static on the timescale of the electron motion, the dephasing term in the action of Eq. (4.9) is a purely geometrical effect without any reference to the dynamics of the trajectories, as may be expected from motion in a static random magnetic field with the correlator (4.8).

Moreover, it is easy to see that for a closed trajectory (or a pair of trajectories forming a closed loop), a static uniform gauge field drops out, as expected by gauge invariance. The path integral formulation also allows to derive a relation between weak localization and mesoscopic conductance fluctuations in a similar way as has been done in Section 2.3 for Coulomb interaction. This calculation is presented in Section 4.3. As a result, the weak localization correction may be calculated instead of the amplitude of mesoscopic conductance fluctuations wherever it is more convenient.

For the static case (4.7), Aronov and Wölfle [53, 55] obtained the Cooperon amplitude

$$\langle \mathcal{C}(0, 0, t_0) \rangle = \int_{\mathbf{r}(-t_0)=0}^{\mathbf{r}(t_0)=0} \mathcal{D}[\mathbf{r}(t)] \exp\{ -S_0 - \Delta S \} \quad (4.10)$$

with the dephasing action

$$\begin{aligned} \Delta S &= -\frac{1}{2\pi} \frac{e^2 T}{\chi} \int_{-t}^t dt_1 dt_2 \dot{\mathbf{r}}(t_1) \cdot \dot{\mathbf{r}}(t_2) \ln \frac{|\mathbf{r}(t_1) - \mathbf{r}(t_2)|}{l} \\ &= -\frac{1}{2\pi} \frac{e^2 T}{\chi} \oint d\mathbf{r}_1 \cdot \oint d\mathbf{r}_2 \ln \frac{|\mathbf{r}_1 - \mathbf{r}_2|}{l} \\ &= 2 \frac{e^2 T}{\chi} \int dA_1 \int dA_2 \delta(\mathbf{r}_1 - \mathbf{r}_2) . \end{aligned} \quad (4.11)$$

If a part of the enclosed area A is encircled n times, this area should be weighted with the factor n^2 since the δ -function can be satisfied in n different ways for each of the integrations,

$$\Delta S = \frac{2e^2 T}{\chi} \sum_i n_i^2 A_i , \quad (4.12)$$

where $n_i \in \mathbb{Z}$ is the number of times the area A_i is encircled. The area weighted with the square of the winding numbers is known as the non-oriented (Amperean) area.

For an estimate of Eq. (4.12), the authors of Ref. [55] argued that for weak disorder the factors n_i^2 in Eq. (4.12) can be replaced by 1. Inserting the area covered by a diffusive particle in the time t_0 , $A = Dt_0$, into Eq. (4.12), the action ΔS becomes linear in time. Using the free-fermion result for the susceptibility, $\chi = e^2/12\pi m = e^2 D/12\pi g$ with the dimensionless conductance g , the estimate results in

$$\frac{1}{\tau_\varphi} \sim gT . \quad (4.13)$$

This estimate, however, has some limitations as the temperature is lowered: As dephasing becomes weaker, longer trajectories will contribute more to the path integral. As a result, the probability of multiple return processes increases with decreasing temperature. This temperature dependence is not accounted for in Eq. (4.13). Indeed, in Ref. [75] Wölfle obtained a logarithmic correction factor to Eq. (4.13) using a quasiclassical propagator accounting for diffusive and ballistic propagation. In Section 4.4.1 this result is reproduced from a different starting point, eliminating the need to account for ballistic propagation explicitly. This is possible since the multiple-return processes are a large-scale effect which do not depend sensitively on details of the disorder.

4.3 Relation of weak localization and conductance fluctuations

In this section, the relation between weak localization and conductance fluctuations first demonstrated in Ref. [85] and more generally proven in Section 2.3 is examined for the situation when slow transverse gauge field fluctuations are present in a system where the time-reversal symmetry is not broken except by the gauge field fluctuations.³ The static approximation (4.7) is used to describe the gauge field fluctuations. Moreover, the following hierarchy of timescales is assumed:

$$\frac{L^2}{D} \ll \omega_{\text{gauge field}}^{-1} \ll \text{measurement duration} \ll \text{experiment time} . \quad (4.14)$$

This means that an individual electron experiences a static gauge field configuration during the time it spends in the sample, but in contrast the duration of a measurement is long enough relative to the gauge field dynamics to perform a complete ensemble average over the gauge field configurations. Finally, the two measurements are well separated in time so there are no correlations between the gauge field configurations seen by different measurements.

For convenience, instead of writing down a relation analogous to Eq. (2.41), again only the diffuson part of the conductance fluctuations will be considered, assuming that the conductance fluctuations are measured at a sufficiently high average magnetic field superimposed over the fluctuating contribution, or that harmonics of the Aharonov-Bohm effect are considered, where the amplitude of the harmonics is determined solely by the diffuson part [89].

Consider first the situation $l \ll L_T \ll L_\varphi$: In this case the regime of interest is $T \gg E_c$, and the function (2.12) can be approximated as a delta function in the same way as done in Section 2.3. For a static gauge field configuration $\mathbf{a}(\mathbf{r})$, the amplitude of mesoscopic conductance fluctuations can be written in analogy to Eq. (2.42) as

$$\begin{aligned} \langle \delta G^2 \rangle = & \frac{4e^4 D^2}{3\pi T L^4} \int d^d \mathbf{R}_1 \int d^d \mathbf{R}_2 \int_0^\infty dt \int_{\mathbf{r}_1(0)=\mathbf{R}_2}^{\mathbf{r}_1(t)=\mathbf{R}_1} \mathcal{D}[\mathbf{r}_1(t)] \int_{\mathbf{r}_2(0)=\mathbf{R}_2}^{\mathbf{r}_2(t)=\mathbf{R}_1} \mathcal{D}[\mathbf{r}_2(t)] \\ & \times \left\langle \exp \left\{ - \int_0^t dt'_1 \left[\frac{\dot{\mathbf{r}}_1^2(t'_1)}{4D} + ie \dot{\mathbf{r}}_1(t'_1) [\mathbf{a}_1[\mathbf{r}_1(t'_1)] - \mathbf{a}_2[\mathbf{r}_1(t'_1)]] \right] \right. \right. \\ & \left. \left. - \int_0^t dt'_2 \left[\frac{\dot{\mathbf{r}}_2^2(t'_2)}{4D} + ie \dot{\mathbf{r}}_2(t'_2) [\mathbf{a}_1[\mathbf{r}_2(t'_2)] - \mathbf{a}_2[\mathbf{r}_2(t'_2)]] \right] \right\} \right\rangle . \quad (4.15) \end{aligned}$$

³This is not the case for the Composite-Fermion system: due to the static screening of the impurities the disorder also breaks the time-reversal symmetry. In this situation, the Cooperon should be regarded as an auxiliary quantity useful for the calculation of mesoscopic conductance fluctuations, as is done in the next section.

Clearly, a static gauge field, $\mathbf{a}_1 = \mathbf{a}_2$, drops out of Eq. (4.15). In the opposite limit (4.14), correlators between different measurements vanish, $\langle \mathbf{a}_1 \mathbf{a}_2 \rangle = 0$. Performing the average over Gaussian variables $\mathbf{a}(\mathbf{r})$ results in 16 gauge-field induced terms in the exponent. Half of them correlates gauge fields from the same measurement (giving identical terms), so that in the static approximation given by Eq. (4.14) the result is

$$\begin{aligned}
 \langle \delta G^2 \rangle &= \frac{4e^4 D^2}{3\pi T L^4} \int \mathbf{d}^d \mathbf{R}_1 \int \mathbf{d}^d \mathbf{R}_2 \int_0^\infty dt \int_{\mathbf{r}_1(0)=\mathbf{R}_2}^{\mathbf{r}_1(t)=\mathbf{R}_1} \mathcal{D}[\mathbf{r}_1(t)] \int_{\mathbf{r}_2(0)=\mathbf{R}_2}^{\mathbf{r}_2(t)=\mathbf{R}_1} \mathcal{D}[\mathbf{r}_2(t)] \\
 &\times \exp \left\{ - \int_0^t dt' \left[\frac{\dot{\mathbf{r}}_1^2(t')}{4D} + \frac{\dot{\mathbf{r}}_2^2(t')}{4D} \right] \right. \\
 &\quad - e^2 \int_0^t dt'_1 dt'_2 \left[\dot{\mathbf{r}}_1(t'_1) \left\langle \mathbf{a}[\mathbf{r}_1(t'_1)] \mathbf{a}[\mathbf{r}_1(t'_2)] \right\rangle \dot{\mathbf{r}}_1(t'_2) \right. \\
 &\quad \quad + \dot{\mathbf{r}}_2(t'_1) \left\langle \mathbf{a}[\mathbf{r}_2(t'_1)] \mathbf{a}[\mathbf{r}_2(t'_2)] \right\rangle \dot{\mathbf{r}}_2(t'_2) \\
 &\quad \quad - \dot{\mathbf{r}}_1(t'_1) \left\langle \mathbf{a}[\mathbf{r}_1(t'_1)] \mathbf{a}[\mathbf{r}_2(t'_2)] \right\rangle \dot{\mathbf{r}}_2(t'_2) \\
 &\quad \quad \left. \left. - \dot{\mathbf{r}}_2(t'_1) \left\langle \mathbf{a}[\mathbf{r}_2(t'_1)] \mathbf{a}[\mathbf{r}_1(t'_2)] \right\rangle \dot{\mathbf{r}}_1(t'_2) \right] \right\} . \quad (4.16)
 \end{aligned}$$

Using the transformation (2.43), this is equal to

$$\begin{aligned}
 \langle \delta G^2 \rangle &= \frac{4e^4 D^2}{3\pi T L^4} \int \mathbf{d}^d \mathbf{R} \int_0^\infty dt \int \mathcal{D}[\mathbf{r}(t)] \\
 &\times \exp \left\{ - \int_{-t}^t dt' \frac{\dot{\mathbf{r}}^2}{4D} - e^2 \int_{-t}^t dt'_1 dt'_2 \dot{\mathbf{r}}(t'_1) \left\langle \mathbf{a}[\mathbf{r}(t'_1)] \mathbf{a}[\mathbf{r}(t'_2)] \right\rangle \dot{\mathbf{r}}(t'_2) \right\} . \quad (4.17)
 \end{aligned}$$

This can be related to the weak localization correction evaluated in the presence of a static random gauge field $\mathbf{a}(\mathbf{r})$ by rescaling the gauge field correlator by a factor 2,

$$\begin{aligned}
 \langle \delta G^2 \rangle (T) &= \frac{4e^4 D^2}{3\pi T L^4} \int \mathbf{d}^d \mathbf{R} \int_0^\infty dt \int_{\mathbf{r}(-t)=\mathbf{R}}^{\mathbf{r}(t)=\mathbf{R}} \mathcal{D}[\mathbf{r}(t)] \\
 &\times \exp \left\{ - \int_{-t}^t dt' \frac{\dot{\mathbf{r}}^2}{4D} \right\} \left\langle \exp \left\{ -2ie \int_{-t}^t dt' \dot{\mathbf{r}}(t') \frac{1}{\sqrt{2}} \mathbf{a}[\mathbf{r}(t')] \right\} \right\rangle . \quad (4.18)
 \end{aligned}$$

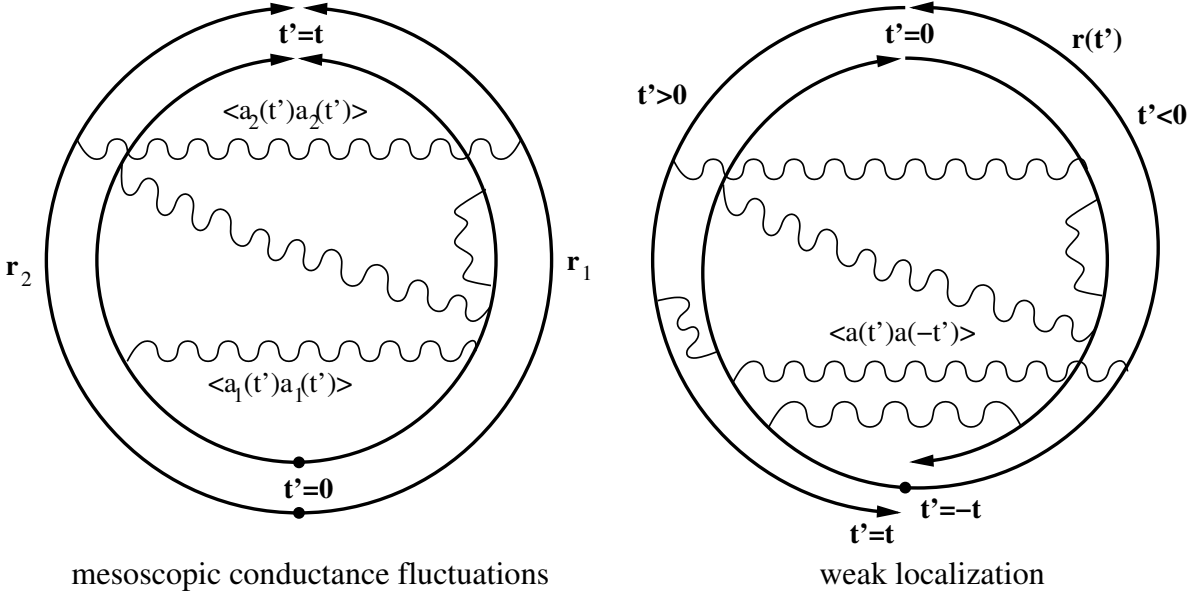


Figure 4.1: The transformation (2.43) can also be used in the presence of quasistatic gauge field fluctuations to establish the connection between weak localization and mesoscopic conductance fluctuations. The effects of ensemble averaging on conductance fluctuations is mapped onto the effect of time-reversal breaking on weak localization. The extra gauge field lines compared to Fig. 2.6 indicate that the gauge field correlator is static in the present case, as opposed to local in time in the case of screened Coulomb interaction. As a result, the allowed gauge field lines for the case of conductance fluctuations are more restricted than for the Cooperon, modifying the relation (4.20) compared to Eq. (2.50).

For thermal gauge field fluctuations this is equivalent to changing the temperature by a factor of 2,

$$\langle \delta G^2 \rangle (T) = \frac{e^2 D}{3TL^2} \left| \delta G_{WL} \left(\frac{T}{2} \right) \right|, \quad d = 1, \quad L_T \ll L_\varphi, \quad (4.19)$$

while in two dimensions, due to the different short-scale cutoffs (see Section 2.3), the result is

$$\langle \delta G^2 \rangle (T) = \frac{e^2 D}{3TL^2} \left| \delta G_{WL} \left(\frac{T}{2} \right) \right|_{l \rightarrow L_T}, \quad d = 1, 2, \quad L_T \ll L_\varphi. \quad (4.20)$$

This result applies to the dephasing effect of transverse magnetic fluctuations given by Eq. (4.5), which is small in the parameter v_F/c . For the Composite-Fermion system, as is seen in the following sections, the dephasing effect of gauge field fluctuations is

strong, $l \ll L_\varphi \ll L_T$, so that the thermal factor (2.12) should be evaluated in the limit $T \ll E_c$, as presented in detail in Appendix F. The result is most conveniently expressed by introducing an extrinsic dephasing rate $1/\tau_\varphi^*$,

$$\langle \delta G^2 \rangle (T) = \frac{3e^2 D}{2\pi L^2} \left| \frac{\partial}{\partial (1/\tau_\varphi^*)} \delta G_{WL} \left(\frac{T}{2} \right) \right|, \quad L_T \gg L_\varphi. \quad (4.21)$$

It should be emphasized that the different prefactors in Eqs. (4.20), (4.21) arise from the different regimes in which the thermal factor is evaluated. The information about the dephasing effects is contained in the quantities δG^2 and δG_{WL} and their respective temperature arguments only. In particular, the dephasing rates associated with both quantities are the same up to a numerical coefficient.

Compared to the case of Coulomb interaction, Eq. (2.50), in Eq. (4.20) and (4.21) a relative factor of 2 is present in the temperature arguments. The reason for this is that, as indicated in Fig. 4.1, the gauge field correlators should in the static case be drawn between all points on the time-reversed paths, while for conductance fluctuations the limitation applies that the two measurements are uncorrelated.⁴

Again, as has been discussed in Section 2.3, the presented transformation connects harmonics of the h/e and of the $h/2e$ Aharonov-Bohm effect as well, just by restricting the path integrals to include only paths with the desired winding numbers. It has thus been shown that the relation between weak localization and conductance fluctuations (or between the h/e and the $h/2e$ Aharonov-Bohm effect) is valid in the presence of transverse gauge field fluctuations just as it is in the case of scalar potential fluctuations.

The validity of Eqs. (4.20), (4.21) is not trivial, since weak localization is insensitive to ensemble averaging but suppressed by breaking of time-reversal symmetry, but on the other hand the diffuson part of mesoscopic conductance fluctuations is suppressed by ensemble averaging and not by time-reversal breaking. However, since the gauge field fluctuations are slow on the scale of the electron motion *and* break time-reversal symmetry, the different suppression effects on the two quantities are mapped onto each other.

Since the relations (4.20), (4.21) can be traced back to the gauge field breaking the time-reversal symmetry, slow *external* noise not breaking time-reversal symmetry [31] will lead to an ensemble averaging effect during a measurement but not to a suppression of weak localization. The relations⁵ (2.50) and (4.20) or (4.21) are therefore useful to distinguish between different sources of dephasing.

⁴Another situation where the relation between weak localization and conductance fluctuations is modified is the case of spin-orbit scattering [85].

⁵note that for Coulomb interaction even the Aharonov-Bohm dephasing length (2.34) is larger than L_T (by a factor $\sim (\xi/R)^{1/2}$, where ξ is the localization length), and therefore it is not necessary to formulate Eq. (2.50) for the opposite situation.

4.4 Weak localization with slow transverse gauge field fluctuations

4.4.1 Two-dimensional case

In this section, the Cooperon amplitude and the weak localization correction are calculated for a system of electrons coupled to a fluctuating gauge field with the correlator (4.7). In the half-filled lowest Landau level, time reversal symmetry is broken by the strong magnetic field. The calculation of the weak-localization correction should then be taken just as a convenient way to calculate mesoscopic conductance fluctuations via the relation (4.20).

The object of interest is the Cooperon $\mathcal{C}(0, 0, t_0)$, which in the presence of static transverse gauge field fluctuations can be written as a path integral,

$$\mathcal{C}(0, 0, t_0) = \int_{\mathbf{r}(-t_0)=0}^{\mathbf{r}(t_0)=0} \mathcal{D}[\mathbf{r}(t)] \exp\{-S_0 + iS_1\} \quad (4.22)$$

with

$$S_0 = \int_{-t_0}^{t_0} dt \frac{\dot{\mathbf{r}}^2(t)}{4D} \quad (4.23)$$

and⁶

$$S_1 = -2e \int_{-t_0}^{t_0} dt \dot{\mathbf{r}}(t) \cdot \mathbf{a}[\mathbf{r}(t)] . \quad (4.24)$$

Averaging over the gauge field configurations with Gaussian weight, using $\langle \exp\{i\varphi\} \rangle = \exp\{-\langle \varphi^2 \rangle / 2\}$ for Gaussian variables φ , the result is (see also Eq. (4.10))

$$\langle \mathcal{C}(0, 0, t_0) \rangle = \int_{\mathbf{r}(-t_0)=0}^{\mathbf{r}(t_0)=0} \mathcal{D}[\mathbf{r}(t)] \exp\{-S_0 - \Delta S\} \quad (4.25)$$

with

$$\Delta S = 2e^2 \int_{-t_0}^{t_0} dt_1 \int_{-t_0}^{t_0} dt_2 \dot{r}_\alpha(t_1) \left\langle a_\alpha[\mathbf{r}(t_1)] a_\beta[\mathbf{r}(t_2)] \right\rangle \dot{r}_\beta(t_2) . \quad (4.26)$$

⁶for ease of reading, the coupling constant describing the fermion-gauge field coupling will be set equal to the electron charge, as applicable to the Composite-Fermion system.

It is convenient to define an averaged action $\langle \Delta S \rangle(t_0)$ with the property [75]

$$\begin{aligned} \langle \mathcal{C}(0, 0, t_0) \rangle &= \exp\{-\langle \Delta S \rangle(t_0)\} \int_{\mathbf{r}(-t_0)=0}^{\mathbf{r}(t_0)=0} \mathcal{D}[\mathbf{r}(t)] \exp\{-S_0\} \\ &= \exp\{-\langle \Delta S \rangle(t_0)\} \mathcal{C}^{(0)}(0, 0, t_0) , \end{aligned} \quad (4.27)$$

where $\mathcal{C}^{(0)}(0, 0, t_0) = (4\pi Dt_0)^{-d/2}$ is the unperturbed Cooperon in d dimensions.

To second order in the coupling constant e , $\langle \Delta S \rangle$ can be evaluated as the average of ΔS weighted with the unperturbed Cooperon,

$$\langle \Delta S \rangle(t_0) = \frac{1}{\mathcal{C}^{(0)}(0, 0, t_0)} \int_{\mathbf{r}(-t_0)=0}^{\mathbf{r}(t_0)=0} \mathcal{D}[\mathbf{r}(t)] \exp\{-S_0\} \Delta S[\mathbf{r}(t), t_0] \quad (4.28)$$

The integral can be identified as the term second order in e of an expansion of the Cooperon $\mathcal{C} = (-D\nabla^2)^{-1} = (D\hat{\mathbf{q}}^2)^{-1}$ after coupling to the gauge field by the substitution $-i\nabla \rightarrow (-i\nabla - e\mathbf{a})$, $\hat{\mathbf{q}} \rightarrow (\hat{\mathbf{q}} - e\mathbf{a})$,

$$\mathcal{C} = \mathcal{C}^{(0)} + eD\mathcal{C}^{(0)} \{a_\alpha, \hat{q}_\alpha\} \mathcal{C}^{(0)} - e^2 D\mathcal{C}^{(0)} a_\alpha a_\alpha \mathcal{C}^{(0)} + e^2 D^2 \mathcal{C}^{(0)} \{a_\alpha, \hat{q}_\alpha\} \mathcal{C}^{(0)} \{a_\beta, \hat{q}_\beta\} \mathcal{C}^{(0)} , \quad (4.29)$$

where $\{\cdot, \cdot\}$ is the anticommutator. Averaging over the gauge field fluctuations,

$$\langle \mathcal{C} \rangle = \mathcal{C}^{(0)} - e^2 D\mathcal{C}^{(0)} \langle a_\alpha a_\alpha \rangle \mathcal{C}^{(0)} + e^2 D^2 \mathcal{C}^{(0)} \langle \{a_\alpha, \hat{q}_\alpha\} \mathcal{C}^{(0)} \{a_\beta, \hat{q}_\beta\} \rangle \mathcal{C}^{(0)} . \quad (4.30)$$

The second and third term of the right hand side are the complete set of terms second order in e and therefore must add up to the integral in Eq. (4.28). The corresponding processes are shown in Fig. 4.2. The averaged action $\langle \Delta S \rangle$ can thus be written as

$$\begin{aligned} \langle \Delta S \rangle &= (4\pi Dt_0)^{d/2} \int \frac{d\omega}{2\pi} \exp\{i\omega t_0\} \int \frac{d^d q}{(2\pi)^d} \int \frac{d^d k}{(2\pi)^d} \frac{1}{(D\mathbf{q}^2 - i\omega)^2} e^2 D \\ &\times \left[-\langle a_\alpha a_\alpha \rangle_{\mathbf{k}} + 4D \frac{1}{D(\mathbf{q} - \mathbf{k})^2 - i\omega} \left(q - \frac{k}{2} \right)_\alpha \langle a_\alpha a_\beta \rangle_{\mathbf{k}} \left(q - \frac{k}{2} \right)_\beta \right] \end{aligned} \quad (4.31)$$

with the static transverse gauge field correlator given by Eq. (4.7). In $d = 2$, the action can be written as⁷

$$\begin{aligned} \langle \Delta S \rangle &= 4\pi Dt_0 \frac{e^2 DT}{\chi} \int \frac{d\omega}{2\pi} \exp\{i\omega t_0\} \int_0^\infty \frac{q dq}{2\pi} \int_0^\infty \frac{k dk}{2\pi} \int_0^{2\pi} \frac{d\varphi}{2\pi} \frac{1}{(Dq^2 - i\omega)^2} \\ &\times \frac{1}{k^2} \left[-1 + 4D \frac{q^2 \sin^2 \varphi}{Dq^2 - 2Dqk \cos \varphi + Dk^2 - i\omega} \right] , \end{aligned} \quad (4.32)$$

⁷note that Eq. (4.32) bears a close similarity to Eq. (21) of Ref. [75], which was derived in a different way (including ballistic propagation). Here the first term (-1) in brackets takes the role of the ballistic term of Ref. [75]. As a result, the following derivation of Eq. (4.36) follows closely Ref. [75].

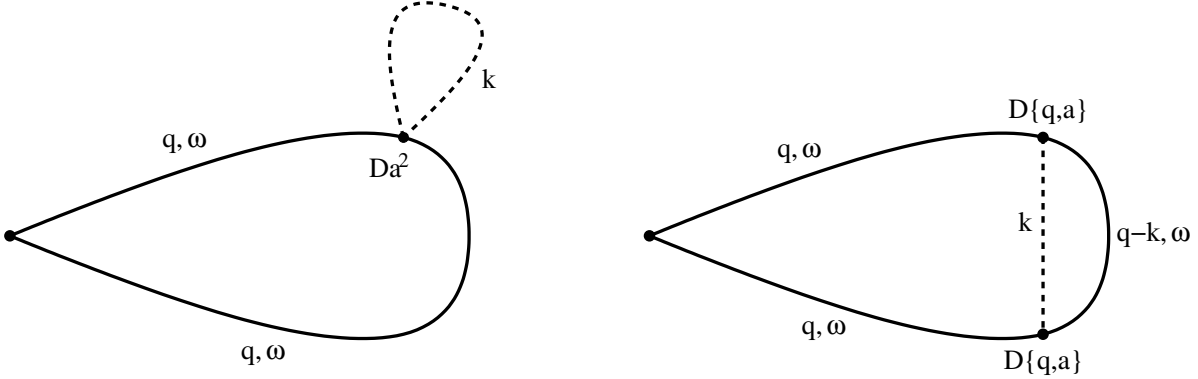


Figure 4.2: Return processes second order in the interaction with static gauge field fluctuations. The processes correspond to the second and third term of the right hand side of Eq. (4.30). The solid lines denote the unperturbed Cooperon, while the dashed lines denote the gauge field propagator $\langle \mathbf{a} \mathbf{a} \rangle_{\mathbf{k}}$ given by Eq. (4.7).

where φ is the angle between the directions of the momenta \mathbf{q} and \mathbf{k} . In writing down Eq. (4.32) the fact was used that the gauge field correlator is transverse, projecting onto the direction perpendicular to \mathbf{k} .

This integral is dominated by small $q, \omega \sim Dq^2$ and *larger* k : Power-counting shows that the k -integral is logarithmic, where the upper cutoff will be the inverse elastic mean free path l^{-1} beyond which the diffusive description is invalid. Furthermore, knowing that a static uniform gauge field must have no effect, it can be anticipated that the integrand must vanish for $k \rightarrow 0$. The second term in brackets will serve as a low- k cutoff for the first one, cancelling it in the limit $k \rightarrow 0$. The k -integral will thus be logarithmic in the interval $[L_\omega^{-1}, l^{-1}]$, where $L_\omega = (D/\omega)^{1/2}$. Since most of the weight is located at k well above typical $q \sim L_\omega^{-1}$, it is possible to neglect the term $2D\mathbf{q} \cdot \mathbf{k}$ in the denominator of Eq. (4.32) compared to Dk^2 . However, it is useful to keep the term Dq^2 : since then the approximation is valid for both $q \ll k$ and $q \gg k$ it will allow to check that the integrand indeed vanishes for $k \rightarrow 0$.

It serves as a consistency check to verify gauge invariance: A *longitudinal* part of the gauge field correlator should not contribute to Eq. (4.31), since a *static* longitudinal gauge field should have no observable effect. It is easily checked in the limit of $q, \omega \rightarrow 0$ that the second term of Eq. (4.31) cancels the first one. To verify the cancellation exactly for all q and ω would require a calculation beyond the diffusion approximation. The results of the present calculation are however due to large-scale (diffusive) physics and insensitive to short-scale details.

The angular integration in Eq. (4.32) is trivial after neglecting the term dependent on

the angle between \mathbf{q} and \mathbf{k} ,

$$\begin{aligned} \langle \Delta S \rangle &= 4\pi D t_0 \frac{e^2 D T}{\chi} \int \frac{d\omega}{2\pi} \exp\{i\omega t_0\} \int_0^\infty \frac{q dq}{2\pi} \int_0^\infty \frac{k dk}{2\pi} \\ &\times \frac{1}{k^2} \left[-1 + 2D \frac{q^2}{Dq^2 + Dk^2 - i\omega} \right], \end{aligned} \quad (4.33)$$

and integrating over q results in

$$\begin{aligned} \langle \Delta S \rangle &= 4\pi D t_0 \frac{e^2 D T}{\chi} \frac{1}{4\pi D} \int \frac{d\omega}{2\pi} \exp\{i\omega t_0\} \int_0^\infty \frac{dk}{2\pi} \\ &\times \frac{1}{k} \left[\frac{1}{i\omega} - \frac{2}{Dk^2} + 2 \frac{i\omega - Dk^2}{(Dk^2)^2} \ln \frac{-i\omega}{Dk^2 - i\omega} \right], \end{aligned} \quad (4.34)$$

where the first term in brackets is the result of the first term in brackets of Eq. (4.33) and the other two terms are the result of the second term of Eq. (4.33). It is seen that the first term in brackets gives a logarithmic integral with the upper cutoff set by the elastic mean free path l , beyond which the diffusive description is not valid, and the lower cutoff set by the other two terms at the scale L_ω (see also Fig. 4.3). In the limit $k \rightarrow 0$ the integrand indeed vanishes $\propto k$, so that the leading contribution to the integral is given by the logarithmic term:

$$\begin{aligned} \langle \Delta S \rangle &= 4\pi D t_0 \frac{e^2 D T}{\chi} \frac{1}{4\pi D} \int \frac{d\omega}{2\pi} \exp\{i\omega t_0\} \left[\frac{1}{i\omega} \frac{1}{2\pi} \ln \frac{L_\omega}{l} + \text{subleading terms} \right] \\ &\simeq 4\pi D t_0 \frac{e^2 D T}{\chi} \frac{1}{8\pi^2 D} \int \frac{d\omega}{2\pi} \frac{\sin \omega t_0}{\omega} \ln \frac{L_\omega}{l}. \end{aligned} \quad (4.35)$$

Since this integral is dominated by $\omega \sim 1/t_0$, it can be evaluated to logarithmic accuracy by substituting $\ln \frac{L_\omega}{l} \simeq \frac{1}{2} \ln \frac{t_0}{\tau}$, where τ is the elastic scattering time. Using the Landau diamagnetic susceptibility of free fermions [11], $\chi = 1/12\pi m$, to substitute $e^2 D/\chi = 12\pi g$ with g the dimensionless conductance, the result is

$$\langle \Delta S \rangle = \frac{3}{2} g T t_0 \ln \frac{t_0}{\tau}, \quad (4.36)$$

which is identical to Eq. (25) of Ref. [75]. This result has thus been reproduced in a purely *diffusive* calculation without the need of taking ballistic propagation into account in detail. This could be expected since the relevant physics happens on the large length scales of diffusive propagation and does not depend on the details of microscopic scattering processes.

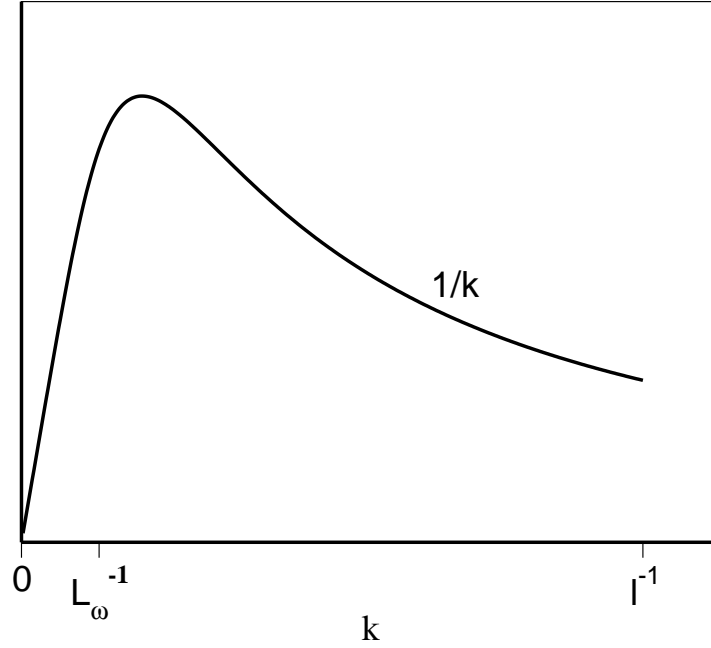


Figure 4.3: Plot of the absolute value of the integrand of Eq. (4.34) as a function of the gauge field momentum k . In the transverse gauge, the logarithmic contribution arises from the first term in brackets and is regularized at the lower limit by the other terms.

Once $\langle \Delta S \rangle(t_0)$ is known, the amplitude of the weak-localization correction can be evaluated as

$$\begin{aligned}
 \delta\sigma_{\text{WL}} &= -\frac{2e^2 D}{\pi} \int_{\tau}^{\infty} dt_0 \langle \mathcal{C}(0, 0, t_0) \rangle \\
 &= -\frac{2e^2 D}{\pi} \int_{\tau}^{\infty} dt_0 \mathcal{C}^{(0)}(0, 0, t_0) \exp\{-\langle \Delta S \rangle(t_0)\} \\
 &= -\frac{2e^2 D}{\pi} \int_{\tau}^{\infty} dt_0 \frac{1}{4\pi D t_0} \exp\left\{-\frac{3}{2} g T t_0 \ln \frac{t_0}{\tau}\right\} \\
 &= -\frac{e^2}{2\pi^2} \int_1^{\infty} \frac{dx}{x} \exp\left\{-\frac{3}{2} g T \tau x \ln x\right\} , \tag{4.37}
 \end{aligned}$$

At very low temperatures,

$$T \ll \frac{2}{3g\tau} , \quad (4.38)$$

the exponential factor serves just as a cutoff for the logarithmic integral (4.37), with the result

$$\delta\sigma_{\text{WL}} = -\frac{e^2}{2\pi^2} \ln \frac{\tau_\varphi}{\tau} , \quad (4.39)$$

where τ_φ is defined by $\langle \Delta S \rangle(t_0 = \tau_\varphi) = 1$,

$$\frac{1}{\tau_\varphi} = \frac{3}{2} gT \ln \frac{2}{3gT\tau} . \quad (4.40)$$

The logarithmic correction to τ_φ , which was first found in Ref. [75], is due to the possibility of paths forming multiple loops [55, 75], which results in an enhancement of the non-oriented area enclosed. The dephasing rate (4.40) is large in the parameter $g \gg 1$ and much larger than the dephasing rate induced by the Coulomb interaction, which is [29, 72] proportional to the sheet *resistance* instead of the conductance.

A typical dephasing length arising from Eq. (4.40) is calculated in Appendix G,

$$L_\varphi \sim 0.3 \mu\text{m} , \quad (4.41)$$

satisfying $L_\varphi > l$ at temperatures $T \lesssim 30 \text{ mK}$.

It should be emphasized that, although the dephasing rate (4.40) is much larger than the inverse temperature, this does not indicate a breakdown of the Fermi liquid picture. The dephasing rate (4.40) is mostly the result of an ensemble average⁸ over slow gauge field fluctuations, which are approximately static on the timescale of the electron motion. *Individual* particles retain phase coherence much longer than stated by Eq. (4.40). A related situation has also been found in Ref. [83] for the dephasing rate applicable to mesoscopic fluctuations of the Coulomb drag between two layers with each layer containing a half-filled Landau level.

At higher temperatures, $T \gg 2/3g\tau$, the integral (4.37) is dominated by $x \sim 1$, i.e. by $t_0 \sim \tau$, and the results derived for the diffusive regime cannot be used. However, in view of the large dephasing rate (4.40), the regime of interest for quantum interference phenomena is clearly the low-temperature regime given by Eq. (4.38).

A comment is in order here regarding the static approximation (4.7) for the gauge field fluctuations. In the transversal gauge, the leading contribution to the action (4.36) comes from the first process shown in Fig. 4.2 alone. For this process the integrals over the momenta and frequencies of the particle and the gauge field factorize. The results (4.36), (4.39), (4.40) obtained in this section therefore do not require the static approximation for their validity. However, the static approximation is checked in Appendix G and found to be well satisfied for typical semiconductor samples.

⁸The notion of ensemble averaging of course applies when mesoscopic conductance fluctuations are calculated using the relation (4.20). If actually weak localization is considered, the dephasing rate (4.40) is due to time-reversal breaking.

4.4.2 Quasi-onedimensional case

In view of the fact that multiple returns give rise to a logarithmic correction to the phase relaxation rate in two dimensions, it is interesting to consider the quasi-onedimensional case. Two effects can be expected to compete: The probability of returning to a given point decays more slowly with increasing time in quasi-one dimension than in two dimensions. On the other hand, the confinement in the transverse direction limits the geometric area which can be enclosed by diffusive paths. It is therefore not trivial what happens to the non-oriented area enclosed by a typical path in quasi-one dimension.

In the following, the device of interest will be a wire of length L and width b , where $l \ll b \ll L$. The momenta of the electrons, $\mathbf{q} = (q_{||}, q_{\perp})$, and of the gauge field fluctuations, $\mathbf{k} = (k_{||}, k_{\perp})$, are therefore quantized in the transverse direction.

In general, the directions of \mathbf{q} , \mathbf{k} , and the $||$ direction can all be different. The quasi-onedimensional version of Eq. (4.31) then is

$$\begin{aligned} \langle \Delta S \rangle &= (4\pi D t_0)^{1/2} \int \frac{d\omega}{2\pi} \exp\{i\omega t_0\} \int \frac{dq_{||}}{2\pi} \sum_{q_{\perp}} \int \frac{dk}{2\pi} \frac{1}{b} \sum_{k_{\perp}} \frac{1}{(Dq_{||}^2 + Dq_{\perp}^2 - i\omega)^2} \\ &\times e^2 D \left[-\langle a_{\alpha} a_{\alpha} \rangle_{\mathbf{k}} + 4D \frac{1}{D(\mathbf{q} - \mathbf{k})^2 - i\omega} \left(q - \frac{k}{2} \right)_{\alpha} \langle a_{\alpha} a_{\beta} \rangle_{\mathbf{k}} \left(q - \frac{k}{2} \right)_{\beta} \right], \end{aligned} \quad (4.42)$$

where the indices α, β run over the directions $||, \perp$. From Eq. (4.42) it is seen that higher modes of the transverse component of the electron momentum, $q_{\perp} > 0$, are less important than higher modes of the gauge field momentum \mathbf{k} . This allows to consider only the lowest (zeroth) transverse mode of q , as could be expected from a quasi-onedimensional diffusive system. However both components of the momentum \mathbf{k} of the gauge field fluctuations need to be kept, since in strictly one dimension (with no transverse components of the momenta taken into account) Eq. (4.42) would trivially reduce to zero.

When keeping only the $||$ component of q , for consistency also only the component $a_{||}$ should be kept in Eq. (4.29). Eq. (4.42) can thus be reduced to

$$\begin{aligned} \langle \Delta S \rangle &= (4\pi D t_0)^{1/2} \int \frac{d\omega}{2\pi} \exp\{i\omega t_0\} \int \frac{dq}{2\pi} \int \frac{dk}{2\pi} \frac{1}{b} \sum_{k_{\perp}} \frac{1}{(Dq^2 - i\omega)^2} e^2 D \\ &\times \left[-\langle a_{||} a_{||} \rangle_{\mathbf{k}} + 4D \frac{1}{D(\mathbf{q} - \mathbf{k})^2 - i\omega} \left(q - \frac{k}{2} \right)_{||} \langle a_{||} a_{||} \rangle_{\mathbf{k}} \left(q - \frac{k}{2} \right)_{||} \right], \end{aligned} \quad (4.43)$$

where the gauge field correlator is again given by Eq. (4.7), and the momenta are given by $\mathbf{q} = (q, 0)$ and $\mathbf{k} = (k, k_{\perp})$. Again, as in Eq. (4.32), gauge invariance is satisfied in the limit of small q, ω , which is what is to expect from the diffusive formulation. Similar to the twodimensional case, in the transversal gauge (4.7) only the first term in brackets of Eq. (4.43) gives the leading contribution, the difference to the twodimensional case

being that the second term is not needed for regularization. Consequently, since the first term is independent of the gauge field frequency the static approximation can be relaxed also in the wire geometry, however, as shown in Appendix G, it is well satisfied for typical parameters.

It is important to remember that the integral over q is the continuum limit of a discrete sum over momenta allowed by the system size L . Therefore, when the integrals over q and ω do not commute, the integral over ω should be taken first. This is the case in quasi-one dimension for the first term in brackets, which would give a divergence for low ω if the q -integral would be performed first. For the leading contribution (the first term in brackets in Eq. (4.43)), performing the ω -integration results in

$$\langle \Delta S \rangle = (4\pi D t_0)^{1/2} \frac{e^2 D T}{\chi} \int \frac{dq}{2\pi} t_0 \exp\{-D q^2 t_0\} \int \frac{dk_{\parallel}}{2\pi} \frac{1}{b} \sum_{k_{\perp}} \frac{1}{k_{\parallel}^2 + k_{\perp}^2} . \quad (4.44)$$

The \mathbf{k} -sum/integral thus factorizes from the rest and the sum over $k_{\perp} = n\pi/b$, $n = 1, 2, \dots$ (the term with $n = 0$ vanishes, $\delta_{\parallel\parallel} - k_{\parallel} k_{\parallel}/k_{\parallel}^2 = 0$) is cut off at the upper limit at the scale of the inverse elastic mean free path l^{-1} ,

$$\frac{1}{b} \int \frac{dk_{\parallel}}{2\pi} \sum_{k_{\perp}} \frac{1}{k_{\parallel}^2 + k_{\perp}^2} = \frac{1}{b} \sum_{k_{\perp}} \frac{1}{2|k_{\perp}|} = \frac{1}{2\pi} \left(\gamma + \ln \frac{b}{l} \right) \simeq \frac{1}{2\pi} \ln \frac{b}{l} , \quad (4.45)$$

where $\gamma \approx 0.577$ is Euler's constant. The q -integral can now be taken without discretization,

$$\langle \Delta S \rangle = 6 g_{\square} T t_0 \ln \frac{b}{l} , \quad (4.46)$$

where (again) g_{\square} is the dimensionless conductance of a square segment of the wire.

Note that the system size L does not appear explicitly, as expected for a quantity which should not need this cutoff, since for “short” times $t_0 \ll D/L^2$ the closed trajectories of duration t_0 should not be influenced by the system size.

So compared to Eq. (4.36) the logarithm is cut off by the wire width b , instead of L_{ω} in two dimensions. The two competing effects, confinement of the geometry and enhancement of the return probability, almost cancel in their effect on the non-oriented area enclosed by a typical closed diffusive path, the difference being only that the logarithmic factor is absent. The dephasing rate in quasi-one dimension, defined by $\langle \Delta S \rangle(t_0 = \tau_{\varphi}) = 1$, is found to be

$$\frac{1}{\tau_{\varphi}} = 6 g_{\square} T \ln \frac{b}{l} . \quad (4.47)$$

Remarkably, as already indicated by the form of the action (4.46) being linear in t_0 , there are no infrared singularities arising in quasi-one dimension, resulting in the dephasing rate (4.47) linear in the temperature. This is in contrast to the twodimensional result (4.36), which features the additional factor logarithmic in t_0 . In view of the gauge field

correlator (4.7) being very singular at low momenta and the phase space volume in quasi-one dimension favouring low momenta, this deserves extra attention. In strictly one dimension of course no magnetic field exists. For the quasi-onedimensional wire this does not apply, but a related feature of Eq. (4.43) is that the zeroth transverse mode of the gauge field fluctuations does not contribute to the action. Intuitively, this follows from the fact that it can not contribute to the random flux of magnetic field which is encircled by a closed path. For the higher transverse modes, any possible infrared problems are already cut off by the width of the wire, so that on length scales larger than the wire width no peculiarities of the infrared cutoff can arise.

As a result, it can be expected that the dephasing rate for the Aharonov-Bohm geometry does not differ from the dephasing rate for the singly-connected quasi-onedimensional geometry in the same significant way as it does for the case of Coulomb interaction (considered in Chapter 2). In Section 4.5 this question is addressed and it is confirmed that the dephasing rate for the Aharonov-Bohm situation is indeed up to a numerical factor the same as Eq. (4.47).

The weak localization amplitude is easily calculated from Eq. (4.46),

$$\begin{aligned}
 \delta\sigma_{\text{WL}} &= -\frac{2e^2 D}{\pi} \int_{\tau}^{\infty} dt_0 \langle \mathcal{C}(0, 0, t_0) \rangle \\
 &= -\frac{2e^2 D}{\pi} \int_{\tau}^{\infty} dt_0 \frac{1}{(4\pi D t_0)^{1/2}} \exp\{-\langle \Delta S \rangle(t_0)\} \\
 &= -\frac{e^2}{\sqrt{6}\pi} g_{\square}^{-1/2} \left(\frac{D}{T}\right)^{1/2} \left(\ln \frac{b}{l}\right)^{-1/2}; \tag{4.48}
 \end{aligned}$$

this equation is valid in the regime in which the two-dimensional dephasing length $L_{\varphi} = (D\tau_{\varphi})^{1/2}$ with τ_{φ} given by Eq. (4.40) is larger than the transverse dimension of the wire b . For typical semiconductor samples this is calculated in Appendix G, where a dephasing length of

$$L_{\varphi} \sim 0.15 \mu\text{m} \tag{4.49}$$

is found. The quasi-onedimensional description introduced in this section therefore applies to wires with a width of the order of $0.1 \mu\text{m}$ or less.

The result for the action (4.46) should be related to the twodimensional result (4.36) in the following way: A factor $t_0^{1/2}$ can be attributed to the typical geometrical area enclosed by paths of duration t_0 ; this factor is the equivalent of the factor t_0 in Eq. (4.36). Another factor is due to the effect of multiple returns, which have an enhanced probability in low dimensions so that instead of the logarithmic correction in Eq. (4.36) an extra *algebraic* factor $t_0^{1/2}$ arises in Eq. (4.46). This factor can be understood in the following way (see Fig. 4.4): A closed path covers an area of size $\sim t_0^{1/2}$ in every unconstrained dimension. In quasi-one dimension, the area enclosed extends $\sim t_0^{1/2}$ in the longitudinal direction,

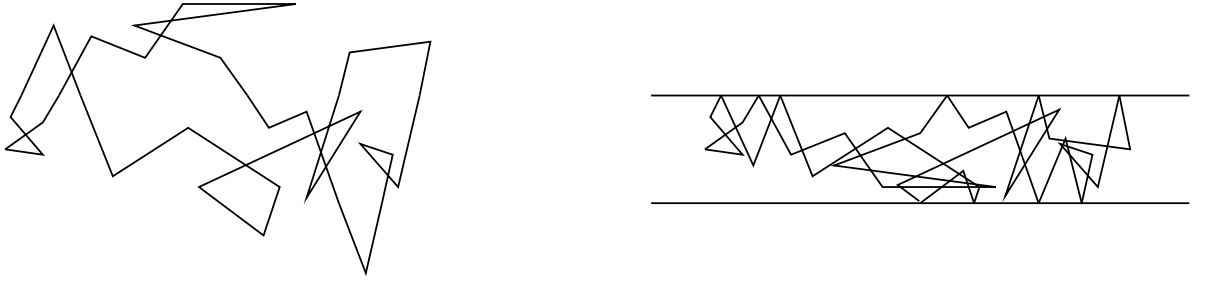


Figure 4.4: Left: a typical closed path in two dimensions. Right: a similar closed path in quasi-one dimension, obtained by reflecting the twodimensional version at the boundaries. The confinement in the transversal direction makes the trajectory return more often to a given area, which is encircled in a random direction each time.

and a given cross-section of the wire is visited $\sim t_0^{1/2}$ times. The path winds around this given point with a random sign each time, the winding number being therefore $\sim t_0^{1/4}$. The non-oriented area is obtained by adding up all enclosed patches weighted with the square of the respective winding numbers. As a result, the power of t_0 entering Eq. (4.46) is $(t_0^{1/4})^2 t_0^{1/2} = t_0$, and as a result the dephasing rate in quasi-one dimension (4.47) is proportional to the temperature, the temperature thus appearing to the same power as in the twodimensional case (4.40). This differs from the Coulomb interaction [29, 85] in the remarkable way that the different geometric effects combine in quasi-one dimension to eliminate infrared divergences.

4.5 Aharonov-Bohm oscillations with slow transverse gauge field fluctuations

When considering $h/2e$ Aharonov-Bohm oscillations of rings formed of quasi-one-dimensional wires, only Cooperon paths with winding number one contribute. In Chapter 2 it has been shown that the finite minimum length of these paths leads to a parametrically different dephasing rate which is much larger than the dephasing rate for weak localization. This reflects the fact that in the regime of strong dephasing the probability of retaining coherence throughout such a path is small and paths which are not typical diffusive paths, but rather atypically straight ones, contribute most to the Aharonov-Bohm amplitude.

On the other hand, in the case of gauge-field fluctuations the action (4.46) and the dephasing rate (4.47) for the simple wire show no sign of long-time/infrared divergence. It may therefore be expected that the dephasing rate applicable to Aharonov-Bohm oscillations will not exceed the one for the plain wire in the same way as in the case of

Coulomb interaction, where the difference in the dephasing rates arises from the different cutoff procedures applicable to the respective situations (see Section 2.2.4).

In Section 2.2.3 it has been argued that in the strong-dephasing situation it is sufficient to consider paths which do not extend into the leads, since this will lead to extra dephasing, effectively removing these paths from the class giving the leading contribution to the Aharonov-Bohm interference. The same argument holds when dephasing is caused by gauge field interactions. It should be noted that the effect of a static random gauge field depends only on the geometry of the trajectory under consideration, not on the dwell time which could be spent in the leads. One might try to imagine a situation where the gauge field interaction is absent or weak in the leads. In this case the part of the trajectory exploring the lead can just be removed and the discussion can also be restricted to trajectories within the ring.

The difference to the calculations in Sections 4.4.1 and 4.4.2 is that, instead of closed Cooperon paths, Cooperons with winding number one in the ring geometry are considered. In other words, the Cooperon paths now have endpoints with a separation of $2\pi R$ in unfolded coordinate space, where R is the radius of the ring. The action corresponding to Eq. (4.43) then becomes

$$\begin{aligned} \langle \Delta S \rangle_{2\pi R} = & \frac{1}{\mathcal{C}^{(0)}(0, 2\pi R, t_0)} \int \frac{d\omega}{2\pi} e^{i\omega t_0} \int \frac{dq}{2\pi} e^{iq 2\pi R} \int \frac{dk}{2\pi} \frac{1}{b} \sum_{k_\perp} \frac{1}{(Dq^2 - i\omega)^2} e^2 D \times \\ & \left[-\langle a_{||} a_{||} \rangle_{\mathbf{k}} + 4D \frac{1}{D(\mathbf{q} - \mathbf{k})^2 - i\omega} \left(q - \frac{k}{2} \right)_{||} \langle a_{||} a_{||} \rangle_k \left(q - \frac{k}{2} \right)_{||} \right], \end{aligned} \quad (4.50)$$

with the unperturbed Cooperon with winding number one

$$\mathcal{C}^{(0)}(0, 2\pi R, t_0) = \frac{1}{(4\pi D t_0)^{1/2}} \exp \left\{ -\frac{(2\pi R)^2}{4D t_0} \right\}. \quad (4.51)$$

Along the lines of the calculation presented in Section 4.4.2, the result is

$$\begin{aligned} \langle \Delta S \rangle_{2\pi R} &= \frac{1}{\mathcal{C}^{(0)}(0, 2\pi R, t_0)} \frac{e^2 D T}{\chi} \frac{1}{2\pi} \ln \left(\frac{b}{l} \right) t_0 \int \frac{dq}{2\pi} \exp \{ i q 2\pi R - D q^2 t_0 \} \\ &= \frac{1}{\mathcal{C}^{(0)}(0, 2\pi R, t_0)} \frac{e^2 D T}{\chi} \frac{1}{2\pi} \ln \left(\frac{b}{l} \right) t_0 \frac{\exp \left\{ -\frac{(2\pi R)^2}{4D t_0} \right\}}{(4\pi D t_0)^{1/2}} \\ &= 6 g_{\square} T t_0 \ln \frac{b}{l}, \end{aligned} \quad (4.52)$$

in other words $\langle \Delta S \rangle$ averaged over Cooperons with winding number one is the same as averaged over all closed Cooperon paths in the plain wire geometry, Eq. (4.46). The

amplitude of $\hbar/2e$ Aharonov-Bohm oscillations then is

$$\begin{aligned}
 \langle \delta g \rangle_{\hbar/2e} &= C_{\hbar/2e} D \int_0^\infty dt_0 \langle \mathcal{C}(0, 2\pi R, t_0) \rangle \\
 &= C_{\hbar/2e} D \int_0^\infty dt_0 \mathcal{C}^{(0)}(0, 2\pi R, t_0) \exp\{-\langle \Delta S \rangle_{2\pi R}\} \\
 &\equiv C_{\hbar/2e} D \int_0^\infty dt_0 \frac{1}{(4\pi D t_0)^{1/2}} \exp\{-S_{AB}\} .
 \end{aligned} \tag{4.53}$$

Here $S_{AB}(t_0)$ is defined as

$$S_{AB}(t_0) = \frac{(2\pi R)^2}{4D t_0} + \langle \Delta S \rangle_{2\pi R} , \tag{4.54}$$

b is the linewidth of the ring, and $C_{\hbar/2e}$ is a coefficient related to the geometry [89] which will not be evaluated here. In the regime of strong dephasing, the action $S_{AB}(t_0)$ is large for all t_0 and the integral can be evaluated by the saddle-point method:

$$\langle \delta g \rangle_{\hbar/2e} = C_{\hbar/2e} D \frac{1}{(4\pi D t_0^{\text{opt}})^2} \exp\{-S_{AB}^{\text{opt}}\} \sqrt{2\pi} \left[\frac{\partial^2}{\partial t_0^2} S_{AB} \right]_{t_0=t_0^{\text{opt}}}^{-1/2} , \tag{4.55}$$

where t_0^{opt} is the time where $S_{AB}(t_0)$ assumes its minimum value S_{AB}^{opt} . The evaluation of the saddle-point is performed in Appendix H, with the result

$$\begin{aligned}
 \langle \delta g \rangle_{\hbar/2e} &= C_{\hbar/2e} \sqrt{6} g_{\square}^{-1/2} \left(\frac{D}{T} \right)^{1/2} \left(\ln \frac{b}{l} \right)^{-1/2} \\
 &\times \exp \left\{ -\sqrt{6} g_{\square}^{1/2} (T t_{AB})^{1/2} \left(\ln \frac{b}{l} \right)^{1/2} \right\} ,
 \end{aligned} \tag{4.56}$$

where the time t_{AB} is defined as the timescale set by the ring circumference,

$$t_{AB} = \frac{(2\pi R)^2}{D} . \tag{4.57}$$

In particular, the saddle-point is located at $t_0^{\text{opt}} \ll t_{AB}$ (see Eq. (H.1)), meaning that the optimal paths are much straighter than typical diffusive ones. Eq. (4.56) is valid in the strong-dephasing regime $S_{AB}^{\text{opt}} \gg 1$ (see Eq. (H.2)). Writing the exponential factor of the Aharonov-Bohm amplitude (4.56) in the form $\exp\{-2\pi R/L_\varphi\} = \exp\{-(t_{AB}/\tau_\varphi^{\text{AB}})^{1/2}\}$,

equivalent to introducing $1/\tau_\varphi^{\text{AB}}$ as a mass of the CF diffuson propagator [17, 38], the dephasing rate $1/\tau_\varphi^{\text{AB}}$ is found to be

$$\frac{1}{\tau_\varphi^{\text{AB}}} = 6 g_\square T \ln \frac{b}{l} , \quad (4.58)$$

which, as expected from the long-time behaviour of the action (4.46), is the same as the dephasing rate for the quasi-onedimensional wire, Eq. (4.47).

4.6 Fast versus slow gauge field fluctuations

Having seen that mesoscopic conductance fluctuations of the fermion-gauge field system are strongly suppressed by an ensemble averaging effect rather than “true” decoherence (i.e. loss of phase memory of the individual particles), a question to be asked is whether the effects of “slow” gauge field fluctuations (with frequencies $\omega \lesssim 1/\tau_\varphi$) and “fast” gauge field fluctuations (with frequencies $\omega \gtrsim 1/\tau_\varphi$) can be separated. Then the (loss of) phase memory of the individual particles could be accessed, which would have important consequences for the validity of the Fermi-liquid picture of the half-filled lowest Landau level. Unfortunately, both conductance fluctuations and weak localization do to leading order not allow this. What is needed is a quantum interference effect which is sensitive to neither time-reversal breaking nor ensemble averaging.

The weak-localization contribution of second order in the disorder is such a quantity. Several contributions to it are given by diffusons only, and therefore insensitive to time-reversal breaking by gauge-field fluctuations (see Figs. 4.5, 4.6). Since weak localization also is an ensemble-averaged quantity, it is also insensitive to fluctuations which are static on the timescale of the coherent electron motion ($\omega \lesssim 1/\tau_\varphi$). So the two-diffuson contributions to weak localization fulfil both requirements, being sensitive only to fluctuations with frequencies $\omega \gtrsim 1/\tau_\varphi$. The different interference effects and by which type of fluctuations they are affected are summarized in Table 4.1.

The process shown in the left of Fig. 4.5 can be characterized by the following path integral:

$$\delta g_{\text{WL}}^{2\text{-loop}} \sim \int_{[\mathbf{r}]=[\mathbf{r}_1]+[\mathbf{r}_2]} \mathcal{D}[\mathbf{r}(t)] \exp \left\{ - \int_{-t_0}^{t_0} dt' \frac{\dot{\mathbf{r}}^2}{4D} - ie \int_{-t_0}^{t_0} dt' \left[\dot{\mathbf{r}}_1(t') \mathbf{a}[\mathbf{r}_1(t'), t'] - \dot{\mathbf{r}}_2(t') \mathbf{a}[\mathbf{r}_2(t'), t'] \right] \right\} , \quad (4.59)$$

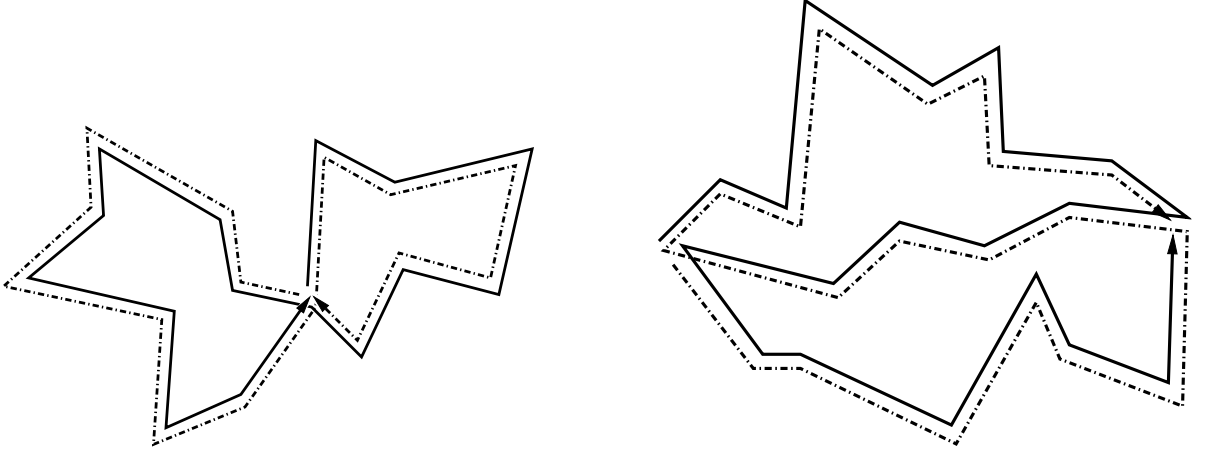


Figure 4.5: Left: A set of two trajectories visiting the same two sets of impurity sites, each set in the same order but one trajectory visiting one set first and the other trajectory visiting the other set first, returning to the origin in between. The two trajectories thus accumulate the same phase, independent of breaking of time-reversal symmetry, and interfere constructively, giving a contribution second order in $1/g$ to the weak localization effect. Right: Another set of trajectories with the same feature of accumulating the same phase although visiting the impurity sites in different orders.

where the two paths $\mathbf{r}_1, \mathbf{r}_2$ visit the same sets of impurities,⁹

$$\begin{aligned} \mathbf{r}_2(t' \geq 0) &= \mathbf{r}_1(t' - t_0) , \\ \mathbf{r}_2(t' \leq 0) &= \mathbf{r}_1(t' + t_0) , \\ \mathbf{r}_1(t' = \pm t_0) &= \mathbf{r}_1(t' = 0) . \end{aligned} \quad (4.60)$$

This allows to write the path integral as

$$\begin{aligned} \delta g_{\text{WL}}^{2\text{-loop}} \sim & \int_{\mathbf{r}_{1,2}(0)=\mathbf{r}_{1,2}(t)} \mathcal{D}[\mathbf{r}_1(t)] \mathcal{D}[\mathbf{r}_2(t)] \exp \left\{ - \int_0^{t_0} dt' \left[\frac{\dot{\mathbf{r}}_1^2}{4D} + \frac{\dot{\mathbf{r}}_2^2}{4D} \right] \right. \\ & - ie \int_0^{t_0} dt' \left[\dot{\mathbf{r}}_1(t') \left[\mathbf{a}[\mathbf{r}_1(t'), t'] - \mathbf{a}[\mathbf{r}_1(t'), t' - t_0] \right] \right. \\ & \left. \left. - \dot{\mathbf{r}}_2(t') \left[\mathbf{a}[\mathbf{r}_2(t'), t'] - \mathbf{a}[\mathbf{r}_2(t'), t' - t_0] \right] \right] \right\} . \end{aligned} \quad (4.61)$$

⁹Here it is assumed for simplicity that the times spent visiting each of the two sets of impurities are equal. This simplifies the notation but does not affect the general argument.

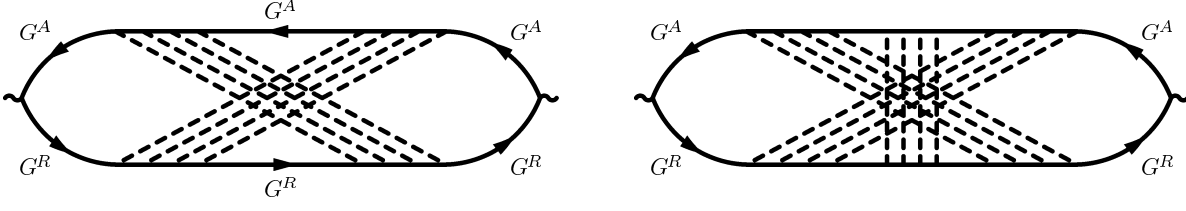


Figure 4.6: Diagrammatic representations of the processes shown in Fig. 4.5.

effect affected by	mesoscopic conductance fluctuations	weak localization (1-loop)	weak localization (2-loop)
scalar fluctuations with $\omega \lesssim 1/\tau_\varphi$	(yes)*	no	no
scalar fluctuations with $\omega \gtrsim 1/\tau_\varphi$	yes	yes	yes
vector fluctuations with $\omega \lesssim 1/\tau_\varphi$	yes, by ensemble averaging	yes, by time-reversal breaking	yes, by time-reversal breaking (Cooperon part), no (diffuson part)
vector fluctuations with $\omega \gtrsim 1/\tau_\varphi$	yes	yes	yes

Table 4.1: Overview to which type of electromagnetic fluctuations the different quantum interference phenomena are sensitive. “Fast” fluctuations with frequencies $\omega \gtrsim 1/\tau_\varphi$ always lead to “true” dephasing, while “slow” fluctuations with frequencies $\omega \lesssim 1/\tau_\varphi$ result in ensemble-averaging and (for vector fluctuations) time-reversal breaking effects, to which not all quantities are sensitive. In particular, the diffuson contribution to weak localization in two-loop order is sensitive to neither ensemble averaging nor time-reversal breaking. In any case, the fluctuations need to have momenta larger than the inverse dephasing length (or the inverse system size for the Aharonov-Bohm configuration), since otherwise they can be gauged away by a global gauge transformation. * note that the screened Coulomb propagator has not enough weight at low frequencies for this to be important. However, similar considerations apply to external (i.e. not arising from diffusive electron motion) slow fluctuations which do not break time-reversal symmetry, e.g. $1/f$ noise [31, 44, 73, 101].

It is immediately obvious that a (quasi)static random gauge field which does not change on the time scale t_0 drops out, and this two-loop contribution to weak localization is only affected by gauge field fluctuations which are fast on the time scale of the electron motion.¹⁰

However, it seems that second-order weak localization is not reliably accessible in experiments. Being second order in $1/g$, where g is the dimensionless conductance, it is a very small quantity from the start. Since it is (as required) insensitive to magnetic fields, it cannot be examined by magnetoresistance effects. Its temperature dependence is masked by the temperature dependences of Altshuler-Aronov type corrections [29] in first order in $1/g$ and cannot be accessed separately.

It is instructive to compare the effect of *fast* gauge field fluctuations on one-loop weak localization to the effect of all fluctuations, which has been considered in Section 4.4.1. As has been discussed in Section 4.4.1, the first term in brackets of Eq. (4.34), giving the leading contribution, does not depend on the validity of the static approximation. Therefore a direct comparison is possible. Restricting the frequency integration to frequencies $\omega_{\text{gf}} \gtrsim \tau_{\varphi}^{\text{true}}$, where $\tau_{\varphi}^{\text{true}}$ is the “true” dephasing rate denoting the loss of phase memory of a single (non-ensemble averaged) particle and should be determined self-consistently,¹¹ the result is

$$\begin{aligned} \int_{|\omega_{\text{gf}}| \gtrsim 1/\tau_{\varphi}^{\text{true}}} \frac{d\omega_{\text{gf}}}{2\pi} \langle a_{\alpha} a_{\beta} \rangle_{\mathbf{k}, \omega_{\text{gf}}} &= \int_{|\omega_{\text{gf}}| \gtrsim 1/\tau_{\varphi}^{\text{true}}} \frac{d\omega_{\text{gf}}}{2\pi} \frac{2T}{\sigma \omega_{\text{gf}}^2 + \sigma \left(\frac{\chi k^2}{\sigma} \right)^2} \delta_{\alpha\beta}^{\perp}(\mathbf{k}) \\ &= \frac{2T}{\pi \chi k^2} \delta_{\alpha\beta}^{\perp}(\mathbf{k}) \arctan \frac{\chi k^2 \tau_{\varphi}^{\text{true}}}{\sigma} \end{aligned} \quad (4.62)$$

instead of Eq. (4.7). The low- k behaviour of the first term in brackets in Eq. (4.34) is now regularized by the arctan factor of Eq. (4.62) instead of the second term in brackets. The logarithmic contribution to the integral vanishes completely if the dephasing time $\tau_{\varphi}^{\text{true}}$ satisfies

$$\tau_{\varphi}^{\text{true}} \lesssim 12\pi g^2 \tau, \quad (4.63)$$

because then the arctan can be expanded for all momenta up to the order of l^{-1} (see Fig. 4.7).

As a result, the action corresponding to fast gauge field fluctuations evaluates to

$$\langle \Delta S_{\text{fast}} \rangle \simeq \frac{T t_0 \tau_{\varphi}^{\text{true}}}{8\pi^2 g \tau}, \quad (4.64)$$

¹⁰For Coulomb interaction, it has been found in Ref. [69] that diffuson and Cooperon propagators decay in the same way in the long-time limit.

¹¹note that while the conditions $k \gtrsim L_{\varphi}^{-1}$ and $\omega \gtrsim \tau_{\varphi}^{-1}$ are equivalent for the screened Coulomb interaction, due to the slow dynamics of the gauge field here $k \gtrsim L_{\varphi}^{-1}$ is the stronger condition.

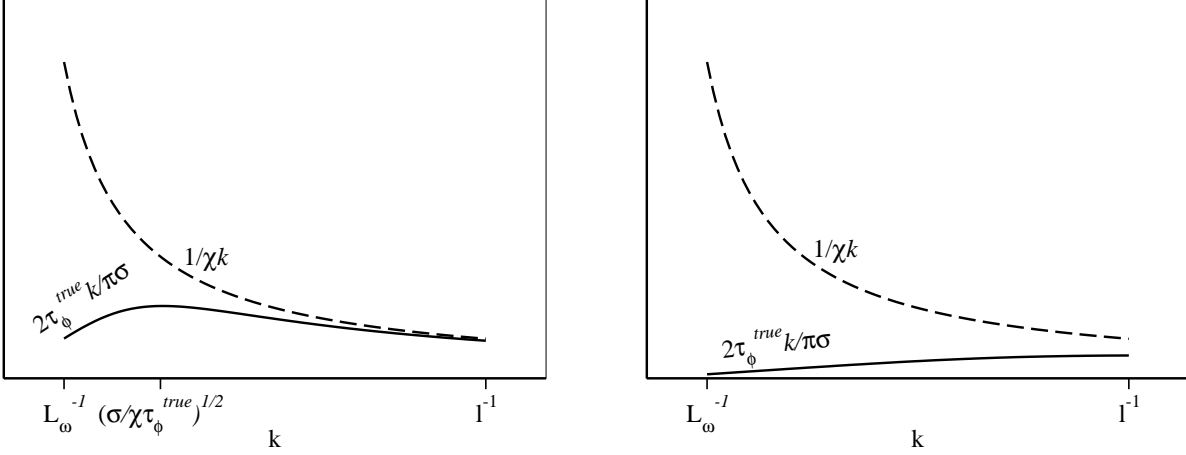


Figure 4.7: Left: the contribution of *fast* gauge field fluctuations with frequencies $\omega_{\text{gf}} \gtrsim 1/\tau_\phi^{\text{true}}$ to the action (4.64) (solid line) compared to the contribution of all gauge field fluctuations (dashed line) to the action (4.36). While the contribution of all gauge field fluctuations arising from the first term in brackets of Eq. (4.34) is regularized for low momenta by the other terms at the scale L_ω^{-1} (see also Fig. 4.3), the contribution of *fast* fluctuations is regularized self-consistently by the arctan factor in Eq. (4.62) at the scale $k_{\text{min}} = (\sigma/\chi\tau_\phi^{\text{true}})^{1/2} = (12\pi g^2/\tau_\phi^{\text{true}})^{1/2}$. For not too long dephasing times $\tau_\phi^{\text{true}} \lesssim 12\pi g^2\tau$ this contribution degenerates to the one shown in the right, with the logarithmic contribution vanishing. The dephasing rate (4.66) due to fast fluctuations is smaller than the inverse temperature in a wide parameter range, confirming the Fermi liquid picture.

while the action corresponding to the effect of all gauge field fluctuations is given by Eq. (4.36). From Eq. (4.64) it is seen that

$$\langle \Delta S_{\text{fast}} \rangle \lesssim T t_0 \quad \text{for} \quad \tau_\phi^{\text{true}} \lesssim 8\pi^2 g\tau, \quad (4.65)$$

in agreement with the Fermi liquid picture, and the “true” dephasing rate is evaluated self-consistently by the condition $\langle \Delta S_{\text{fast}} \rangle(t_0 = \tau_\phi^{\text{true}}) = 1$ to be

$$\frac{1}{\tau_\phi^{\text{true}}} = \left(\frac{T}{8\pi^2 g\tau} \right)^{1/2}, \quad (4.66)$$

which is well compatible with the diffusive regime $T\tau \ll 1$ considered in this chapter. Using the dephasing rate (4.66), the condition (4.63) for τ_ϕ^{true} used in the evaluation of the action (4.64) translates to the condition on the temperature

$$T \gtrsim \frac{1}{18g^3\tau}. \quad (4.67)$$

This means that the condition (4.63), allowing the expansion of the arctan factor in Eq. (4.62), is justified for every realistic sample, and the spectrum of fast fluctuations contributing to “true” dephasing (shown in the right of Fig. 4.7) is very different from the one shown in Fig. 4.3, which leads to an ensemble-averaging or time-reversal breaking effect only.

A more interesting restriction is set by the temperature scale

$$T \approx \frac{1}{8\pi^2 g \tau} , \quad (4.68)$$

at which even the dephasing rate (4.66) *due to fast fluctuations only* becomes of the order of the temperature. At this temperature, the interval for thermal gauge field fluctuations with frequencies ω_{gf} in the range $1/\tau_{\varphi}^{\text{true}} \lesssim \omega_{\text{gf}} \lesssim T$ collapses. The scale given Eq. (4.68) computes to less than 1 mK for typical samples and therefore is of little experimental relevance, however what happens at such low temperatures deserves a more detailed theoretical study.

All the above arguments can also be directly transferred to the wire geometry once the momentum scale set by the arctan factor in Eq. (4.62) exceeds the scale set by the inverse wire width.

So indeed, as has been argued in Section 4.4.1, the dephasing rate due to “fast” gauge field fluctuations, Eq. (4.66), is much smaller than the dephasing rate arising from all gauge field fluctuations, Eq. (4.40), which is mostly due to an ensemble averaging effect. The “true” dephasing rate, Eq. (4.40), being smaller than the temperature in a parametrically large region of the diffusive regime, is compatible with the Fermi liquid picture for the composite fermions in the presence of a fluctuating Chern-Simons field in the parameter range of experimental relevance.

4.7 Summary

This chapter has focused on the effect of transverse gauge field fluctuations on quantum interference phenomena.

While the effects of transverse electromagnetic fluctuations on electrons are relativistically small, for composite-fermion systems, where the electron-gauge field coupling is of order unity, the dephasing rates in both two and quasi-one dimensions exceed the dephasing rates arising from Coulomb interaction by orders of magnitude.

For good metals (when the conductance is large), characteristic frequencies of the gauge field are much slower than the electron dynamics, so that each of the electrons essentially moves in a static gauge field configuration. Unlike the small energy transfers associated with Coulomb scattering in low dimensions, the random phases associated with the trajectories in the presence of gauge field fluctuations are a topological effect, which can be described in terms of the geometry of the trajectories alone. While earlier estimates [55] related the dephasing in a straightforward way to the area enclosed by

typical paths, a refined argument [75] produces an additional logarithmic correction. This correction is due to the fact that, as already pointed out in Ref. [55], it is actually the non-oriented area enclosed by a path which should be taken instead of the geometrical area. The non-oriented area is defined as the geometrical area weighted with the square of the number of times a particular part is encircled. Compared to the estimate from Ref. [55], where the non-oriented area was set equal to the geometrical area, the non-oriented area is enhanced by the effect of multiple returns to a given point. This turns out to be particularly important in low dimensions.

In Section 4.4.1, it has been shown that the earlier result of Ref. [75] can be obtained, using a perturbative expansion in the coupling to the gauge field, in a diffusive formulation without explicitly taking ballistic propagation into account. The logarithmic correction to the dephasing rate, Eq. (4.40), compared to the estimate from Ref. [55], is due to multiple return processes which happen on large scales and do not depend on the details of the short-scale physics.

In Section 4.4.2, the diffusive formulation of Section 4.4.1 has been transferred to quasi-one-dimensional wires. Due to the confined geometry an algebraic correction $\sim t_0^{1/2}$ arises instead of the logarithmic one in two dimensions. Since the important quantity is the non-oriented area enclosed by closed paths, the effect of multiple returns on the non-oriented area thus almost neutralizes the effect of the confinement in the lateral direction. As a result, the dephasing rate in two dimensions (4.40) differs from the one in quasi-one dimension (4.47) only by a logarithmic factor. Remarkably, the different effects in the wire geometry combine in a way that no infrared divergences arise in the fermion-gauge field system. The differences in the low-momentum cutoffs applicable to the two geometries, which have been discussed in Section 2.2.4, thus are irrelevant in the context of transverse gauge field fluctuations. As a result, the dephasing rates due to gauge field fluctuations in the wire geometry (4.47) and in the Aharonov-Bohm geometry (4.58) are the same, unlike in the case of Coulomb interaction. The dephasing effect can be thought of to happen in a local fashion along the wires forming the ring, and thus does not differ from the dephasing in the singly-connected geometry.

The validity of the static approximation for the gauge field fluctuations has been confirmed for typical parameters of semiconductor samples. Moreover the calculations have shown that the results are quite insensitive to a relaxation of the static approximation, as in the leading order the integrations over the frequencies of the fermions and the gauge field fluctuations factorize.

The relation of weak localization and mesoscopic conductance fluctuations in the presence of Coulomb interaction [85], which has been traced back in Section 2.3 to the two quantities being given by the same path integral, has been shown in Section 4.3 to exist in a similar way also in the presence of slow transverse gauge field fluctuations. Ultimately this is caused by the ensemble averaging effect of the static gauge field fluctuations having the same effect on conductance fluctuations as the time-reversal breaking of the gauge field fluctuations has on the weak localization amplitude. The calculated results on weak localization can therefore be used via the relation (4.20) or (4.21) to

express mesoscopic conductance fluctuations of a fermion-gauge field system.

The results presented in this chapter have some interesting implications for the observability of quantum interference in transport phenomena of composite fermion systems: To access the diffusive temperature regime, for which this chapter is written, low but accessible temperatures of the order of 30 mK are needed. Typical dephasing lengths to be expected are of the order of tenths of microns. Further, the quasi-one-dimensional regime can be realized using wires with widths of the order of $0.1 \mu\text{m}$. The dephasing lengths in simple wires and in the Aharonov-Bohm geometry are similar to the dephasing length in two dimensions and differ from it only by numerical and logarithmic factors.

Although the calculated dephasing rates exceed the thermal broadening by large factors, this does not invalidate the Fermi liquid picture [3] of the fermion-gauge field systems: The dephasing rates (4.40), (4.47) are mainly due to an ensemble averaging effect over the gauge field configurations. The phase distribution of the fermions within the ensemble broadens much faster than the individual particle loses its phase memory. In Section 4.6, it has been explicitly checked that the “true” dephasing rate due to fast gauge field fluctuations, Eq. (4.66), is smaller than the inverse temperature down to very low temperatures. The dephasing rate (4.40), due to ensemble averaging over the gauge field fluctuations, exceeds the “true” one by a factor which is parametrically large in the conductance g . The Fermi liquid picture thus remains valid in the experimentally relevant parameter range, since the individual particles keep their phase memory much longer than the time needed to broaden the phase distribution of the ensemble. The “true” dephasing rate of the individual particles is accessible through neither mesoscopic conductance fluctuations nor one-loop weak localization, since the former are suppressed by the ensemble averaging and the latter is suppressed by the time-reversal breaking of the slow fluctuations. The diffuson contribution to two-loop weak localization would in principle give access to the effect of the fast fluctuations alone, since it is not affected by either ensemble averaging or time-reversal breaking. However, it seems that this is difficult to measure experimentally due to its insensitivity to magnetic fields and the small magnitude of this effect compared to the Altshuler-Aronov correction. It remains to be seen whether there exists another experimental setup in which the “true” phase coherence of Composite Fermions could be better observed.

At very low temperatures, as given by Eq. (4.68), the “true” dephasing rate due to fast gauge field fluctuations alone cannot be easily estimated by Eq. (4.66), since the details of the spectrum of thermal fluctuations need further consideration. The properties of the fermion-gauge field system at such low temperatures call for a closer examination, which is beyond the limits of this thesis.

5 Conclusions

The interplay of interaction and disorder is one of the key topics in mesoscopic physics. Especially lowdimensional samples show a rich variety of phenomena related to both. This thesis has focused on dephasing effects in quantum transport arising from electron-electron interaction.

For diffusive lowdimensional systems, momenta and momentum transfers of the order of the inverse system size dominate the behaviour. Chapter 2 has considered Aharonov-Bohm oscillations of conductance in a ring formed of quasi-onedimensional wires. While h/e and $h/2e$ oscillations are related to mesoscopic conductance fluctuations and weak localization respectively, they differ from them in the way that Aharonov-Bohm interference takes place on a global scale between topologically different paths. Important trajectories therefore have a minimum length which is set by the size of the ring. This condition holds even when the dephasing length becomes much smaller than the path length, and therefore differs from the usual self-consistency condition that only inelastic processes with momentum transfers greater than the inverse dephasing length contribute to dephasing. Instead, momentum transfers of the order of the inverse system size determine the dephasing, resulting in the dephasing length (2.34), which differs from the usual one given by Eq. (1.11). The naive assumption (2.1) should therefore be replaced by the presented results (2.30), (2.33), which are derived from a microscopic theory. Using the path-integral formalism, the relation (2.41) between weak localization and mesoscopic conductance fluctuations has also been proven on a more general ground and naturally extended to the equivalent relation (2.48) between h/e and $h/2e$ Aharonov-Bohm oscillations.

When a sample is far from equilibrium, several new phenomena arise. Chapter 3 developed a theory of conductance fluctuations out of equilibrium. Several different regimes result in an interesting nonmonotonic behaviour of the conductance fluctuations as a function of the voltage. When the voltage V is increased beyond linear response, there is a broad regime $V_c \ll V \ll gV_c$ in which inelastic effects are negligible but fluctuations of the electrochemical potential result in an enhancement of conductance fluctuations. This can ultimately be traced back to be an effect of electron-electron interaction, as the electrochemical potential arises from screening of the Coulomb interaction on lengthscales larger than the screening length. A fully noninteracting picture treated by scattering theory, assuming just different concentrations of charge carriers, would miss this effect. As the phase space for inelastic scattering effects is opened up further with increasing voltage, it turns out that these become important at voltages $V \gtrsim gV_c$. For the strong-dephasing regime $V \gg gV_c$, the asymptotic behaviour (3.99) has been found. It is the

result of a position-dependent dephasing effect, which is due to the available phase space changing with the position-dependent electron distribution function along the sample. The power law (3.99) is given by regions with weak dephasing in the vicinity of the reservoirs and the scaling of these regions with the voltage. The experimental results from Refs. [86, 87] are explained well by the presented theory on the basis of electron-electron interaction alone, without the need to consider electron-phonon scattering.

Finally, Chapter 4 addressed the effect of gauge field fluctuations. The systems under consideration differ from electrons interacting only via the Coulomb interaction in a remarkable way: The dynamics of the gauge field introduce new timescales, being much slower than the electron motion. Moreover, the dephasing due to the transverse part of the gauge field is not related to energy exchange, but rather to topological properties of the electron trajectories, and is mostly a broadening of the phase within the ensemble average over quasistatic gauge field configurations rather than loss of phase memory of the single particle. Remarkably, a relation between weak localization and mesoscopic conductance fluctuations can be derived similar to the case of Coulomb interaction, the effects of time-reversal breaking on weak localization and the effect of ensemble averaging on mesoscopic conductance fluctuations being mapped onto each other. While the (apparent) dephasing rate (4.40), including those effects, is much larger than the inverse temperature, the “true” dephasing rate (4.66) describing loss of phase memory of the single Composite Fermion remains smaller than the inverse temperature for experimentally relevant parameters, in agreement with the Fermi liquid picture of the half-filled lowest Landau level. However, no reasonably accessible effect displaying this “true” dephasing rate has been identified so far, second-order weak localization being of mostly theoretical interest. Interestingly, although the gauge field correlator is very singular at low momenta and the momenta characteristic for the behaviour of lowdimensional systems are given by the lowest available momenta in a more pronounced way as the dimensionality is lowered, the quasi-onedimensional fermion-gauge field system exhibits a dephasing rate which is linear in the temperature. The logarithmic correction of the twodimensional system turns out to be absent in the wire. As a result, the peculiarities of the infrared cutoff from Chapter 2 do not carry over to the fermion-gauge field system, and the dephasing rates for the singly-connected wire geometry and for the Aharonov-Bohm geometry are identical.

While the behaviour of interacting electrons in disordered systems is understood quite well, some open questions exist regarding the properties of Composite Fermion systems. Most directly encountered in the present thesis was the existence of the temperature scale given by Eq. (4.68), at which the estimated “true” dephasing rate becomes of the order of the temperature and the spectrum of thermal gauge field fluctuations with frequencies $\omega_{\text{gf}} \lesssim T$ vanishes. The behaviour of the system in this regime has not yet been understood and calls for further investigation.

A Preexponential factor of Aharonov-Bohm oscillations

In this appendix, the preexponential factor accompanying the exponential factor (2.30) is calculated by the standard method of performing Gaussian integrations over small deviations from the optimal solution [19]. Only the parametric dependence of the prefactor will be considered, neglecting numerical factors of order unity.

First, consider small offsets of the initial and final points of the paths from their optimal position. The second-order variation of the action $\delta^2 S$ will be a quadratic form of the offsets, $\delta^2 S = u_{ij} \delta\Theta_i \delta\Theta_j$, where $i = 1, 2$. Using that $\delta^2 S \sim 1$ for $\delta\Theta_i \sim 1$, it follows that

$$(\det u_{ij})^{-1/2} \sim \frac{1}{S}. \quad (\text{A.1})$$

Second, there is a possibility for small deviations of the paths from the instanton solution, $\theta_i = \theta_i^{\text{opt}} + \delta\theta_i$. The fluctuation term

$$\int_0^0 \mathcal{D}[\delta\theta_1(\tau')] \int_0^0 \mathcal{D}[\delta\theta_2(\tau')] \exp \left\{ -\frac{1}{2} \frac{\delta^2 S}{\delta\dot{\theta}_i \delta\dot{\theta}_j} \delta\dot{\theta}_i \delta\dot{\theta}_j \Big|_{\theta_{i,j}^{\text{opt}}} - \frac{1}{2} \frac{\delta^2 S}{\delta\theta_i \delta\theta_j} \delta\theta_i \delta\theta_j \Big|_{\theta_{i,j}^{\text{opt}}} \right\} \quad (\text{A.2})$$

factorizes from the action of the optimal paths due to the quadratic form of the exponent in Eq. (2.15). It can be identified as the path integral representation of the propagator of an harmonic oscillator with parameters $m \sim R^2/D$ and $m\omega^2 \sim RT/D\nu$. There are two such factors (one for each of the paths), yielding together

$$\left[(m\omega)^{1/2} \right]^2 \sim \frac{T^{1/2} R^{3/2}}{\nu^{1/2} D}. \quad (\text{A.3})$$

Eqs. (A.1), (A.3) thus cancel in the preexponential factor.

Finally, there is a Gaussian integration over the deviations of the time τ spent on the path from its optimal value $\tau_{\text{opt}} \sim (\nu R/T)^{1/2}$. The corresponding factor can be estimated as

$$\left(\frac{\partial^2 S}{\partial \tau^2} \right)_{\tau=\tau_{\text{opt}}}^{-1/2} \sim \left(\frac{S}{\tau_{\text{opt}}^2} \right)^{-1/2} \sim \frac{\nu^{3/4} D^{1/2}}{T^{3/4} R^{1/4}}. \quad (\text{A.4})$$

Alternatively, it can be obtained in the following way: To account for deviations from the optimal duration τ_{opt} of the paths, consider the particle tunnelling not with zero

energy, but with a small energy E_0 , which can be viewed as a function of the time τ elapsed on the path. The action then is

$$S = \int_0^\tau d\tau' \left\{ \frac{8TR}{\nu D} \left[\theta(\tau') - \frac{2}{\pi} \theta^2(\tau') \right] + E_0(\tau) \right\} \quad (\text{A.5})$$

and its second derivative with respect to τ is

$$\frac{\partial^2 S}{\partial \tau^2} = \frac{8TR}{\nu D} \left[\dot{\theta}(\tau) - \frac{4}{\pi} \theta(\tau) \dot{\theta}(\tau) \right] + 2 \frac{\partial E_0(\tau)}{\partial \tau} + t \frac{\partial^2 E_0(\tau)}{\partial \tau^2} . \quad (\text{A.6})$$

Setting $\tau = \tau_{\text{opt}}$ (which is equivalent to setting $E_0 = 0$), the first term vanishes since $\dot{\theta} = 0$, and the second term vanishes since $\frac{\partial \tau}{\partial E_0} \sim -\frac{D^{1/2}\nu}{TE_0^{1/2}}$ at $E_0 \rightarrow 0$. Using

$$\frac{\partial^2 E_0}{\partial \tau^2} = -\frac{\tau''(E_0)}{[\tau'(E_0)]^3}, \text{ as well as}$$

$$\begin{aligned} \tau_{\text{opt}} &= 2 \int_0^{\pi/2} \frac{d\theta}{\dot{\theta}} \\ &= \int_0^{\pi/2} \frac{d\theta}{\left[\frac{8T}{\nu R} \left(\theta - \frac{\gamma+1}{\pi} \theta^2 \right) \right]^{1/2}} \\ &= \left(\frac{\nu R}{8T} \right)^{1/2} \frac{\pi^{1/2} (\pi - \arccos \gamma)}{(\gamma + 1)^{1/2}} \end{aligned} \quad (\text{A.7})$$

(see also Eqs. (2.30), (2.31)), it is seen that

$$\left(\frac{\partial^2 S}{\partial \tau^2} \right)_{\tau=\tau_{\text{opt}}} \sim \frac{R^{1/2} T^{3/2}}{D \nu^{3/2}}, \quad (\text{A.8})$$

which is equivalent to Eq. (A.4).

Combining Eqs. (A.1), (A.3), and (A.4) with the exponential factor (2.30), the result is Eq. (2.33).

B Keldysh diagram for the current

Here the derivation of Eq. (3.36) is given, which relates the current to the impurity averaged diagonal Keldysh function.

We begin by expressing the averaged Keldysh function $\langle G^K(x_1, x_2) \rangle$ using the averaged diagonal Keldysh function $\langle G^K(x, x) \rangle$. The self-energy equation for the matrix Green's function can be written as

$$\text{Diagram: Double line with arrow pointing left} = \text{Diagram: Plain line with arrow pointing left} + \text{Diagram: Plain line with arrow pointing left, followed by a dashed loop, followed by a double line with arrow pointing left}, \quad (\text{B.1})$$

with the plain lines denoting the unperturbed Green's function $\hat{G}^{(0)}$ and the double lines denoting the full Green's function \hat{G} (in the following impurity averaging is implied). Using Eq. (3.33), this results in the equation of motion

$$\left(i \frac{\partial}{\partial t} - H \right) \hat{G}(\mathbf{r}, t; \mathbf{r}', t') = \mathbb{I} \delta(\mathbf{r} - \mathbf{r}') \delta(t - t') + \frac{1}{2\pi\nu\tau} \int dt'' \hat{G}(\mathbf{r}, t; \mathbf{r}, t'') \hat{G}(\mathbf{r}, t''; \mathbf{r}', t') \quad (\text{B.2})$$

with $H = -\frac{1}{2m}\nabla^2 + U(\mathbf{r}) + e\phi(\mathbf{r})$. Changing to the Fourier representation and using Eq. (3.34) as well as $G^{R,A}(\mathbf{r}, \mathbf{r}) = \mp i\pi\nu$ with Eq. (B.2) and the corresponding equation with the operators acting from the right, the matrix Green's function satisfies

$$(\epsilon - H) \hat{G} = \mathbb{I} + \frac{i}{2\tau} \begin{pmatrix} -1 & 2[2n(\mathbf{r}) - 1] \\ 0 & 1 \end{pmatrix} \begin{pmatrix} G^R & G^K \\ 0 & G^A \end{pmatrix}, \quad (\text{B.3})$$

$$\hat{G}(\epsilon - H) = \mathbb{I} + \frac{i}{2\tau} \begin{pmatrix} G^R & G^K \\ 0 & G^A \end{pmatrix} \begin{pmatrix} -1 & 2[2n(\mathbf{r}) - 1] \\ 0 & 1 \end{pmatrix}. \quad (\text{B.4})$$

Adding Eqs. (B.3), (B.4), the off-diagonal component is equal to

$$(\epsilon - \hat{H}) G^K + G^K (\epsilon - \hat{H}) = \frac{i}{\tau} [(2n_\epsilon - 1) G^A + G^R (2n_\epsilon - 1)] . \quad (\text{B.5})$$

Using the gradient expansion [35], one finds

$$G^K(\mathbf{r}, \mathbf{p}) = \frac{i}{\tau} \left\{ [2n_\epsilon(\mathbf{r}) - 1] G^R(\mathbf{p}) G^A(\mathbf{p}) + i\nabla n_\epsilon(\mathbf{r}) [G^R(\mathbf{p}) \nabla_p G^A(\mathbf{p}) - G^A(\mathbf{p}) \nabla_p G^R(\mathbf{p})] \right\}. \quad (\text{B.6})$$

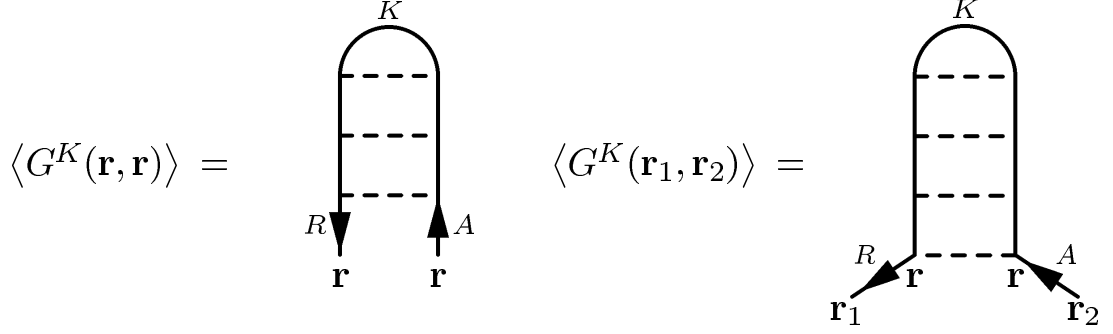


Figure B.1: Diagrammatic representation of the relation between the averaged Keldysh function $\langle G^K(\mathbf{r}_1, \mathbf{r}_2) \rangle$ and the averaged diagonal Keldysh function $\langle G^K(\mathbf{r}, \mathbf{r}) \rangle$, Eq. (B.7), which is used in the derivation of Eq. (3.36).

This is equivalent to the relation

$$\langle G^K(\mathbf{r}_1, \mathbf{r}_2) \rangle = \frac{1}{2\pi\nu\tau} \int d\mathbf{r} \langle G^R(\mathbf{r}_1, \mathbf{r}) \rangle \langle G^K(\mathbf{r}, \mathbf{r}) \rangle \langle G^A(\mathbf{r}, \mathbf{r}_2) \rangle . \quad (\text{B.7})$$

This relation can be easily understood diagrammatically, see Fig. B.1. Using the relation (3.7) between the function $G^{-+} = (G^K + G^A - G^R)/2$ and the electron density matrix ρ , one finds

$$I_x(\mathbf{r}) = \frac{(-e)}{m} \int \frac{d\epsilon}{2\pi} \nabla G^{-+}(\mathbf{r}, \mathbf{r}') \Big|_{\mathbf{r}'=\mathbf{r}} . \quad (\text{B.8})$$

The contribution from the term $G^A - G^R$ is proportional to the spectral density and does not depend on the state of the system. Therefore only the Keldysh function G^K contributes to the current [35], which can now conveniently be calculated by a change to momentum space,

$$\begin{aligned} \langle I_x(\mathbf{r}) \rangle &= \frac{(-e)}{2m} \frac{\partial}{\partial x} \int \frac{d\epsilon}{2\pi} \langle G_\epsilon^K(\mathbf{r}, \mathbf{r}') \rangle \Big|_{\mathbf{r}'=\mathbf{r}} \\ &= \frac{(-e)}{2} \int \frac{d\epsilon}{2\pi} \int \frac{d^d p}{(2\pi)^d} G_\epsilon^R(\mathbf{p} + \mathbf{q}) G_\epsilon^A(\mathbf{p}) \frac{ip_x}{m} \frac{1}{2\pi\nu\tau} \langle G_\epsilon^K(\mathbf{r}, \mathbf{r}) \rangle \\ &= \frac{-ie}{2} \int \frac{d\epsilon}{2\pi} \int \frac{d^d p}{(2\pi)^d} \frac{\mathbf{p}\mathbf{q}}{m} \frac{p_x}{m} (G_\epsilon^R)^2 G_\epsilon^A \frac{1}{2\pi\nu\tau} \langle G_\epsilon^K(\mathbf{r}, \mathbf{r}) \rangle \\ &= \frac{-iep_F^2}{2m^2d} 2\pi i\nu\tau^2 q_x \frac{1}{2\pi\nu\tau} \int \frac{d\epsilon}{2\pi} \langle G_\epsilon^K(\mathbf{r}, \mathbf{r}) \rangle \\ &= \frac{e}{2} D q_x \int \frac{d\epsilon}{2\pi} \langle G_\epsilon^K(\mathbf{r}, \mathbf{r}) \rangle \\ &= \frac{e}{4\pi i} D \frac{\partial}{\partial x} \int d\epsilon \langle G_\epsilon^K(\mathbf{r}, \mathbf{r}) \rangle , \end{aligned} \quad (\text{B.9})$$

which is just Eq. (3.36).

To obtain the kinetic equation (3.35), one subtracts Eqs. (B.3), (B.4), and obtains

$$(\epsilon - H) G^K - G^K (\epsilon - H) = 0 . \quad (\text{B.10})$$

The commutator is in the quasiclassical approximation equal to the Poisson bracket $\{(\epsilon - H), \hat{G}\}$. For a stationary situation,

$$\frac{p}{m} \frac{\partial}{\partial \mathbf{r}} G^K(\mathbf{r}, \mathbf{p}) - \nabla[U(\mathbf{r}) + e\phi(\mathbf{r})] \frac{\partial}{\partial \mathbf{p}} G^K(\mathbf{r}, \mathbf{p}) = 0 . \quad (\text{B.11})$$

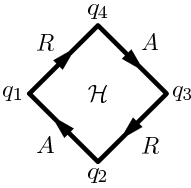
Averaging over the disorder potential, on diffusive lengthscales this describes a random walk, resulting in Eq. (3.35).

C Keldysh diagrams for current fluctuations

In this appendix, the diagrams are calculated which arise in the Keldysh technique and contribute to the correlation function of currents (see Sec. 3.2.2). We will show that the sum of all the diagrams is equal to Eq. (3.37).

We begin by presenting the expressions for the vertex factors (Hikami boxes). Because of their local character (the electron Green's function decays exponentially on the scale of the mean free path l , which is much smaller than the system size L), they can be calculated in the momentum space.

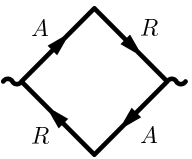
The right Hikami box (containing two Keldysh vertices) of the diagram a-diff is of second order in the incoming momenta q :



The diagram shows a diamond-shaped loop with four vertices. The top vertex is labeled q_4 , the bottom vertex q_2 , the left vertex q_1 , and the right vertex q_3 . The edges are labeled with arrows and letters: the top edge is labeled R with an arrow pointing right, the bottom edge is labeled A with an arrow pointing left, the left edge is labeled A with an arrow pointing down, and the right edge is labeled R with an arrow pointing up. The center of the diamond is labeled \mathcal{H} .

$$= 2\pi\nu D\tau^4 \left(-2q_2q_4 + q_1^2 + q_3^2 \right) , \quad (\text{C.1})$$

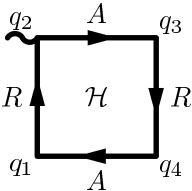
where D is the diffusion constant, ν is the density of states, τ is the elastic scattering time, the q_i are the incoming momenta, and $q_1 + q_2 + q_3 + q_4 = 0$. The left box, containing two velocity vertices, is thus only needed to zeroth order:



The diagram shows a diamond-shaped loop with four vertices. The top edge is labeled A with an arrow pointing right, the bottom edge is labeled R with an arrow pointing left, the left edge is labeled R with an arrow pointing down, and the right edge is labeled A with an arrow pointing up. The vertices are represented by wavy lines.

$$= 4\pi\nu D\tau^2 . \quad (\text{C.2})$$

For the diagram b-diff the vertex factors are needed to first order in the momenta:



The diagram shows a square-shaped loop with four vertices. The top edge is labeled A with an arrow pointing right, the bottom edge is labeled A with an arrow pointing left, the left edge is labeled R with an arrow pointing down, and the right edge is labeled R with an arrow pointing up. The vertices are labeled with incoming momenta: top-left is q_2 , top-right is q_3 , bottom-left is q_1 , and bottom-right is q_4 . The center of the square is labeled \mathcal{H} .

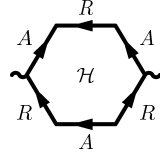
$$= 4\pi i\nu D\tau^3 q_4 . \quad (\text{C.3})$$

The vertex factors of a-coop and b-coop are the same as the vertex factors of b-diff up to extra signs arising from the direction of the Greens functions. The vertex factors of the

diagrams c-diff and c-coop are only needed to zeroth order. Since these diagrams contain only one diffuson/Cooperon, this gives a result of the same order in the momenta as the other diagrams (containing one more diffuson/Cooperon) evaluated up to second order in the momenta.



$$= 0 , \quad (C.4)$$



$$= -4\pi\nu D\tau^4 . \quad (C.5)$$

Calculating the vertex factors, the formulas

$$\int \frac{d^d p}{(2\pi)^d} (G^R)^n (G^A)^m = 2\pi\nu i^{m-n} \binom{m+n-2}{n-1} \tau^{m+n-1} \quad (C.6)$$

and

$$\int \frac{d^d p}{(2\pi)^d} (\mathbf{p} \cdot \mathbf{q}_1) (\mathbf{p} \cdot \mathbf{q}_2) = \int \frac{d^d p}{(2\pi)^d} \frac{p^2}{d} \mathbf{q}_1 \cdot \mathbf{q}_2 \quad (C.7)$$

have been used.

Using the vertex factors (C.1)–(C.5) and changing to real space representation, the expressions corresponding to the diagrams shown in Figs 3.1, 3.2 are (written for a quasi-one-dimensional wire)

$$\begin{aligned} \langle \delta I(V_1) \delta I(V_2) \rangle_{\text{a-diff}} &= \left(\frac{e}{4\pi i} \right)^2 \left(\frac{1}{2\pi\nu\tau} \right)^2 4\pi\nu D\tau^4 2\pi\nu D\tau^2 \int d\epsilon_1 d\epsilon_2 \int \frac{dx_1 dx_2}{L^2} \\ &\times \left[2 \frac{\partial}{\partial x_1} G_{\epsilon_1}^K(x_1) \frac{\partial}{\partial x_2} G_{\epsilon_2}^K(x_2) \mathcal{P}_{\epsilon_1-\epsilon_2} \mathcal{P}_{\epsilon_2-\epsilon_1} \right. \\ &\quad - \frac{\partial^2}{\partial x_1^2} \mathcal{P}_{\epsilon_1-\epsilon_2} \mathcal{P}_{\epsilon_2-\epsilon_1} G_{\epsilon_1}^K(x_1) G_{\epsilon_2}^K(x_2) \\ &\quad \left. - \mathcal{P}_{\epsilon_1-\epsilon_2} \frac{\partial^2}{\partial x_2^2} \mathcal{P}_{\epsilon_2-\epsilon_1} G_{\epsilon_1}^K(x_1) G_{\epsilon_2}^K(x_2) \right] , \quad (C.8) \end{aligned}$$

$$\begin{aligned} \langle \delta I(V_1) \delta I(V_2) \rangle_{\text{b-diff}} &= \left(\frac{e}{4\pi i} \right)^2 \left(\frac{1}{2\pi\nu\tau} \right)^2 (4\pi\nu D\tau^3)^2 \int d\epsilon_1 d\epsilon_2 \int \frac{dx_1 dx_2}{L^2} \\ &\times \left[\frac{\partial}{\partial x_1} \mathcal{P}_{\epsilon_1-\epsilon_2} \frac{\partial}{\partial x_2} \mathcal{P}_{\epsilon_1-\epsilon_2} G_{\epsilon_1}^K(x_1) G_{\epsilon_2}^K(x_2) + \text{c.c.} \right] \quad (C.9) \end{aligned}$$

$$\langle \delta I(V_1) \delta I(V_2) \rangle_{\text{c-diff}} = 0 , \quad (C.10)$$

$$\begin{aligned} \langle \delta I(V_1) \delta I(V_2) \rangle_{\text{a-coop}} &= \left(\frac{e}{4\pi i} \right)^2 \left(\frac{1}{2\pi\nu\tau} \right)^2 (4\pi\nu D\tau^3)^2 \int d\epsilon_1 d\epsilon_2 \int \frac{dx_1 dx_2}{L^2} \\ &\quad \times \mathcal{P}_{\epsilon_1-\epsilon_2} \mathcal{P}_{\epsilon_2-\epsilon_1} \frac{\partial}{\partial x_1} G_{\epsilon_1}^K(x_1) \frac{\partial}{\partial x_2} G_{\epsilon_2}^K(x_2) , \quad (\text{C.11}) \end{aligned}$$

$$\begin{aligned} \langle \delta I(V_1) \delta I(V_2) \rangle_{\text{b-coop}} &= \left(\frac{e}{4\pi i} \right)^2 \left(\frac{1}{2\pi\nu\tau} \right)^2 (4\pi\nu D\tau^3)^2 \int d\epsilon_1 d\epsilon_2 \int \frac{dx_1 dx_2}{L^2} \\ &\quad \times \left(\frac{\partial^2}{\partial x_1 \partial x_2} \mathcal{P}_{\epsilon_1-\epsilon_2} \right) \mathcal{P}_{\epsilon_1-\epsilon_2} G_{\epsilon_1}^K(x_1) G_{\epsilon_2}^K(x_2) , \quad (\text{C.12}) \end{aligned}$$

$$\begin{aligned} \langle \delta I(V_1) \delta I(V_2) \rangle_{\text{c-coop}} &= \left(\frac{e}{4\pi i} \right)^2 \left(\frac{1}{2\pi\nu\tau} \right)^2 (-4\pi\nu D\tau^4) \int d\epsilon_1 d\epsilon_2 \int \frac{dx_1 dx_2}{L^2} \\ &\quad \times \delta(x_1 - x_2) \mathcal{P}_{\epsilon_1-\epsilon_2} G_{\epsilon_1}^K(x_1) G_{\epsilon_2}^K(x_2) , \quad (\text{C.13}) \end{aligned}$$

where $\mathcal{P}_{\epsilon_1-\epsilon_2}(x_1, x_2)$ is the diffusion propagator satisfying the equation

$$\left\{ D \frac{\partial^2}{\partial x_1^2} + i \left[\epsilon_1 + \phi_1(x_1) - \epsilon_2 - \phi_2(x_1) \right] \right\} \mathcal{P}_{\epsilon_1-\epsilon_2}(x_1, x_2) = -\frac{1}{2\pi\nu\tau^2} \delta(x_1 - x_2) , \quad (\text{C.14})$$

and $\phi_{1,2}$ are the electrochemical potentials corresponding to the voltages $V_{1,2}$. Using the identity

$$\frac{1}{4} \frac{\partial^2}{\partial x_1 \partial x_2} \mathcal{P}^2(x_1, x_2) = \left[\frac{\partial^2}{\partial x_1 \partial x_2} \mathcal{P}(x_1, x_2) - \frac{1}{4\pi\nu D\tau^2} \delta(x_1 - x_2) \right] \mathcal{P}(x_1, x_2) , \quad (\text{C.15})$$

the diagrams combine to

$$\begin{aligned} \langle \delta I(V_1) \delta I(V_2) \rangle_{\text{a-diff} + \text{b-diff}} &= -\frac{e^2}{(2\pi)^2} (D\tau^2)^2 \int d\epsilon_1 d\epsilon_2 \left[|\mathcal{P}_{\epsilon_1-\epsilon_2}|^2 + \frac{1}{2} \text{Re} \mathcal{P}_{\epsilon_1-\epsilon_2}^2 \right] \\ &\quad \times \frac{\partial}{\partial x_1} G^K(x_1) \frac{\partial}{\partial x_2} G^K(x_2) , \quad (\text{C.16}) \end{aligned}$$

$$\langle \delta I(V_1) \delta I(V_2) \rangle_{\text{c-diff}} = 0 , \quad (\text{C.17})$$

$$\begin{aligned} \langle \delta I(V_1) \delta I(V_2) \rangle_{\text{a-coop}} &= -\frac{e^2}{(2\pi)^2} (D\tau^2)^2 \int d\epsilon_1 d\epsilon_2 \int \frac{dx_1 dx_2}{L^2} |\mathcal{P}_{\epsilon_1-\epsilon_2}|^2 \\ &\quad \times \frac{\partial}{\partial x_1} G^K(x_1) \frac{\partial}{\partial x_2} G^K(x_2) , \quad (\text{C.18}) \end{aligned}$$

$$\begin{aligned} \langle \delta I(V_1) \delta I(V_2) \rangle_{\text{b-coop} + \text{c-coop}} &= -\frac{e^2}{(2\pi)^2} (D\tau^2)^2 \int d\epsilon_1 d\epsilon_2 \int \frac{dx_1 dx_2}{L^2} \frac{1}{2} \text{Re} \mathcal{P}_{\epsilon_1-\epsilon_2}^2 \\ &\quad \times \frac{\partial}{\partial x_1} G^K(x_1) \frac{\partial}{\partial x_2} G^K(x_2) . \quad (\text{C.19}) \end{aligned}$$

Adding up these equations and rescaling the propagator by a factor $2\pi\nu D\tau^2$, $\mathcal{D} = 2\pi\nu D\tau^2 \mathcal{P}$, the result is Eq. (3.37).

D Crossover between the linear response and the high-voltage enhancement

In this appendix, the variance $\langle \delta g^2 \rangle$ is calculated as a function of the bias voltage in the full range from the UCF regime $V/V_c \ll 1$ to the Larkin-Khmelnitskii asymptotic regime $V/V_c \gg 1$.

In addition to the asymptotics given by Eq. (3.52), there are contributions to the variance of the conductance which do not grow proportionally to V/V_c asymptotically but dominate in the intermediate regime. First of all, there is a constant contribution, Eq. (3.45),

$$\langle \delta g^2 \rangle_0 = \frac{8}{15} , \quad (\text{D.1})$$

which gives the familiar UCF result in the limit of zero bias voltage. Second, there are the contributions from the term $\langle \delta g^2 \rangle_1$, Eq. (3.46), containing one energy integration, which can be evaluated as

$$\begin{aligned} \langle \delta g^2 \rangle_{1, \text{Abs}} &= 32 \int_0^{V/V_c} dz \frac{\partial}{\partial \alpha} \text{Tr} \left[2 |\Pi_{V/V_c - z}|^2 \right]_{\alpha=0} \\ &= 64 \sum_{n=1}^{\infty} \frac{(V/V_c)^2}{2n^8 \pi^8 + 2n^4 \pi^4 (V/V_c)^2} \\ &= \frac{1}{45} \left(\frac{V_c}{V} \right)^2 \left\{ 720 + 16 \left(\frac{V}{V_c} \right)^2 \right. \\ &\quad \left. - 360 (-1)^{1/4} \sqrt{\frac{V}{V_c}} \left[\cot \left\{ (-1)^{1/4} \sqrt{\frac{V}{V_c}} \right\} + \coth \left\{ (-1)^{1/4} \sqrt{\frac{V}{V_c}} \right\} \right] \right\} \end{aligned} \quad (\text{D.2})$$

and

$$\begin{aligned}
 \langle \delta g^2 \rangle_{1, \text{Re}} &= 32 \int_0^{V/V_c} dz \frac{\partial}{\partial \alpha} \text{Tr Re } \Pi_{V/V_c - z}^2 \Big|_{\alpha=0} \\
 &= \frac{8}{45} - 16 \sum_{n=1}^{\infty} \frac{(V/V_c)^2 - n^4 \pi^4}{[n^4 \pi^4 + (V/V_c)^2]^2} .
 \end{aligned} \tag{D.3}$$

In the limit $V/V_c \rightarrow \infty$, the sum of Eqs. (D.2) and (D.3) saturates at $8/15$. Then there is the part of $\langle \delta g^2 \rangle_2$ containing $\text{Re } \Pi^2$, which also does not contribute to the linear asymptotic behaviour but gives a contribution which saturates towards a constant as the voltage is increased:

$$\begin{aligned}
 \langle \delta g^2 \rangle_{2, \text{Re}} &= -16 \int_0^{V_1/V_c} dz_1 \int_0^{V_2/V_c} dz_2 \frac{\partial^2}{\partial \alpha^2} \text{Tr Re } \Pi_{z_1 - z_2}^2 \Big|_{\alpha=0} \\
 &= 32 \sum_{m, n > 0} \frac{2 (V/V_c)^2 [m^4 \pi^4 + m^2 n^2 \pi^4 + n^4 \pi^4 + (V/V_c)^2]}{m^2 n^2 \pi^4 [m^4 \pi^4 + (V/V_c)^2] [n^4 \pi^4 + (V/V_c)^2]} \left(\langle n | y | m \rangle \right)^2 \\
 &\xrightarrow{V \rightarrow \infty} 0.1905 ,
 \end{aligned} \tag{D.4}$$

where again $|n\rangle = \sqrt{2} \sin(n\pi y)$. Finally, the $|\Pi|^2$ contribution to $\langle \delta g^2 \rangle_2$ is also modified at finite V/V_c compared to its asymptotics given by Eq. (3.52). It is evaluated in detail in Ref. [89]. The sum of all the contributions is the result shown graphically in Figs. 3.5, 3.6.

E Subleading terms in the high-voltage strong-dephasing regime

In this appendix it is shown that the two subleading terms, $\langle \delta g^2 \rangle_0$ and $\langle \delta g^2 \rangle_1$, remain indeed smaller than the leading term, $\langle \delta g^2 \rangle_2$, in the strong-dephasing regime. Taking again advantage of the Fourier transform (3.81), the cross-term $\langle \delta g^2 \rangle_1$ is evaluated as follows,

$$\begin{aligned}
\langle \delta g^2 \rangle_1 &= 32 V_c \frac{\partial}{\partial V_1} \Big|_{V_1=V_2=V} \int_{(V_1-V_2)/V_c}^{V_1/V_c} d\epsilon \Xi_\epsilon \\
&= 32 V_c \frac{\partial}{\partial V_1} \Big|_{V_1=V_2=V} \int_{-\infty}^{\infty} d\tau \tilde{\Xi}(\tau) \int_{(V_1-V_2)/V_c}^{V_1/V_c} d\epsilon [\cos \epsilon \tau + i \sin \epsilon \tau] \\
&= 32 V_c \int_{-\infty}^{\infty} d\tau \frac{\partial}{\partial V_1} \Big|_{V_1=V_2=V} \tilde{\Xi}(\tau) \frac{1}{\tau} \left[\sin \frac{V\tau}{V_c} + i - i \cos \frac{V\tau}{V_c} \right] \\
&\quad + 32 \int_{-\infty}^{\infty} d\tau \tilde{\Xi}(\tau) \left[\cos \frac{V\tau}{V_c} - 1 + i \sin \frac{V\tau}{V_c} \right] . \tag{E.1}
\end{aligned}$$

Using the approximation

$$\frac{1}{\tau} \sin \frac{V\tau}{V_c} \simeq \pi \delta(\tau) \tag{E.2}$$

valid for $V \gg V_c$, and the fact that $\frac{\partial}{\partial V_1} \tilde{\Xi}(\tau) \Big|_{V_1=V_2=V}$ is even in τ , this is to leading order in V_c/V equal to

$$\langle \delta g^2 \rangle_1 = 32 \left[\pi V_c \frac{\partial}{\partial V_1} \tilde{\Xi}(0) \Big|_{V_1=V_2} + \int dt \tilde{\Xi}(t) \right] . \tag{E.3}$$

The last term in brackets is equal to twice the equilibrium term $\langle \delta g^2 \rangle_0$, and can be neglected if that one can. Using the rescaled variables (3.89)–(3.93), the first term in brackets evaluates to

$$\langle \delta g^2 \rangle_1 = 32\sqrt{2} \pi \frac{\partial}{\partial v} \tilde{Q} \Big|_{v=0} \int_0^1 \frac{dy}{p^{1/3}} , \tag{E.4}$$

where

$$\left\{ -\frac{\partial}{\partial \eta^2} + |\eta| + iv\eta \right\} \tilde{Q}(v, \eta) = \delta(\eta) . \quad (\text{E.5})$$

Eq. (E.5) can be treated using the same cutoff procedure as used in the evaluation of (3.99), resulting in

$$\langle \delta g^2 \rangle_1 \sim \left(\frac{gV_c}{V} \right)^{5/4} . \quad (\text{E.6})$$

This clearly decays faster than Eq. (3.99) in the strong-dephasing regime $V \gg gV_c$ and is smaller than Eq. (3.99) by a factor of $1/g$ at the beginning of the strong dephasing regime $V \sim gV_c$. It thus can be safely neglected.

The check of $\langle \delta g^2 \rangle_0$ goes a slightly different route. Setting $V_1 = V_2 = V$ in Eq. (3.78) leads to

$$\begin{aligned} \Xi_0 = & 2 \int_0^1 dy_1 dy_2 \int_0^\infty d\tau_1 d\tau_2 \int_{\xi_1(0)=y_2}^{\xi_1(\tau_1)=y_1} \mathcal{D}[\xi_1(t_1)] \int_{\xi_2(0)=y_2}^{\xi_2(\tau_2)=y_1} \mathcal{D}[\xi_2(t_2)] \\ & \times \exp \left\{ - \int_0^{\tau_1} dt_1 \frac{\dot{\xi}_1^2}{4} - \int_0^{\tau_2} dt_2 \frac{\dot{\xi}_2^2}{4} \right. \\ & \left. - \frac{2V}{gV_c} F(y_2) |\tau_1 - \tau_2| - \frac{2V}{gV_c} \int_0^{\min(\tau_1, \tau_2)} dt |\xi_1 - \xi_2| y_2(1 - y_2) \right\} . \quad (\text{E.7}) \end{aligned}$$

The above equation represents two trajectories with durations τ_1, τ_2 , respectively. During the time interval between the shorter and the longer of these times there is only one trajectory, resulting in strong suppression of interference by bare fluctuations. Therefore relevant trajectories will have similar durations, $\tau_1 \approx \tau_2$, allowing to factorize the suppression arising from the time difference and the suppression arising from the relative coordinate:

$$\begin{aligned} \Xi_0 = & 2\sqrt{2} \int_0^1 dy \int_0^\infty d\tau_1 \int_0^{\tau_1} d\tau_2 \\ & \times \exp \left\{ - \frac{2V}{gV_c} F(y) |\tau_1 - \tau_2| \right\} \\ & \times \int_{\xi(0)=0}^{\xi(\tau_1)=0} \mathcal{D}\xi(t_1) \exp \left\{ - \int_0^{\tau_1} dt \left[\frac{\dot{\xi}^2}{4} + \frac{2V}{gV_c} \sqrt{2} |\xi| y(1 - y) \right] \right\} . \quad (\text{E.8}) \end{aligned}$$

The integral over τ_2 can now be performed,

$$\begin{aligned} \Xi_0 = & \sqrt{2} \frac{gV_c}{V} \int_0^1 \frac{dy}{F(y)} \int_0^\infty d\tau \left(1 - \exp \left\{ -\frac{2V}{gV_c} F(y) \tau \right\} \right) \\ & \times \int_{\xi(0)=0}^{\xi(\tau)=0} \mathcal{D}[\xi(t)] \exp \left\{ -\int_0^\tau dt \left[\frac{\dot{\xi}^2}{4} + \frac{2V}{gV_c} \sqrt{2} |\xi| y(1-y) \right] \right\} , \end{aligned} \quad (\text{E.9})$$

as well as the reduction of the path integral to a dimensionless differential equation using the variables (3.89)–(3.93):

$$\begin{aligned} \Xi_0 = & \sqrt{2} \frac{gV_c}{V} \int_0^1 \frac{dy}{F(y) \left[\frac{2V}{gV_c} \sqrt{2} y(1-y) \right]^{1/3}} \int_0^\infty dt \\ & \times \left(1 - \exp \left\{ -\frac{\frac{2V}{gV_c} F(y) t}{\left[\frac{2V}{gV_c} \sqrt{2} y(1-y) \right]^{2/3}} \right\} \right) \mathcal{I}(0, t) , \end{aligned} \quad (\text{E.10})$$

where

$$\left\{ \frac{\partial}{\partial t} - \frac{\partial}{\partial \eta^2} + |\eta| \right\} \mathcal{I}(\eta, t) = \delta(\eta) \delta(t) . \quad (\text{E.11})$$

This integral is again dominated by y close to the reservoirs at 0 or 1, and should be cut off at a distance $\sim y_c$, where y_c is given by Eq. (3.98). Note that the exponential function cannot be expanded in y and $1-y$ since by the cutoff relation $y_c \sim (gV_c/V)^{1/4}$ the coefficient in the exponent is of order 1. It is however sufficient to calculate an upper bound of the expression by neglecting the exponential function compared to unity. The result is

$$\langle \delta g^2 \rangle_0 \sim g \frac{V_c}{V} , \quad (\text{E.12})$$

which has the same asymptotic power law as Eq. (3.99) but is smaller by a factor $\sim 1/g$. It is thus proven that the term dominating the conductance fluctuations in the strong-dephasing regime is given by Eq. (3.99).

F Thermal averaging factor for $T \ll E_c$

In this appendix, the expression (2.11) for conductance fluctuations is evaluated for the regime of interest for Composite Fermion systems, $l \ll L_\varphi \ll L_T$, resulting in Eq. (4.21). The dephasing effects on weak localization and mesoscopic conductance fluctuations are purely geometrical and do not contain any reference to the dynamics of the electrons. Therefore only the thermal factor appearing in the relation (4.20) needs to be re-evaluated.

Since due to the strong dephasing effect the temperature is much lower than the Thouless energy, the thermal factor (2.12) needs to be taken in the limit of small $T(t - t')$,

$$\tilde{\delta}(t - t') = \frac{3}{\pi} T, \quad T(t - t') \ll 1. \quad (\text{F.1})$$

As a result, the expression (2.11) for conductance fluctuations contains two time integrations, and the transformation (2.43) cannot be used directly. It is convenient to introduce an extrinsic dephasing rate $1/\tau_\varphi^*$, which represents a mass of the diffuson and Cooperon propagators. $1/\tau_\varphi^*$ may be set to zero in the end of the calculation. The conductance fluctuations can now be written as

$$\langle \delta G^2 \rangle = \frac{4e^4 D^2}{\pi^2 L^4} \int \mathbf{dr}_1 \mathbf{dr}_2 \int_0^\infty dt_1 dt_2 \mathcal{D}(\mathbf{r}_1, \mathbf{r}_2, t_1) \exp\{-t_1/\tau_\varphi^*\} \mathcal{D}(\mathbf{r}_2, \mathbf{r}_1, t_2) \exp\{-t_2/\tau_\varphi^*\}. \quad (\text{F.2})$$

Using the transformation

$$\mathbf{r}(t') = \begin{cases} \mathbf{r}_1(t_1 + t') , & -t_1 \leq t' \leq 0 \\ \mathbf{r}_2(t_2 - t') , & 0 \leq t' \leq t_2 \end{cases} \quad (\text{F.3})$$

to join the paths in analogy to Eq. (2.43) (see Fig. F.1), the result is

$$\begin{aligned} \langle \delta G^2 \rangle &= \frac{4e^2 D^2}{\pi^2 L^4} \int \mathbf{dr}_1 \int_0^\infty dt_1 dt_2 \mathcal{D}(\mathbf{r}_1, \mathbf{r}_1, t_1 + t_2) \exp\{-(t_1 + t_2)/\tau_\varphi^*\} \\ &= \frac{4e^2 D^2}{\pi^2 L^4} \int \mathbf{dr}_1 \int_0^\infty dt t \mathcal{C}(\mathbf{r}_1, \mathbf{r}_1, t) \exp\{-t/\tau_\varphi^*\} \\ &= \frac{4e^2 D^2}{\pi^2 L^4} \int \mathbf{dr}_1 \int_0^\infty dt \left(-\frac{\partial}{\partial(1/\tau_\varphi^*)} \right) \mathcal{C}(\mathbf{r}_1, \mathbf{r}_1, t) \exp\{-t/\tau_\varphi^*\}, \quad (\text{F.4}) \end{aligned}$$

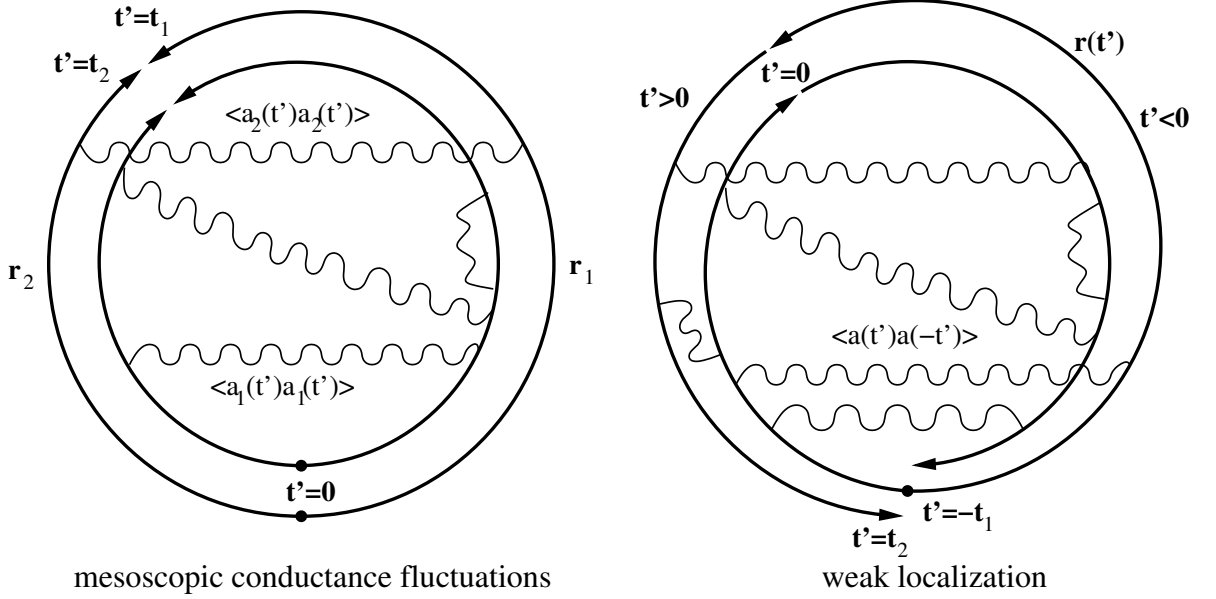


Figure F.1: When the thermal factor (2.12) is evaluated at low temperatures $T \ll E_c$, the two paths do not need to have equal durations, in contrast to the high-temperature case for which Fig. 4.1 is drawn. Using the transformation (F.3), the relation (4.21) between conductance fluctuations and weak localization is derived, which differs from Eq. (4.20) only in the thermal factor. The mapping between the *dephasing* effects associated with both quantities holds at all temperatures.

where the diffuson propagator has been replaced by the Cooperon propagator assuming that the disorder alone does not break time-reversal symmetry. Interchanging differentiation and integration and restoring the dephasing terms resulting from the coupling to the gauge field fluctuations results in

$$\langle \delta G^2 \rangle (T) = \frac{e^2 D}{\pi L^2} \left| \frac{\partial}{\partial (1/\tau_\varphi^*)} \delta G_{WL} \left(\frac{T}{2} \right) \right|, \quad L_T \gg L_\varphi. \quad (\text{F.5})$$

At low temperatures, the part $\sim \text{Re } \mathcal{D}^2$ of Eq. (1.12) also needs to be taken into account. As a result, the conductance fluctuations are enhanced by a factor of 3/2, leading to the stated result, Eq. (4.21).

G Consistency checks for the fermion-gauge field system

In this appendix, some consistency checks for the fermion-gauge field system considered in Sections 4.4.1, 4.4.2 are performed. A typical semiconductor sample with

$$\text{dimensionless conductance } g = g_{\square} \sim 30 \quad (\text{G.1})$$

$$\text{Fermi energy } E_F \sim 30 \text{ K} \quad (\text{G.2})$$

$$\text{temperature } T \sim 30 \text{ mK} \quad (\text{G.3})$$

$$\text{elastic scattering time } \tau \sim 1 \text{ K}^{-1} \quad (\text{G.4})$$

$$\text{electron sheet density } n \sim 10^{15} \text{ m}^{-2} \quad (\text{G.5})$$

is assumed, which is well in the diffusive regime $T\tau \lesssim 1$ considered in Chapter 4.

Although not needed to obtain the result (4.36), an estimate shows that for typical gauge field frequencies the static approximation is indeed valid: In two dimensions, typical gauge field frequencies ω_{gf} are given by $\omega_{\text{gf}} \sim \chi k^2 / \nu D$ with typical k from the range $L_{\omega}^{-1} \dots l^{-1} \ll k_F$. Together with Eq. (4.40), it is seen that relevant gauge field frequencies satisfy

$$\begin{aligned} \omega_{\text{gf}} \tau_{\varphi} &\sim \frac{\chi k^2}{\nu D} \frac{2}{3gT \ln \frac{2}{3gT\tau}} \\ &\sim \frac{1}{36\pi^2} \underbrace{\frac{k^2}{k_F^2}}_{\ll 1} \underbrace{\frac{1}{g^2}}_{\sim 10^{-3}} \underbrace{\frac{E_F}{T}}_{\sim 10^3} \underbrace{\frac{1}{\ln \frac{2}{3gT\tau}}}_{\approx 1} \\ &\ll 1, \quad d = 2 \end{aligned} \quad (\text{G.6})$$

for typical semiconductor samples with parameters as stated above. In other words, for these samples during the time τ_{φ} in which the phase memory of the ensemble gets randomized the gauge field configuration of an ensemble member does not change much.

The validity of the static approximation for the wire geometry is checked in a similar way as in the twodimensional case. Typical gauge field frequencies ω_{gf} are given by $\omega_{\text{gf}} \sim \chi k^2 / \sigma = k^2 / 12\pi g_{\square} \nu$ with $k = \pi/b, 2\pi/b, \dots, \pi/l$. Using $\nu = m/\pi = k_F^2 / (2\pi E_F)$

and Eq. (4.47), it can be estimated that

$$\begin{aligned}
 \omega_{\text{gf}}\tau_\varphi &\sim \frac{1}{72\pi} \frac{k^2}{\nu g_\square^2 T} \frac{1}{\ln(b/l)} \\
 &\sim \frac{1}{36} \underbrace{\frac{1}{g_\square^2}}_{\sim 10^{-3}} \underbrace{\frac{E_F}{T}}_{\sim 10^3} \underbrace{\frac{k^2}{k_F^2}}_{\ll 1} \underbrace{\frac{1}{\ln(b/l)}}_{< 1} \\
 &\ll 1, \quad d = 1.
 \end{aligned} \tag{G.7}$$

Another consistency check to perform in two dimensions is that $L_\varphi > l$ in order for the diffusive description to be valid. Using $L_\varphi = (D\tau_\varphi)^{1/2}$ with τ_φ given by Eq. (4.40), the result is

$$\begin{aligned}
 k_F L_\varphi &= \left(\frac{4DmE_F}{3gT \ln \frac{2}{3gT\tau}} \right)^{1/2} \\
 &= \left(\frac{4}{3} \right)^{1/2} \left(\frac{E_F}{T} \right)^{1/2} \left(\ln \frac{2}{3gT\tau} \right)^{-1/2} \\
 &\approx \left(\frac{E_F}{T} \right)^{1/2}.
 \end{aligned} \tag{G.8}$$

Comparing this to $k_F l = E_F \tau$, the condition for $L_\varphi > l$ in two dimensions is

$$T \lesssim \frac{1}{E_F^2 \tau} \sim 30 \text{ mK}, \tag{G.9}$$

which is a regime of experimental relevance. An estimate of the dephasing lengths L_φ to expect can be obtained in the following way from Eq. (4.40): Using $L_\varphi = (D\tau_\varphi)^{1/2}$ with $D = g/m$ and $D = v_F \tau / 2$ gives

$$\begin{aligned}
 L_\varphi &= \left(\frac{2D}{3gT \ln \frac{2}{3gT\tau}} \right)^{1/2} \\
 &= \left(\frac{4E_F}{3k_F^2 T \ln \frac{4E_F}{3Dk_F^2 T \tau}} \right)^{1/2} \\
 &= \frac{2}{\sqrt{3}} \frac{1}{\sqrt{4\pi n}} \left(\frac{E_F}{T} \right)^{1/2} \left(\ln \frac{8E_F}{3Tk_F^2 l^2} \right)^{-1/2}.
 \end{aligned} \tag{G.10}$$

The argument of the logarithm is of order unity, and the dephasing length for a typical sample as characterized above is estimated as stated in Eq. (4.41),

$$L_\varphi \sim 0.3 \mu\text{m} . \quad (\text{G.11})$$

Typical gauge field frequencies at wavevectors of the order of L_φ^{-1} are

$$\begin{aligned} \omega_{\text{gf}} &\sim \frac{\chi L_\varphi^{-2}}{\sigma} \\ &= \frac{L_\varphi^{-2}}{12\pi g\nu} \\ &= \frac{L_\varphi^{-2} 2\pi E_F}{12\pi g k_F^2} \\ &= \frac{E_F}{24\pi n g L_\varphi^2} \\ &\approx 2 \cdot 10^7 \text{ s}^{-1} . \end{aligned} \quad (\text{G.12})$$

For the wire of width b , instead of checking that $L_\varphi > l$, the relation $L_\varphi > b$ needs to be verified. Using $D = g_\square/m$, $k_F = \sqrt{4\pi n}$, and approximating the logarithm by unity, the dephasing length is calculated from Eq. (4.47) as

$$\begin{aligned} L_\varphi &= (D\tau_\varphi)^{1/2} \\ &= \left(\frac{1}{6 m T \ln(b/l)} \right)^{1/2} \\ &= \left(\frac{1}{12 \pi} \right)^{1/2} \frac{1}{\sqrt{n}} \left(\frac{E_F}{T} \right)^{1/2} \left(\ln \frac{b}{l} \right)^{-1/2} \\ &\sim 0.15 \mu\text{m} , \quad d = 1 , \end{aligned} \quad (\text{G.13})$$

which is slightly less than the corresponding result (4.41) in two dimensions and sets the scale for a wire with the given parameters to be considered as quasi-onedimensional.

H Saddle-point evaluation of the $\hbar/2e$ amplitude with gauge field fluctuations

In this appendix the details of the evaluation of the saddle-point equation (4.55) are presented for reference. The factors entering Eq. (4.55) are given by

$$t_0^{\text{opt}} = \frac{1}{2} t_{\text{AB}}^{1/2} \left(6 g_{\square} T \ln \frac{b}{l} \right)^{-1/2} \quad (\text{H.1})$$

$$S_{\text{AB}}^{\text{opt}} = t_{\text{AB}}^{1/2} \left(6 g_{\square} \ln \frac{b}{l} \right)^{1/2} T^{1/2} \quad (\text{H.2})$$

$$\left. \frac{\partial^2 S_{\text{AB}}}{\partial t_0^2} \right|_{t_0=t_0^{\text{opt}}} = t_{\text{AB}}^{-1/2} \left(6 g_{\square} \ln \frac{b}{l} \right)^{3/2} T^{3/2} , \quad (\text{H.3})$$

where the time t_{AB} is defined as the timescale set by the ring circumference,

$$t_{\text{AB}} = \frac{(2\pi R)^2}{D} . \quad (\text{H.4})$$

Combining the factors, the result is Eq. (4.56). Note that in the regime of strong dephasing considered, the saddle-point is located at $t_0^{\text{opt}} \ll t_{\text{AB}}$, indicating the special character of the paths giving the leading contribution.

Bibliography

- [1] L. Onsager, *Reciprocal Relations in Irreversible Processes. II.*, Phys. Rev. **38**, 2265 (1931).
- [2] D. Bohm and D. Pines, *A Collective Description of Electron Interactions: III. Coulomb Interactions in a Degenerate Electron Gas*, Phys. Rev. **92**, 609 (1953).
- [3] L. D. Landau, *The Theory of a Fermi Liquid*, Zh. Eksp. Teor. Fiz. **30**, 1058 (1956) [Sov. Phys. JETP **3**(6), 920 (1957)].
L. D. Landau, *Oscillations in a Fermi Liquid*, Zh. Eksp. Teor. Fiz. **32**, 59 (1957) [Sov. Phys. JETP **5**(1), 101 (1957)].
L. D. Landau, *On the Theory of The Fermi Liquid*, Zh. Eksp. Teor. Fiz. **35**, 97 (1958) [Sov. Phys. JETP **35**(8), 70 (1959)].
- [4] P. W. Anderson, *Absence of Diffusion in Certain Random Lattices*, Phys. Rev. **109**, (1958).
- [5] Y. Aharonov and D. Bohm, *Significance of Electromagnetic Potentials in the Quantum Theory*, Phys. Rev. **115**, 485 (1959).
- [6] A. A. Rukhadze and V. P. Silin, *Electrodynamics of Media with Spatial Dispersion*, Soviet Physics Uspekhi **4**, 459 (1961).
- [7] A. A. Abrikosov, L. P. Gorkov, and I. E. Dzyaloshinski, *Methods of Quantum Field Theory in Statistical Physics*, Dover Publications (1963).
- [8] L. V. Keldysh, *Diagram technique for nonequilibrium processes*, Zh. Eksp. Teor. Fiz. **47**, 1515 (1964) [Sov. Phys. JETP **20**, 1018 (1965)].
- [9] Sh. M. Kogan and A. Ya. Shul'man, *Theory of Fluctuations in a Nonequilibrium Electron Gas*, Zh. Eksp. Teor. Fiz. **56**, 862 (1969) [Sov. Phys. JETP **29**(3), 467 (1969)].
- [10] A. I. Larkin and Yu. N. Ovchinnikov, *Nonlinear conductivity of superconductors in the mixed state*, Zh. Eksp. Teor. **68**, 1915 (1975) [Sov. Phys. JETP **41**, 960 (1976)].
- [11] L. D. Landau, E. M. Lifschitz, and L. P. Pitajewski, *Course of Theoretical Physics, Volume 5: Statistical Physics Part I*, (1976).

- [12] L. D. Landau, E. M. Lifschitz, and L. P. Pitajewski, *Course of Theoretical Physics, Volume 10: Physical Kinetics*, Chapter X (1979).
- [13] P. W. Anderson, *Local moments and localized states*, Rev. Mod. Phys. **50** (1978).
- [14] E. Abrahams, P. W. Anderson, D. C. Licciardello, and T. V. Ramakrishnan, *Scaling Theory of Localization: Absence of Quantum Diffusion in Two Dimensions*, Phys. Rev. Lett. **42**, 673 (1979).
- [15] L. P. Gor'kov, A. I. Larkin, and D. E. Khmel'nitskii, *Particle conductivity in a two-dimensional random potential*, Pis'ma Zh. Eksp. Teor. Fiz. **30**(4), 248 (1979) [JETP Lett. **30**(4), 228 (1980)].
- [16] B. L. Altshuler, D. Khmel'nitskii and A. I. Larkin, and P. A. Lee, *Magnetoresistance and Hall effect in a disordered two-dimensional electron gas*, Phys. Rev. B **22**, 5142 (1980).
- [17] B. L. Altshuler, A. G. Aronov, and B. Z. Spivak, *The Aaronov-Bohm effect in disordered conductors*, Pis'ma Zh. Eksp. Teor. Fiz. **33**, 101 (1981) [JETP Lett. **33**, 94 (1981)].
- [18] B. L. Altshuler, A. G. Aronov, and D. E. Khmel'nitsky, *Effects of electron-electron collision with small energy transfers on quantum localisation*, J. Phys. C **15**, 7367 (1982).¹
- [19] A. I. Vainshtein, V. I. Zakharov, V. A. Novikov, and M. A. Shifman, *ABC of instantons*, Usp. Fiz. Nauk **136**, 553 (1982).
- [20] R. B. Laughlin, *Anomalous Quantum Hall Effect: An Incompressible Quantum Fluid with Fractionally Charged Excitations*, Phys. Rev. Lett. **50**, 1395 (1983).
- [21] C. P. Umbach, S. Washburn, R. B. Laibowitz, and R. A. Webb, *Magnetoresistance of small, quasi-one-dimensional, normal-metal rings and lines*, Phys. Rev. B **30**, 4048 (1984).
- [22] Dire Straits, *Walk of Life*, Vertigo Records (1985).
- [23] B. L. Altshuler, *Fluctuations in the extrinsic conductivity of disordered conductors*, Pis'ma Zh. Eksp. Teor. Fiz. **41**, 530 (1985) [JETP Lett. **41**, 648 (1985)].
- [24] A. D. Stone, *Magnetoresistance Fluctuations in Mesoscopic Wires and Rings*, Phys. Rev. Lett. **54**, 2692 (1985).

¹Some errors in the numerical coefficients are corrected in Ref. [72].

-
- [25] R. A. Webb, S. Washburn, C. P. Umbach, and R. B. Laibowitz, *Observation of h/e Aharonov-Bohm Oscillations in Normal-Metal Rings*, Phys. Rev. Lett. **54**, 2696 (1985).
- [26] P. A. Lee and A. D. Stone, *Universal Conductance Fluctuations in Metals*, Phys. Rev. Lett. **55**, 1622 (1985).
- [27] B. L. Altshuler and D. E. Khmelnitskii, *Fluctuation Properties of Small Conductors*, Pis'ma Zh. Eksp. Teor. Fiz. **42**, 291 (1985) [JETP Lett. **42**, 359 (1986)].
- [28] S. Washburn, C. P. Umbach, R. B. Laibowitz, and R. A. Webb, *Temperature dependence of the normal-metal Aharonov-Bohm effect*, Phys. Rev. B **32**, 4789 (1985).
- [29] B. L. Altshuler and A. G. Aronov, in *Electron-Electron Interaction in Disordered Conductors*, edited by A. L. Efros and M. Pollak, pp. 1-153 (Elsevier, Amsterdam, 1985).
- [30] C. P. Umbach, C. Van Haesendonck, R. B. Laibowitz, S. Washburn, and R. A. Webb, *Direct observation of ensemble averaging of the Aharonov-Bohm effect in normal-metal loops*, Phys. Rev. Lett. **56**, 386 (1986).
- [31] S. Feng, P. A. Lee, and A. D. Stone, *Sensitivity of the Conductance of a Disordered Metal to the Motion of a Single Atom: Implications for $1/f$ Noise*, Phys. Rev. Lett. **56**, 1960 (1986).
- [32] S. Chakravarty and A. Schmid, *Weak localization: The quasiclassical theory of electrons in a random potential*, Phys. Rep. **140**(4), 193 (1986).
- [33] B. L. Altshuler, and B. I. Shklovskii, *Repulsion of energy levels and conductivity of small metal samples*, Zh. Eksp. Teor. Fiz. **91**, 220 (1986) [Sov. Phys. JETP **64**, 127 (1986)].
- [34] A. I. Larkin and D. E. Khmel'nitskii, *Mesoscopic fluctuations of current-voltage characteristics*, Zh. Eksp. Teor. Fiz. **91**, 1815 (1986) [Sov. Phys. JETP **64**, 1075 (1986)]; Phys. Scr. **T14**, 4 (1986).²
- [35] J. Rammer and H. Smith, *Quantum field-theoretical methods in transport theory of metals*, Rev. Mod. Phys. **58**, 323 (1986).
- [36] P. A. Lee, A. D. Stone, and H. Fukuyama, *Universal conductance fluctuations in metals: Effects of finite temperature, interactions, and magnetic field*, Phys. Rev. B **35**, 1039 (1987).

²Both versions contain minor typographical errors.

- [37] F. P. Milliken, S. Washburn, C. P. Umbach, R. B. Laibowitz, and R. A. Webb, *Effect of partial phase coherence on Aharonov-Bohm oscillations in metal loops*, Phys. Rev. B **36**, 4465 (1987).
- [38] A. G. Aronov and Yu. V. Sharvin, *Magnetic flux effects in disordered conductors*, Rev. Mod. Phys. **59**, 755 (1987).
- [39] C. L. Kane, R. A. Serota, and P. A. Lee, *Long-range correlations in disordered metals*, Phys. Rev. B **37**, 6701 (1988).
- [40] R. A. Webb, S. Washburn, and C. P. Umbach, *Experimental study of nonlinear conductance in small metallic samples*, Phys. Rev. B **37**, 8455 (1988).
- [41] C. L. Kane, P. A. Lee, and D. P. DiVincenzo, *Voltage fluctuations in multilead devices*, Phys. Rev. B **38**, 2995 (1988).
- [42] D. P. DiVincenzo and C. L. Kane, *Voltage fluctuations in mesoscopic metal rings and wires*, Phys. Rev. B **38**, 3006 (1988).
- [43] S. B. Kaplan, *Asymmetric conductance and coherence effects in mesoscopic Si metal-oxide-semiconductor field-effect transistors*, Phys. Rev. B **38**, 7558 (1988).
- [44] A. D. Stone, *Reduction of low-frequency noise in metals by a magnetic field: Observability of the transition between random-matrix ensembles*, Phys. Rev. B **39**, 10736 (1989).
- [45] J. K. Jain, *Composite-fermion approach for the fractional quantum Hall effect*, Phys. Rev. Lett. **63**, 199 (1989).
- [46] A. Stern, Y. Aharonov, and Y. Imry, *Phase uncertainty and loss of interference: A general picture*, Phys. Rev. A **41**, 3436 (1990).
- [47] A. Lopez and E. Fradkin, *Fractional quantum Hall effect and Chern-Simons gauge theories*, Phys. Rev. B **44**, 5246 (1991).
- [48] S. Washburn, *Aharonov-Bohm effects in loops of gold*, in *Mesoscopic Phenomena in Solids*, edited by B. L. Altshuler, P. A. Lee and R. A. Webb, pp. 1-36 (North-Holland, Amsterdam, 1991).
- [49] V. I. Fal'ko, *The Aharonov-Bohm effect in a mesoscopic ring of diluted magnetic alloy*, J. Phys.: Condens. Matter **4**, 3943 (1992).
- [50] A. Müller-Groeling, *Mesoscopic rings with finite aspect ratio: Magnetic-field correlation function*, Phys. Rev. B **47**, 6480 (1993).
- [51] D. C. Ralph, K. S. Ralls, and R. A. Buhrman, *Ensemble studies of nonlinear conductance fluctuations in phase coherent samples*, Phys. Rev. Lett. **70**, 986 (1993).

-
- [52] B. I. Halperin, P. A. Lee, and N. Read, *Theory of the half-filled Landau level*, Phys. Rev. B **47**, 7312 (1993).
- [53] A. G. Aronov and P. Wölfle, *Weak localization of charged quantum particles in a disordered system subject to a strongly fluctuating magnetic field*, Phys. Rev. Lett. **72**, 2239 (1994).
- [54] D. R. Leadley, R. J. Nicholas, C. T. Foxon, and J. J. Harris, *Measurements of the effective mass and scattering times of composite fermions from magnetotransport analysis*, Phys. Rev. Lett. **72**, 1906 (1994).
- [55] A. G. Aronov and P. Wölfle, *Effect of a fluctuating magnetic field on weak localization in a two-dimensional disordered system*, Phys. Rev. B **50**, 16574 (1994).
- [56] A. G. Aronov, E. Altshuler, A. D. Mirlin, and P. Wölfle, *Theory of Shubnikov-de Haas oscillations around the $\nu = 1/2$ filling factor of the Landau level: Effect of gauge-field fluctuations*, Phys. Rev. B **52**, 4708 (1995).
- [57] A. Stern and B. I. Halperin, *Singularities in the Fermi-liquid description of a partially filled Landau level and the energy gaps of fractional quantum Hall states*, Phys. Rev. B **52**, 5890 (1995).
- [58] A. G. Aronov, E. Altshuler, A. D. Mirlin, and P. Wölfle, *Single Particle Relaxation in a Random Magnetic Field*, Europhys. Lett. **29**, 239 (1995) [cond-mat/9404071].
- [59] A. D. Mirlin, E. Altshuler, and P. Wölfle, *Quasiclassical approach to impurity effect on magnetooscillations in 2D metals*, Annalen der Physik **5**, 281 (1996) [cond-mat/9507081].
- [60] R. Schäfer, K. Hecker, H. Hegger, and W. Langheinrich, *Experimental study of mesoscopic fluctuations in nonlinear conductance and magnetoconductance*, Phys. Rev. B **53**, 15964 (1996).
- [61] P. A. Lee, E. R. Mucciolo, and H. Smith, *Dephasing time of composite fermions*, Phys. Rev. B **54**, 8782 (1996).
- [62] Sh. Kogan, *Electronic Noise and Fluctuations in Solids*, (Cambridge University Press, Cambridge, 1996).
- [63] A. D. Mirlin and P. Wölfle, *Quantum corrections to the conductivity of fermion gauge-field models: Application to the half-filled Landau level*, Phys. Rev. B **55**, 5141 (1997).
- [64] Y. Imry, *Introduction to Mesoscopic Physics* (Oxford University Press, New York, 1997).

- [65] H. Pothier, S. Gueron, N. O. Birge, D. Esteve, and M. H. Devoret, *Energy Distribution Function of Quasiparticles in Mesoscopic Wires*, Phys. Rev. Lett. **79**, 3490 (1997).
- [66] R. L. Willet, *Experimental evidence for composite fermions*, Adv. Phys. **46**, 447 (1997).
- [67] A. Lopez and E. Fradkin, *Fermionic Chern-Simons Field Theory for the Fractional Hall Effect*, in *Composite Fermions*, edited by O. Heinonen, World Scientific (London, 1998) [cond-mat/9704055].
- [68] K. E. Nagaev, *Long-range Coulomb interaction and frequency dependence of shot noise in mesoscopic diffusive contacts*, Phys. Rev. B **57**, 4628 (1998).
- [69] D. G. Polyakov and K. V. Samokhin, *Dynamical Scaling at the Quantum Hall Transition: Coulomb Blockade versus Phase Breaking*, Phys. Rev. Lett. **80**, 1509 (1998).
- [70] M. P. Lilly, J. P. Eisenstein, L. N. Pfeiffer, and K. W. West, *Coulomb Drag in the Extreme Quantum Limit*, Phys. Rev. Lett. **80**, 1714 (1998).
- [71] S. Simon, *The Chern-Simons Fermi Liquid Description of Fractional Quantum Hall States*, in *Composite Fermions*, edited by O. Heinonen, pp. 91-194 (World Scientific, Singapore, 1998) [cond-mat/9812186].
- [72] I. L. Aleiner, B. L. Altshuler, and M. E. Gershenson, *Interaction effects and phase relaxation in disordered systems*, Waves Random Media **9**, 201 (1999) [cond-mat/9808053].
- [73] D. Hoadley, P. McConville, and N. O. Birge, *Experimental comparison of the phase-breaking lengths in weak localization and universal conductance fluctuations*, Phys. Rev. B **60**, 5617 (1999).
- [74] Ya. M. Blanter and M. Büttiker, *Shot Noise in Mesoscopic Conductors*, Phys. Rep. **336**, 1 (2000) [cond-mat/9910158].
- [75] P. Wölfle, *Quasiclassical Theory of Phase Relaxation by Gauge Field Fluctuations*, Foundations of Physics **30**(12), 2125 (2000).
- [76] J. Vidal, G. Montambaux, and B. Douçot, *Transmission through quantum networks*, Phys. Rev. B **62**, R16294 (2000).
- [77] F. Pierre, H. Pothier, D. Esteve, and M. H. Devoret, *Energy Redistribution Between Quasiparticles in Mesoscopic Silver Wires*, J. Low Temp. Phys. **118**, 437 (2000) [cond-mat/9912138].

-
- [78] R. Häussler, H. B. Weber, and H. v. Löhneysen, *Voltage Dependence of the Amplitude of Aharonov-Bohm Oscillations in Mesoscopic Metal Rings*, J. Low Temp. Phys. **118**, 467 (2000).
- [79] R. Häussler, *Aharonov-Bohm-Oszillationen in mesoskopischen Metallringen: Einfluß einer Gleichspannung und eines inhomogenen Magnetfeldes*, Ph.D. thesis, Universität Karlsruhe (2000).
- [80] F. Pierre, H. Pothier, D. Esteve, M. H. Devoret, A. B. Gougam, and N. O. Birge, *Probing interactions in mesoscopic gold wires*, Proceedings of the NATO Advanced Research Workshop on Size Dependent Magnetic Scattering, Pesc (Hungary), 2000, edited by V. Chandrasekhar and C. Van Haesendonck, pp. 119ff (Kluwer, 2001) [cond-mat/0012038].
- [81] A. E. Hansen, A. Kristensen, S. Pedersen, C. B. Sørensen, and P. E. Lindelof, *Mesoscopic decoherence in Aharonov-Bohm rings*, Phys. Rev. B **64**, 045327 (2001).
- [82] R. Häussler, E. Scheer, H. B. Weber, and H. v. Löhneysen, *Conductance oscillations in mesoscopic rings: Microscopic versus global phase* Phys. Rev. B **64**, 085404 (2001).
- [83] B. N. Narozhny, I. L. Aleiner, and A. Stern, *Mesoscopic Fluctuations of the Coulomb Drag at $\nu = 1/2$* , Phys. Rev. Lett. **86**, 3610 (2001).
- [84] I. V. Kukushkin, J. H. Smet, K. von Klitzing, and W. Wegscheider, *Cyclotron resonance of composite fermions*, Nature **415**, 409 (2002).
- [85] I. L. Aleiner and Ya. M. Blanter, *Inelastic scattering time for conductance fluctuations*, Phys. Rev. B **65**, 115317 (2002).
- [86] C. Terrier, D. Babić, C. Strunk, T. Nussbaumer, and C. Schönenberger, *The amplitude of non-equilibrium quantum interference in metallic mesoscopic systems*, Europhys. Lett. **59**(3), 437 (2002) [cond-mat/0103486] and private communication.
- [87] C. Terrier, *Non-Equilibrium Coherent Transport in Mesoscopic Conductors*, Ph.D. thesis, Universität Basel (2002).
- [88] F. Pierre and N. O. Birge, *Dephasing by Extremely Dilute Magnetic Impurities Revealed by Aharonov-Bohm Oscillations*, Phys. Rev. Lett. **89**, 206804 (2002).
- [89] T. Ludwig, Diploma thesis, Universität Karlsruhe (2002).
- [90] F. Pierre, A. B. Gougam, A. Anthore, H. Pothier, D. Esteve, and N. O. Birge, *Dephasing of electrons in mesoscopic metal wires*, Phys. Rev. B **68**, 085413 (2003).
- [91] O. Tsyplatyev, I. L. Aleiner, V. I. Fal'ko, and I. V. Lerner, *Applicability of the Ergodicity Hypothesis to Mesoscopic Fluctuations*, Phys. Rev. B **68**, 121301 (2003).

- [92] G. Seelig, S. Pilgram, A. N. Jordan, and M. Büttiker, *Probe-configuration-dependent dephasing in a mesoscopic interferometer*, Phys. Rev. B **68**, 161310(R) (2003).
- [93] T. Ludwig and A. D. Mirlin, *Interaction-induced dephasing of Aharonov-Bohm oscillations*, Phys. Rev. B **69**, 193306 (2004).
- [94] T. Ludwig and A. D. Mirlin, *Mesoscopic Aharonov-Bohm oscillations in metallic rings*, in *Fundamental Problems of Mesoscopic Physics: Interactions and Decoherence*, Proceedings of the NATO Advanced Research Workshop, Granada (Spain), 2003, edited by I. V. Lerner, B. L. Altshuler, and Yu. Gefen, pp. 99-114 (Kluwer, 2004) [cond-mat/0312577].
- [95] M. Ferrier, L. Angers, A. C. H. Rowe, S. Guéron, H. Bouchiat, C. Texier, G. Montambaux, and D. Mailly, *Direct Measurement of the Phase-Coherence Length in a GaAs/GaAlAs Square Network*, Phys. Rev. Lett. **93**, 246804 (2004).
- [96] B. Huard, A. Anthore, F. Pierre, H. Pothier, N. O. Birge, and D. Esteve, *Intensity of Coulomb interaction between quasiparticles in diffusive metallic wires*, Solid State Comm. **131**, 599 (2004) [cond-mat/0404208].
- [97] T. Ludwig, Ya. M. Blanter, and A. D. Mirlin, *Nonequilibrium mesoscopic conductance fluctuations*, Phys. Rev. B **70**, 235315 (2004).
- [98] F. Schopfer, F. Mallet, C. Naud, G. Faini, D. Mailly, L. Saminadayar, and C. Bäuerle, *Observation of h/e conductance oscillations in disordered metallic T_3 network*, in the proceedings of the “Rencontres de Moriond”, *Quantum information and decoherence in nanosystems*, La Thuile (Italy), January/February 2004 [cond-mat/0407200].
- [99] A. Kamenev, *Many-body theory of non-equilibrium systems*, Lecture notes for 2004 Les Houches Summer School, cond-mat/0412296.
- [100] V. M. Galitski, M. G. Vavilov, and L. I. Glazman, *Aharonov-Bohm effect as a probe of interaction between magnetic impurities*, Phys. Rev. Lett. **94**, 096602 (2005).
- [101] A. Trionfi, S. Lee, and D. Natelson, *Time-dependent universal conductance fluctuations and coherence in AuPd and Ag*, Phys. Rev. B **72**, 035407 (2005).
- [102] C. Texier and G. Montambaux, *Dephasing due to electron-electron interaction in a diffusive ring*, Phys. Rev. B **72**, 115327 (2005).
- [103] V. Galitski, *Metallic phase in a two-dimensional disordered Fermi system with singular interactions*, Phys. Rev. B **72**, 214201 (2005).
- [104] H. Bouchiat, private communication (2005).

Acknowledgments

During the time I have worked on this thesis, my disorder has benefitted from interactions with numerous people. First, I wish to thank Alexander Mirlin for his supervision which both was careful in detail and left me room to work my way. I also thank Peter Wölfle for co-refereeing my thesis. I am grateful for the hospitality of the Institut für Theorie der Kondensierten Materie at the University of Karlsruhe, where much of this work was done, and for the flexibility given to me by both the Forschungszentrum Karlsruhe and the University. Further, I thank Yaroslav Blanter for a fruitful collaboration on dephasing effects at high voltages, Section 3.3 and Ref. [97].

It is a pleasure to acknowledge interesting and stimulating discussions with my colleagues, in particular with Igor Aleiner, Boris Altshuler, Norman Birge, Piet Brouwer, John Chalker, Jan von Delft, Vladimir Falko, Lars Fritz, Markus Garst, Leonid Glazman, Igor Gornyi, Hilbert von Löhneysen, Florian Marquardt, Dimitri Polyakov, Achim Rosch, Dirk Schuricht, Christoph Strunk, and Peter Wölfle, as well as receiving a copy of Ref. [102] with detailed remarks from Christophe Texier and Gilles Montambaux prior to publication. Also, I wish to thank Norman Birge for his kind permission to use figures from Ref. [88] for Fig. 1.8, and Hélène Bouchiat for sending me not yet published data [104] confirming the results (2.34), (2.35). Thanks also go to Ferdinand Evers for directing my interest towards condensed matter transport phenomena at an early stage.

While finalizing the thesis, I have received some additional help. I thank Marcus Diem for proofreading and helpful remarks, Andreas Arnold and Stefanie Weidmann for sharing meals, and Inga Fischer for the sweets.

Finally, I want to thank my parents – for everything.